Lawrence Berkeley National Laboratory

Title
Cold Fusion Production and Decay of Neutron-Deficient Isotopes of Dubnium and Development of Extraction Systems for Group V Elements

Permalink
https://escholarship.org/uc/item/6rr6g66n

Author
Gates, Jacklyn M.

Publication Date
2008-11-25

Cold Fusion Production and Decay of Neutron-Deficient Isotopes of Dubnium and

Development of Extraction Systems for Group V Elements

by

Jacklyn Marie Gates

B.S. (Westminster College) 2004

A dissertation submitted in partial satisfaction of the

requirements for the degree of

Doctor of Philosophy

in

Chemistry

in the

GRADUATE DIVISION

of the

UNIVERSITY OF CALIFORNIA, BERKELEY

Committee in charge:

Professor Heino Nitsche, Chair
Professor Joseph Cerny
Professor Jasmina L. Vujic

Fall 2008

The dissertation of Jacklyn Marie Gates is approved:

Chair   Date June 16, 2008

                                                         Date June 23, 2008

                                                         Date July 23, 2008

University of California, Berkeley

Fall 2008

Cold Fusion Production and Decay of Neutron-Deficient Isotopes of Dubnium and

Development of Extraction Systems for Group V Elements

Copyright 2008

by

Jacklyn Marie Gates

Abstract

Cold Fusion Production and Decay of Neutron-Deficient Isotopes of Dubnium and

Development of Extraction Systems for Group V Elements

by

Jacklyn Marie Gates

Doctor of Philosophy in Chemistry

University of California, Berkeley

Professor Heino Nitsche, Chair

Excitation functions for the $1n$ and $2n$ exit channels of the ^{208}Pb(^{51}V,xn)$^{259\text{-}x}$Db reaction were measured. A maximum cross section of the $1n$ exit channel of 2070^{+1100}_{-760} pb was measured at an excitation energy of 16.0 ± 1.8 MeV. For the $2n$ exit channel, a maximum cross section of 1660^{+450}_{-370} pb was measured at 22.0 ± 1.8 MeV excitation energy. The $1n$ excitation function for the ^{209}Bi(^{50}Ti,n)^{258}Db reaction was remeasured, resulting in a cross section of 5480^{+1730}_{-1370} pb at an excitation energy of 16.0 ± 1.6 MeV. Differences in cross section maxima are discussed in terms of the fusion probability below the barrier.

The extraction of niobium (Nb) and tantalum (Ta) from hydrochloric acid and mixed hydrochloric acid/lithium chloride media by bis(2-ethylhexyl) hydrogen phosphate (HDEHP) and bis(2-ethylhexyl) hydrogen phosphite (BEHP) was studied. The goal of the experiments was to find a system that demonstrates selectivity among the members of group five of the Periodic Table and is also suitable for the study of dubnium (Db, $Z = 105$). Experiments with niobium and tantalum were performed with carrier (10^{-6} M),

1

carrier free (10^{-10} M) and trace (10^{-16} M) concentrations of metal using hydrochloric acid solution with concentrations ranging from $1 - 11$ M. The extraction of niobium and tantalum from mixed hydrochloric acid/lithium chloride media by HDEHP and BEHP as a function of hydrogen ion (H^+) concentration was also investigated. The data obtained are used as the basis to discuss the speciation of niobium and tantalum under the conditions studied and to evaluate possible extraction mechanisms.

The $^{74}Se(^{18}O,p3n)^{88g}Nb$ excitation function was measured to determine the best energy for producing the ^{88}Nb used in chemistry experiments. A maximum cross section of 495 ± 5 mb was observed at an ^{18}O energy of 74.0 MeV. The half-life of ^{88g}Nb was measured and determined to be 14.56 ± 0.11 min.

Table of Contents

List of Figures

List of Tables

List of Acronyms

α-HIB   α-hydroxyisobutyric acid

ADC   Analogue to Digital Converter

ARCA   Automated Rapid Chemistry Apparatus

BEHP   Bis-2-Ethylhexyl Hydrogen Phosphite

BGS   Berkeley Gas-filled Separator

Bρ   Magnetic Rigidity

$CHCl_3$ Chloroform

COT   Center-of-Target

D   Distribution Coefficient

DEHPA   2-Ethylhexyl Hydrogen-2-Ethylhexyl Phosphonate

DIBC   Diisobutylcarbinol

DiOPA   Diisooctyldithiophosphinic Acid

DoS   Detector-on-a-Stick

%E   Percent Extracted

EC   Electron Capture

EVR   Evaporation Residue

FBD   Fusion by Diffusion

FCV   Full Column Volume

FPD   Focal Plane Detector

FWHM   Full Width at Half Maximum

GSI   Gesellschaft für Schwerionenforschung

HBr	Hydrobromic Acid
HCl	Hydrochloric Acid
HDEHP	Bis-2-Ethylhexyl Hydrogen Phosphate
HF	Hydrofluoric Acid
HNO_3	Nitric Acid
HPGe	High Purity Germanium
JINR	Joint Institute for Nuclear Research
$La(NO_3)_3$	Lanthanum Nitrate
LBNL	Lawrence Berkeley National Laboratory
LiCl	Lithium Chloride
LLNL	Lawrence Livermore National Laboratory
M1	Gradient-Field Dipole Magnet
M2	Flat-Field Dipole Magnet
MBS	Multi-Branch System
MIBK	Methyl Isobutyl Ketone
MLDS	Maximum Likelihood Decay Fits by the Simplex Method
MWPC	Multi-Wire Proportional Counter
NH_3	Ammonia
ORNL	Oak Ridge National Laboratory
$\bar{q}$	Average Charge
Q1	Quadrupole Magnet
RTC	Recoil Transfer Chamber
SF	Spontaneous Fission

SRIM	Stopping Range of Ions in Matter
TAC	Time-to-Amplitude Converter
TiOA	Triisooctyl Amine
σ	Cross Section

Acknowledgements

Many people have provided me with support and insightful discussions during the time needed to complete this thesis.

First, my advisor Prof. Heino Nitsche who took me on as a grad student even though I had little understanding of transactinides or any of the other subjects I ended up working with for the last four years.

Dr. Ken Gregorich, who rarely complained about the hours I spent in his office asking questions on every topic conceivable. Without his support the work in this dissertation would have taken several more years.

Prof. Ralf Sudowe, who was a staff scientist I was lucky enough to share an office with the first eighteen months. He taught me about aqueous chemistry and convinced me to start working with element 105. During this time and after, he provided invaluable support when I was struggling to understand extraction mechanisms and data. Chris Düllmann, who always made himself available to discuss chemistry or reactions, even after moving to Germany. Darleane Hoffman who was always willing to discuss nuclear physics or chemistry.

Prof. Jon Petter Omtvedt and the SISAK group at the University of Oslo. They hosted me for five months and provided me with many hours of beam time to try various ideas. Without their support, I would have made little progress in extraction chemistry.

Prof. Cody Folden, who was graduating just as I joined the group and shared an office with me during my first year. Throughout my first year he answered numerous questions about heavy element reactions and data analysis. Dr. Liv Stavsetra, Dr. Jan

Dvorak and Dr. Zuzana Dvorakova, postdocs who joined the group during my time here. They provided invaluable support during the last months and years.

Irena Dragojević and Mitch Garcia who joined the group as grad students the same year I did. Our daily discussions about a range of topic (both work related and non), lunches and random vending machine runs helped keep me relatively sane through the years.

The rest of the Nitsche Group, who all participated in many brainstorming sessions, took shifts on my experiments and helped make everything a success. Daniela Leitner and the staff at the 88-Inch Cyclotron. They continually provided the expertise necessary to produce the beams for my experiments.

1　　　Introduction

The production and chemistry of transactinide elements ($Z \geq 104$) is a topic of great interest in current nuclear chemistry research. This dissertation focuses on the production of dubnium (Db, $Z = 105$), and the chemical properties of niobium (Nb, $Z = 41$) and tantalum (Ta, $Z = 73$), the lighter homologues of dubnium. These three elements are all in group V of the periodic table, as can be seen in Fig. 1.1, and are expected to have similar chemical properties [Schädel2003].

1																	18
1 H	2											13	14	15	16	17	2 He
3 Li	4 Be											5 B	6 C	7 N	8 O	9 F	10 Ne
11 Na	12 Mg	3	4	5	6	7	8	9	10	11	12	13 Al	14 Si	15 P	16 S	17 Cl	18 Ar
19 K	20 Ca	21 Sc	22 Ti	23 V	24 Cr	25 Mn	26 Fe	27 Co	28 Ni	29 Cu	30 Zn	31 Ga	32 Ge	33 As	34 Se	35 Br	36 Kr
37 Rb	38 Sr	39 Y	40 Zr	41 Nb	42 Mo	43 Tc	44 Ru	45 Rh	46 Pd	47 Ag	48 Cd	49 In	50 Sn	51 Sb	52 Te	53 I	54 Xe
55 Cs	56 Ba	57+* La	72 Hf	73 Ta	74 W	75 Re	76 Os	77 Ir	78 Pt	79 Au	80 Hg	81 Tl	82 Pb	83 Bi	84 Po	85 At	86 Rn
87 Fr	88 Ra	89+" Ac	104 Rf	105 Db	106 Sg	107 Bh	108 Hs	109 Mt	110 Ds	111 Rg	112 ---	113 ---	114 ---	115 ---	116 ---		

*	58 Ce	59 Pr	60 Nd	61 Pm	62 Sm	63 Eu	64 Gd	65 Tb	66 Dy	67 Ho	68 Er	69 Tm	70 Yb	71 Lu
"	90 Th	91 Pa	92 U	93 Np	94 Pu	95 Am	96 Cm	97 Bk	98 Cf	99 Es	100 Fm	101 Md	102 No	103 Lr

Fig. 1.1: Periodic table of the Elements.

Part I: Cold Fusion Production and Decay of Neutron-Deficient Isotopes of Dubnium

1.1 History of Element 105

Elements beyond Uranium (U) (with the exception of primordial ^{244}Pu [Hoffman1971]) are not found in nature and must be produced in nuclear reactions between lighter isotopes. For transactinides, production is done one atom-at-a-time using particle accelerators. Due to these low production yields, controversy often accompanies discovery.

The discovery of element 105 was contested for many years between two research laboratories: Lawrence Berkeley National Laboratory (LBNL), in the USA and the Joint Institute for Nuclear Research (JINR) in Dubna, Russia. Between 1968 and 1976, several experiments were conducted at the two laboratories. These studies yielded conflicting results regarding the decay properties of element 105 isotopes.

1.1.1 JINR Publications

Starting in 1968, Flerov *et al*. bombarded targets of ^{243}Am with ^{22}Ne [Flerov1968]. The beam energies used were high enough to fuse the two nuclei into a compound nucleus that would then de-excite by the emission of 4-5 neutrons producing ^{260,261}105. To detect the activity, the nuclei recoiling out of the target were stopped in a gas-filled reaction chamber, transported in mixture of nitrogen and helium to a collection wheel, onto which they impinged. A silicon α-detector faced the collection wheel and intercepted α-decays exiting from the face of the wheel. During these experiments, short-lived α-emitters (0.1 s < t$_{1/2}$ < 3 s) with α-particle energies of 9.7 and 9.5 MeV were

observed [Flerov1971]. These activities were attributed to the decay of element 105. Significant α-lines were also observed in the energy region of $8.8 - 9.1$ MeV, and were attributed to products of reactions of the ^{22}Ne beam with lead impurities in the target. According to later publications by Flerov *et al.*: "Suggestions but not definite conclusions on ^{260}105 and ^{261}105, could be drawn from these experiments" [Flerov1971].

To help solidify the claim to the discovery of element 105, an additional set of experiments were undertaken at JINR to study the spontaneous fission (SF) properties of the reaction products from the irradiation of ^{243}Am with ^{20,22}Ne. The reaction products recoiling out of the target were stopped on an endless nickel belt moving at a constant speed past 105 fission fragment detectors. This setup was sensitive enough to detect SF from ^{261,260}105 if the SF branch >1% and $t_{1/2}$ >0.05 s. 58 SF decays were observed with a half-life of 1.8 ± 0.6 s. This activity was attributed to ^{261}105 [Flerov1971].

Following the detection of a short-lived SF activity, a new set of α-detection experiments were undertaken at JINR [Druin1971]. For these experiments, the lead impurities in the ^{243}Am target were reduced. A collimator was also placed behind the target to reduce contamination from transfer products, which have a wider angular distribution than the compound nucleus recoils. Analysis of the data yielded a 9.1-MeV α activity with a half-life of 1.4 s. Decay of this α activity was followed by the decay of a 35-s activity with α-particle energies in the $8.3 - 8.9$ MeV range. The second activity was assigned to ^{257}Lr, produced in the 9.1-MeV α-decay of ^{261}105, based upon the ^{257}Lr decay properties 'known' at that time [Druin1971]. The decay properties of ^{257}Lr were later modified and the half-life was revised from 35 s to 0.7 s [Eskola1971].

A series of chemistry experiments on the 2-s activity from the ^{22}Ne on ^{243}Am reaction were also performed at JINR between 1970 – 1975 [Zvára1974; Zvára1976]. In these experiments, the atoms recoiling out of the target were thermalized in a stream of nitrogen and transported away from the reaction chamber. There they were mixed with another nitrogen stream containing chlorinating agents, either thionyl chloride (SOCl$_2$) or a mixture of SOCl$_2$ and titanium chloride (TiCl$_4$) at 300° C. It was expected that the element 105 reaction products would form volatile chlorides similar to those observed by its lighter homologue, tantalum, while the transfer reaction products would not form volatile complexes <300° C. This would allow for separation of the activity. The volatile products were then flushed through a glass tube with a temperature gradient of 300° C at the entrance, dropping to 50° C over 170 cm. Several mica plate fission detectors were placed inside the tube to track fission fragments from the volatile complexes. ^{170}Hf was also produced in separate reactions and the distribution of SF events as a function of temperature was obtained for comparison with the distribution of possible SF decays from element 105. In the ^{22}Ne + ^{243}Am reaction, no fission fragments were observed in the detectors when SOCl$_2$ was used as the sole chlorinating agent. With the addition of TiCl$_4$ to the gas, 18 fission events were observed around the region that Hf deposits. The chemistry system was not sensitive to lifetime measurements, although a lower limit of 0.2 s was estimated for transport of the atoms from the target to the glass tube (See [Zvára1974; Zvára1976] for a short review or [Hyde1987] for more in-depth results). Later, experiments were conducted using a brominating carrier (a mixture of BBr$_3$ and Br$_2$). Spontaneous fission tracks attributed to the decay of ^{261}105 were observed at higher temperatures than those for niobium [Zvára1976].

1.1.2 LBNL Publications

In 1970 Ghiorso *et al*. announced the synthesis of $^{260}105$ in the reactions of ^{15}N on ^{249}Cf [Ghiorso1970]. The LBNL group chose to use a different method, genetic correlation, to detect and assign observed α-activities. For their experiments, the nuclides recoiling out of the target were slowed in a helium gas stream and transported to a vacuum chamber where they were deposited on the periphery of a wheel. This wheel was periodically rotated to place the collected products next to a series of solid-state detectors. By periodically rotating the wheel, it was possible to get a time-dependent distribution of α-particle decays among the detectors. This allowed for detection of both α-particle energies and half-lives of the α-emitting isotopes of element 105 and observation of the in-growth of the daughter, lawrencium, after decay of the parent. In these spectra, the decay of ^{256}Lr was observed to be preceded by decay of a 1.6 ± 0.3-s activity with α-particle energies of 9.06, 9.10 and 9.14 MeV. This new activity was assigned to $^{260}105$.

Two years later, Ghiorso *et al*. published an additional paper reporting observation of the α-decay of $^{261,262}105$ in reactions of ^{15}N on ^{250}Cf and $^{16,18}O$ on ^{249}Bk [Ghiorso1971b]. The setup for these new experiments was similar to that used for identification of $^{260}105$. Using genetic correlations to the α-decay daughters, $^{257,258}Lr$, Ghiorso *et al*. determined that $^{261}105$ decays by emission of an 8.93 MeV α-particle with a half-life of 1.8 s, while $^{262}105$ has an 8.45 MeV α-decay energy and a half-life of 40 s.

1.1.3   Later Publications

In 1977, the experiments performed by the LBNL group to produce $^{260}105$ were repeated at Oak Ridge National Laboratory (ORNL) [Bemis1977a]. The $^{249}Cf(^{15}N,4n)$ reaction was used to produce the activity. A half-life of 1.52 s and α-particle energies of 9.041, 9.074, and 9.12 MeV were observed, in agreement with the results published by LBNL. Detection of K X-rays was used to definitively assign the α activity to element 105. Later experiments by ORNL in collaboration with Lawrence Livermore National Laboratory (LLNL) investigated the decay properties of $^{262}105$, produced in the $^{249}Bk(^{18}O,5n)$ reaction [Bemis1981]. The half-life of $^{262}105$ was revised to 34.1 ± 4.6 s in these experiments, and a SF branching ratio of $78 \pm 6\%$ was observed.

1.1.4   Controversy

The results from the first experiment in 1968 at JINR were published in an internal report. Thus, with the publication by Ghiorso *et al.*, scientists from both LBNL and JINR began claiming the discovery of element 105. Several articles were written in the next years contesting discovery [Flerov1970; Ghiorso1971a]. In-depth reviews and analysis of data from all experiments were published in the following years [Greenwood2003; Hyde1987; Kratz2003].

For names of the element, LBNL had proposed hahnium (Ha), in honor of Otto Hahn, while JINR proposed nielsbohrium (Ns), in honor of Niels Bohr. Until 1997, publications on element 105 used either name. In addition, several publications used joliotium (Jl), a name proposed by IUPAC in 1994 in an attempt to settle the controversy [Recommendations1994].

Table 1.1: Known isotopes of dubnium and discovery information.

Isotope	Half-life (s)	Decay Properties	Discovery Year	Discovery Reaction(s)	References
^{256}Db	$1.5^{+0.5}_{-0.3}$	E_α = 9.014, 9.120, 9.075, 8.891 MeV b_{EC} = 0.36 ±0.12	2001	^{209}Bi(^{50}Ti,3n)	[Heßberger2001]
^{257}Db	g: $1.50^{+0.19}_{-0.15}$ m: $0.76^{+0.15}_{-0.11}$	E_α = 9.074, 8.967 MeV b_{SF} = ≤ 0.06 E_α = 9.163 MeV b_{SF} ≤ 0.13	1985	^{209}Bi(^{50}Ti,2n)	[Heßberger2001; Heßberger1985]
^{258}Db	$4.4^{+0.9}_{-0.6}$	$E\alpha$ = 9.299, 9.172, 9.078, 9.008 MeV b_α = $0.67^{+0.59}_{-0.95}$ b_{EC} = $0.33^{+0.09}_{-0.05}$	1985	^{209}Bi(^{50}Ti,1n)	[Heßberger2001; Heßberger1985]
^{259}Db	0.51 ± 0.16	E_α = 9.47 MeV	2001	^{241}Am(^{22}Ne,4n)	[Gan2001]
^{260}Db	1.52 ± 0.13	E_α = 9.047, 9.082, 9.128 MeV b_α = 0.904 b_{SF} = 0.096	1968-1970	JINR: ^{243}Am(^{22}Ne,5n) LBNL: ^{249}Cf(^{15}N,4n)	[Flerov1968; Ghiorso1970]
^{261}Db	1.8 ± 0.6	E_α = 8.930 MeV b_α = >0.5 b_{SF} = <0.5	1971	^{250}Cf(^{15}N,4n)	[Ghiorso1971b]
^{262}Db	34.1 ± 4.6	E_α = 8.450, 8.530, 8.670 MeV b_α = 0.64 b_{EC} = 0.33	1971	^{249}Bk(^{18}O,5n)	[Bemis1977b; Ghiorso1971b]
^{263}Db	27^{+10}_{-7}	E_α = 8.35 MeV b_α = 0.43 b_{EC} = 0.57	1992	^{249}Bk(^{18}O,5n)	[Kratz1992]
^{266}Db	21.97 m	$b_{SF/EC}$ = ~1	2006	^{237}Np(^{48}Ca,3n) Daughter of ^{282}113	[Oganessian2007]
^{267}Db	1.2 h	b_{SF} = ~1	2004	^{243}Am(^{48}Ca,4n) Daughter of ^{287}115	[Oganessian2007; Oganessian2004]
^{268}Db	1.2 d	$b_{SF/EC}$ = ~1	2004	^{243}Am(^{48}Ca,3n) Daughter of ^{288}115	[Oganessian2007; Oganessian2004]

After much debate between the groups, it was agreed upon at the 39th IUPAC General Assembly in 1997 that element 105 should be named dubnium. This was done to honor the contributions that JINR had made to the discovery of elements 104 – 106 [Recommendations1997].

1.2   Hot versus Cold Fusion

Transactinides are typically produced in two different types of reactions, termed 'hot' and 'cold' fusion. Hot fusion reactions occur when a deformed actinide target is bombarded with light 'heavy ions'. At energies sufficient for compound nucleus formation, these reactions will leave the compound nucleus with >40 MeV, resulting in the evaporation of 3 - 6 neutrons. Cold fusion is the bombardment of spherical, shell-stabilized lead (Pb) and bismuth (Bi) targets with medium-mass (A > 40) projectiles that leads to compound nuclei with excitation energies of <20 MeV and evaporation of 1 - 2 neutrons.

The known isotopes of Db, their decay properties and discovery information are shown in Table 1.1. The isotopes formed in hot fusion reactions are more neutron rich and tend to have longer half-lives than those formed in the cold fusion reactions.

1.3   Excitation Functions

An excitation function is a measure of cross sections as a function of the energy of the bombarding particle. For the experiments presented in this dissertation, excitation functions for the 1n and 2n exit channels of the $^{208}Pb(^{51}V,xn)^{259-x}Db$ reaction and 1n exit channel of the $^{209}Bi(^{50}Ti,xn)^{259-x}Db$ reaction were investigated. Both of these reactions

are 'cold' fusion reactions and were performed at excitation energies in which the release of 1-2 neutrons was favorable.

1.3.1   Fusion by Diffusion Model

For predicting cold fusion reaction cross sections, Świątecki *et al.* have developed the Fusion by Diffusion (FBD) model [Świątecki2003; Świątecki2005]. According to the FBD model, the cross section is a product of three factors: i) the probability for the target and projectile to become captured in a pocket of their mutual Coulomb + nuclear potential and form a composite system, σ_{cap}. ii) the probability for this composite system to form a compound nucleus, P_{CN}. iii) the probability, $\dfrac{\Gamma_n}{\Gamma_t}$, for the compound nucleus to de-excite by the emission of one neutron in competition with fission and other de-excitation modes times the probability, $P_<$, that after emitting the first neutron, the nucleus is below the threshold for second chance fission or additional neutron emission. The total cross section is then given by:

$$\sigma_{tot} = \sigma_{cap} \times P_{CN} \times \frac{\Gamma_n}{\Gamma_t} P_< \tag{1.1}$$

By producing the same compound nucleus (as done in the $^{208}_{82}\text{Pb}(^{51}_{23}\text{V}, \text{x}n)^{258}_{105}\text{Db}$ and $^{209}_{83}\text{Bi}(^{50}_{22}\text{Ti}, \text{x}n)^{258}_{105}\text{Db}$ reactions), the last term in FBD, $\dfrac{\Gamma_n}{\Gamma_t} P_<$, is identical for the two reactions (ignoring small differences in angular momentum). This allows for the investigation of the product of σ_{cap} and P_{CN}. For two similar reactions, P_{CN} is expected to be similar. However, the more asymmetric target-projectile combinations have smaller

repulsive Coulomb forces, which are expected to result in larger cross sections because of the larger σ_{cap} [Świątecki2003; Świątecki2005].

1.3.1.1 Capture cross section, σ_{cap}

For the $^{208}\text{Pb}(^{51}\text{V,x}n)^{259-x}\text{Db}$ and $^{209}\text{Bi}(^{50}\text{Ti,x}n)^{259-x}\text{Db}$ reactions, differences in the cross sections are expected to be mainly due to σ_{cap}. The classical formula for calculating the cross section to overcome a barrier B, encountered at a separation R, between two mass points colliding with a center of mass energy E can be expressed as:

$$\sigma_{cap} = \pi R^2 \left(1 - \frac{B}{E} \right) \qquad \text{for } E \geq B \qquad\qquad (1.2)$$

$$\sigma_{cap} = 0 \qquad\qquad \text{for } E \leq B$$

However, use of this expression leads to an excitation function measurement consisting of two lines with a discontinuity at $E = B$. In the FBD model, this discontinuity is smoothed by including a distribution of barrier heights centered on B and with a range, υ [Świątecki2003; Świątecki2005]:

$$\sigma_{cap} = \pi R^2 \frac{\upsilon}{2E} \left[X(1 + \text{erf}(X)) + \frac{1}{\sqrt{\pi}} \exp(-X^2) \right] \qquad\qquad (1.3)$$

where $X = \dfrac{E - B}{\upsilon}$

1.3.1.2 Calculating the Barrier, *B*

Prior to forming a composite system, the two nuclei must first overcome a barrier formed from their combined Coulomb and nuclear potentials, represented by B in eqns. (1.2) and (1.3). Świątecki *et al.* have proposed a simple method for calculating these

combined barriers based on a fit to experimental data [Świątecki2005]. For two reactions

with atomic numbers Z_1 and Z_2 and atomic masses A_1 and A_2, B can be estimated by:

$$B = 0.85247z + 0.001361z^2 - 0.00000223z^3 \text{ MeV} \tag{1.4}$$

where $z \equiv \dfrac{Z_1 Z_2}{A_1^{1/3} + A_2^{1/3}}$

In eqn. (1.3), this barrier is distributed using a Gaussian function centered on B

with a width of υ. The value of υ was also determined by extrapolation of experimental

data [Świątecki2005]. The data were best modeled using:

$$\upsilon = CB\sqrt{W_1^2 + W_2^2 + W_0^2} \tag{1.5}$$

where B is calculated as in eqn. (1.4), C is an adjustable parameter set to 0.07767 fm^{-1}

from comparisons with experimental data. $W_0 = 0.41$ fm is a second adjustable parameter

and roughly represents the nuclear vibrations, quantal barrier penetrability etc. W_1 and

W_2 are the rms distributions of the radius vectors specifying the surfaces of the projectile

and target:

$$W_i^2 = \frac{R_i^2 \beta_i^2}{4\pi} \tag{1.6}$$

where R_1 and R_2 are the mean radii taken as $R_i = 1.14A_i^{1/3}$ fm and β is the

deformation parameter listed in [Möller1995] as β_2. σ_{cap} for different reactions can be

calculated using eqn. $(1.3) - (1.5)$. Comparison of σ_{cap} with experimental data gives

indications as to the effect of σ_{cap} on σ_{tot} and is further discussed in Chap. 3.

1.3.1.3   Optimal Beam Energies

When producing isotopes using new reactions, selection of the beam energy is

crucial as limited beam time restricts the number of energies that can be investigated. In

cold fusion reactions, Świątecki *et al.* argue that the maximum of the 1*n* excitation function is a result of competition between two factors that vary with energy: the reaction channel for single neutron emission, $\sigma_{cap} \times P_{CN} \times \dfrac{\Gamma_n}{\Gamma_t}$, and losses in EVR formation due to second chance fission or neutron emission, $P_<$. The reaction channel for single neutron emission increases with increasing bombarding energy; however, $P_<$ decreases with increasing energy once the threshold for second chance fission or neutron emission has been reached [Świątecki2003; Świątecki2005]. The product of $P_<$ and $\sigma_{cap} \times P_{CN} \times \dfrac{\Gamma_n}{\Gamma_t}$ results in a peaked excitation function as is shown in Fig. 1.2.
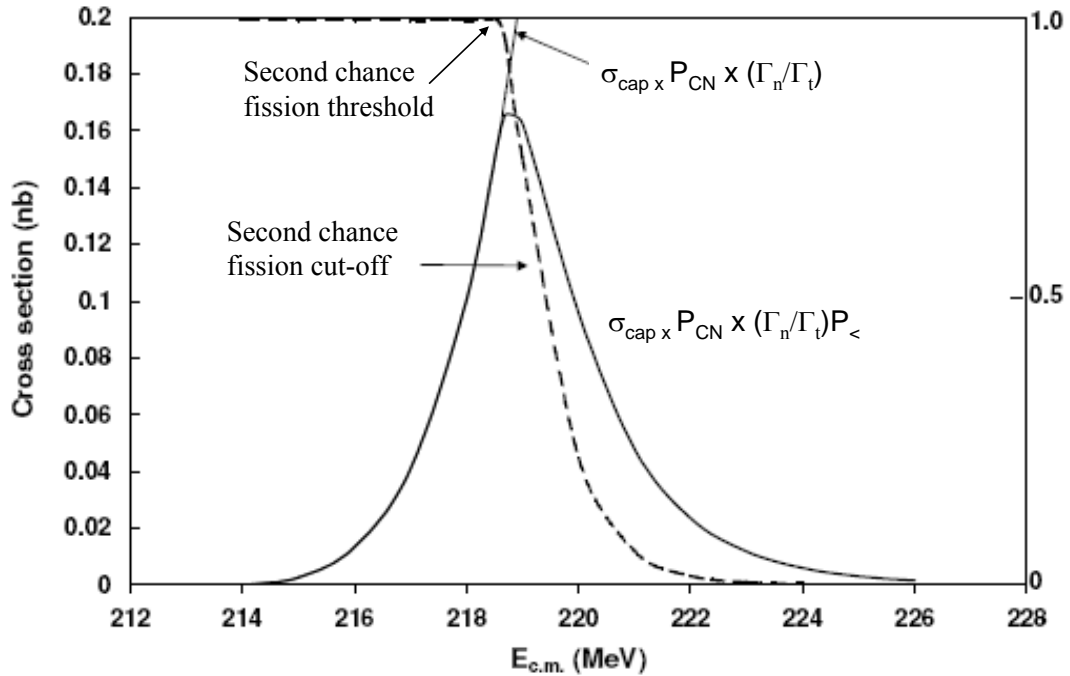
Fig. 1.2: The anatomy of a one-neutron-out excitation function for the ^{58}Fe + ^{208}Pb → ^{265}108 + n (adapted from [Świątecki2005]). The thin solid line represents the cross section for sticking, forming a compound nucleus and then de-exciting by emission of a single neutron (i.e., the single neutron emission reaction channel). The dotted line represents the channel for fission after neutron emission (i.e., 'second chance fission'), which begins to occur when the excitation energy of the compound nucleus after neutron emission is above the fission barrier. The heavy solid line is the product of the two functions, resulting in a peaked excitation function.

12

The FBD model predicts that the maximum of an excitation function will occur when the beam energy maximizes $\sigma_{cap} \times P_{CN} \times \dfrac{\Gamma_n}{\Gamma_t}$ and minimizes contributions due to $P_<$. This occurs at beam energies in which the excitation energy of the resulting compound nucleus is near in energy to the fission barrier after emission of one neutron. Świątecki *et al.* have developed an 'optimum energy rule' to calculate the excitation energy at which the cross section is expected to be the highest:

$$E_{cm,opt} \approx (M_{SP} + M_n) - (M_{proj} + M_{tgt}) + 0.3 \text{ MeV} \tag{1.7}$$

$$= (M_{CN-1} + B_f + M_n) - (M_{proj} + M_{tgt}) + 0.3 \text{ MeV}$$

where $E_{cm,opt}$ is the expected center-of-mass bombarding energy at the maximum of the $1n$ excitation function, M_n is the mass of a neutron, M_{proj} is the mass of the projectile, M_{tgt} is the mass of the target, B_f is the fission barrier of the compound nucleus, M_{SP} is the mass of the saddle point nucleus and M_{CN-1} is the mass of the ground state of the residual nucleus. The 0.3 MeV is a correction factor added after comparisons of theoretical calculations and experimental data. If we assume that the shell correction to the fission barrier is negligible, then the saddle point mass can be approximated by the ground state mass plus the ground state shell correction δ_{CN-1}:

$$E_{cm,opt} \approx (M_{CN-1} + \delta_{CN-1} + M_n) - (M_{proj} + M_{tgt}) + 0.3 \text{ MeV} \tag{1.8}$$

1.3.2 Excitation Function Fits

Excitation functions for reactions are measured at discrete beam energies. While calculations are performed to determine the 'best' bombarding energies, these calculations may be off by several MeV. Targets used in reactions may also be several MeV thick. To best compare excitation functions, it is necessary to 'fit' the data, thus

obtaining information regarding the 'true' cross section as a function of energy. In this dissertation, excitation functions were fitted using the methods described in [Dragojević2008; Gregorich2007]. Studies of various hot and cold fusion excitation functions indicate that their shape can best be modeled with a Gaussian on the low-energy side smoothly joined to an exponential on the high-energy side using:

$$\sigma = \sigma_{max} e^{-(E^* - c)^2 / 2w^2}, E^* \leq \lambda w^2 + c \tag{1.9}$$

$$\sigma = \sigma_{max} e^{\lambda^2 w^2 / 2} e^{-\lambda(E^* - c)}, E^* > \lambda w^2 + c$$

where E^* is the excitation energy, $-\lambda$ is the slope of the exponential line and σ_{max} is the amplitude of the Gaussian with a centriod, c, and a width, w. The number of counts expected at each beam energy, μ, can be calculated by integrating σ over the energy width of the target:

$$\mu_{expected}(L, E_{COT}^*, E_w, \sigma_{max}, w, c, \lambda) = \frac{L}{E_w} \int_{E_{COT}^* - \frac{E_w}{2}}^{E_{COT}^* + \frac{E_w}{2}} \sigma(\sigma_{max}, w, c, \lambda, E) dE \tag{1.10}$$

where L is the one event sensitivity in picobarns, E_{COT}^* is the excitation energy at the center of the target, and E_w is the energy width of the target. The Poisson distribution can then be used to calculate the probability of observing n events when μ are expected at each energy. The relative likelihood, L, that the fit represents the excitation function data is the product of the Poisson probabilities at each of m energies and is given by:

$$L(\sigma_{max}, w, c, \lambda) = \prod_{i=1}^{m} \frac{\mu^{n_i}}{n_i!} \cdot e^{-\mu}. \tag{1.11}$$

The expression obtained is then maximized to obtain the best fitting parameters σ', w', c', and λ'. The fitting curve is obtained from:

$$f(\sigma',w',c',\lambda') = \frac{\mu}{L} \tag{1.12}$$

1.4 Scope of Reactions

In this dissertation, the investigation of the ^{208}Pb(^{51}V,xn) and ^{209}Bi(^{50}Ti,n) excitation functions was undertaken. These two reactions produce the same compound nucleus, which is expected to de-excite in the same way at the same excitation energy, regardless of the production reaction. This reduces the impact of $\frac{\Gamma_n}{\Gamma_{tot}} P_<$ on differences in the cross sections for the two reactions, allowing for the investigation of the product of σ_{cap} and P_{CN}. The ^{209}Bi(^{50}Ti,xn) reaction was previously investigated at GSI [Heßberger2001; Heßberger1985]; however, differences in reaction energies and cross sections occur between the two laboratories [Dragojević2008; Folden III2004a]. To minimize these differences, the ^{209}Bi(^{50}Ti,n) reaction was re-measured at LBNL using the same setup that was used for the ^{208}Pb(^{51}V,xn) reaction.

Part II: Development of Extraction Systems for Group V Elements

The chemistry of group V elements at very low concentrations in aqueous media is of interest to understand the roles that relativistic effects play in the complex formation of these elements. It is predicted [Pershina1996], that relativistic effects in the transactinide elements ($Z \geq 104$) will lead to deviations from chemical trends established by the lighter homologues in a group, as these effects increase with Z^2 of elements

[Pyykkö1988]. To test for deviations, it is necessary to compare the chemical behavior of the transactinide elements to the behavior of the lighter homologues in the group.

1.5   *Relativistic Effects*

With increasing Z of the nucleus, core electrons are more strongly attracted, and consequently, begin to move faster. This leads to a mass, m, increase as:

$$m = \frac{m_0}{\sqrt{1-(v/c)^2}} \tag{1.13}$$

where m_0 is the rest mass of an electron and v is the velocity of the electron. This mass increase has three main results: First, the effective Bohr radius (α_B)

$$\alpha_B = \frac{\hbar^2}{m \cdot c^2} \tag{1.14}$$

decreases for the s and $p_{1/2}$ orbitals. For an element such as dubnium, this results in a 25% relativistic contraction for the 7s orbital as can be seen in Fig. 1.3 [Hoffman2006; Schädel2003]. Second, the relativistic contraction of the s and $p_{1/2}$ orbitals leads to more effective screening of the nuclear charge. As a result, the outer d and f orbitals become more expanded and energetically destabilized. Lastly, levels with l > 0 (p, d, f, … electrons) are split into j = l ± ½. This spin-orbit splitting decreases with increasing l for the same principal quantum number, i.e. the $np_{1/2} - np_{3/2}$ splitting is larger than the $nd_{3/2} - nd_{5/2}$ splitting, which is larger than the $nf_{5/2} - nf_{7/2}$ splitting. All three relativistic effects are on the same order and increase with Z^2 of the nucleus [Pyykkö1988; Schädel2003].
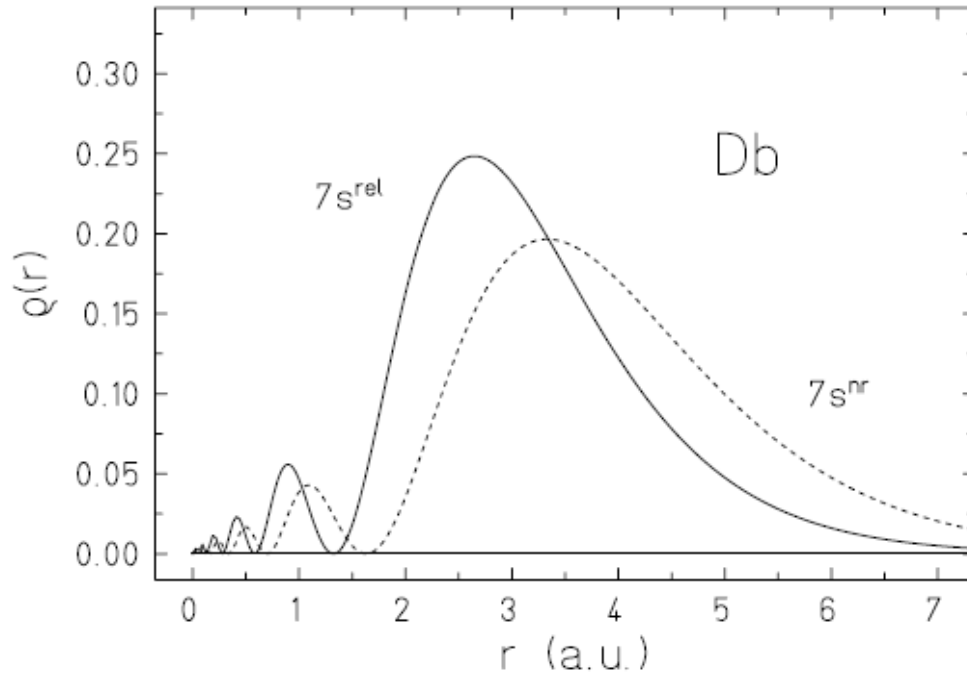
Fig. 1.3: Relativistic (solid line) and non-relativistic (dashed line) radial distributions of the 7s valence electrons in element 105, Db (adapted from [Hoffman2006]).

For the group V elements, relativistic effects have a significant impact on the $s_{1/2}$, $d_{5/2}$ and $d_{3/2}$ orbitals as can be seen in Fig. 1.4. Between niobium, tantalum and dubnium, the spacing between the $d_{5/2}$ and $d_{3/2}$ orbitals increases, and both of those are destabilized in relation to the non-relativistic d orbitals. The $s_{1/2}$ orbitals are increasingly stabilized going down the group. By tantalum, there is only a small spacing between the $s_{1/2}$, $d_{5/2}$ and $d_{3/2}$ orbitals and in dubnium, the $s_{1/2}$, becomes more stabilized than the $d_{5/2}$ and $d_{3/2}$ orbitals. As the expected ground state electronic configuration of dubnium is $[Rn]5f^{14}6d^37s^2$, stabilization of the $7s_{1/2}$ orbitals may result in the presence of trivalent Db(III), something not observed with the lighter homologues [Pershina1993; Pyykkö1988; Schädel2003].
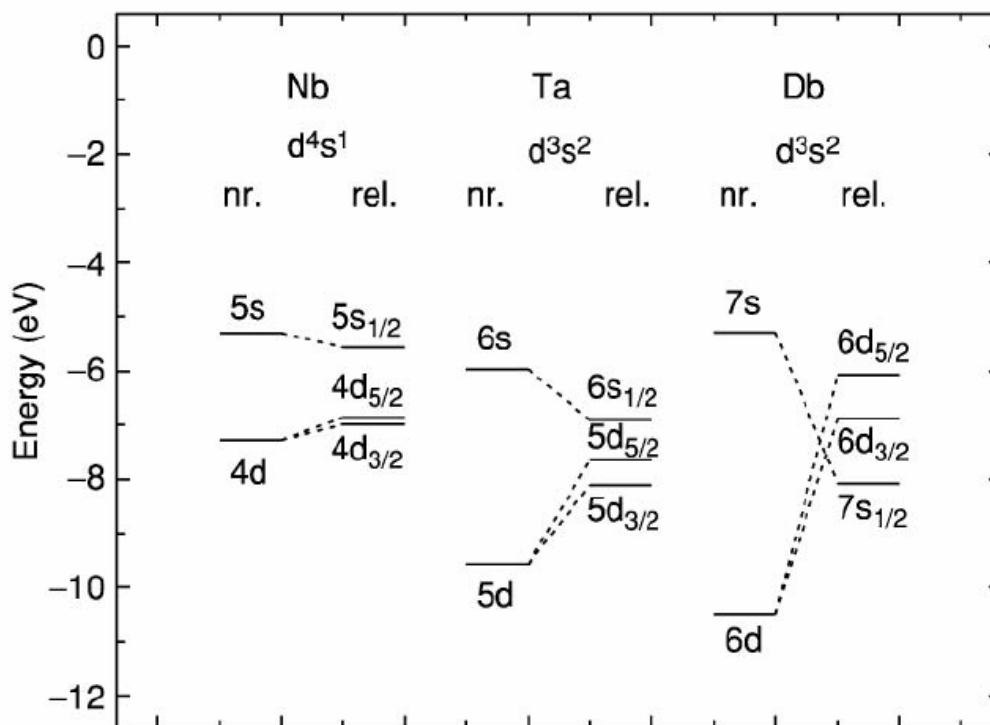
Fig. 1.4: Relativistic and non-relativistic energy levels of the valence ns and (n-1)d electrons for group-5 elements (adapted from [Hoffman2006]).

1.6   *Aqueous Chemistry of Dubnium*

The first aqueous chemistry experiments on Dubnium were performed at LBNL by Gregorich *et al* [Gregorich1988]. ^{262}Db was produced using the ^{249}Bk(^{18}O,5n) reaction. The dubnium EVRs were then thermalized behind the target and captured on potassium chloride (KCl) aerosols and transported to a collection site using a He-gas jet. Niobium and tantalum are known to adsorb to the surface of glass in the presence of nitric acid (HNO$_3$) and the first experiment was designed to test this reaction with dubnium. The aerosols were collected on a glass plate, fumed with 15 M HNO$_3$ and washed with 1.5 M HNO$_3$ and then with acetone. Twenty-six α events were observed

with the decay properties of ^{262}Db or its daughter, ^{258}Lr. Two events were expected from background measurements, leaving ~24 α events from the decay of ^{262}Db or ^{258}Lr, indicating that dubnium does behave as a group V element.

The second experiment was designed to determine whether dubnium behaved more like niobium or more like tantalum. Extrapolations down the periodic table would suggest more tantalum-like behavior. In these experiments, the aerosols were collected and dissolved in a mixture of HNO_3 and hydrofluoric acid (HF). Liquid-liquid extractions were then performed using an organic phase consisting of methyl isobutyl ketone (MIBK). Similar experiments with niobium and tantalum showed that tantalum was extracted by the MIBK while niobium was not. During the dubnium experiments, no α-like events in the energy range of $8.4 - 8.7$ MeV were detected, suggesting that dubnium behaves more like its lighter homologue, niobium [Gregorich1988].

Following the observation of these unexpected dubnium properties, several experiments were undertaken to ascertain more detailed information about the chemical behavior of dubnium. The first of these studies used a microcomputer controlled Automated Rapid Chemistry Apparatus (ARCA II) [Schädel1989] to study the anion exchange properties of niobium, tantalum and dubnium from hydrochloric acid (HCl) and HCl/HF solutions [Kratz1989]. The columns contained triisooctyl amine (TiOA) on an inert support. ^{262}Db produced in the ^{249}Bk(^{18}O,5n) reaction was found to adsorb onto the columns in solutions of 12 M HCl/0.02 M HF or 10 M HCl. Similar behavior was observed for the group V homologues, niobium, tantalum and protactinium. Elutions were then performed to separate out a niobium-protactinium fraction (4 M HCl/0.02 M HF) from the tantalum fraction (6 M HNO_3/0.015 M HF). The

dubnium was observed to be eluted in the niobium-protactinium fraction. A second set of elutions was then performed to separate the protactinium fraction (eluted with 10 M HCl/0.025 M HF) from the niobium fraction (eluted with 6 M HNO$_3$/0.015 M HF). The dubnium activity was observed to be divided equally between the two fractions [Kratz1989]. These studies confirmed the non-tantalum-like behavior of dubnium observed in [Gregorich1988]. The TiOA extractions were later continued by Zimmermann *et al.* [Zimmermann1993]. Using the same chemistry system, they varied the cut between the protactinium and niobium fractions. The authors were able to show that the elution of dubnium occurs nearer to the protactinium than the niobium elution position with an elution sequence of Pa ≥ Db > Nb.

Between the TiOA experiments, additional studies were undertaken to establish whether dubnium behaved more like niobium or protactinium [Gober1992; Schädel1992]. In [Gober1992] [262,263]Db were adsorbed onto a column of diisobutylcarbinol (DIBC) from solutions of concentrated hydrobromic acid (HBr). A niobium fraction was then eluted with 6 M HCl/0.00002 M HF, followed by a protactinium fraction using 0.5 M HCl. The column was then stripped with acetone. Based on the number of [262,263]Db decays observed, less than 45% of the dubnium was extracted into DIBC from the HBr solution, indicating that there is a decreasing extractability from HBr (Pa > Nb > Db). This behavior was assigned to an increasing tendency of the elements to form non-extractable polynegative complexes in concentration HBr solutions [Gober1992].

As noted earlier, the expected ground state electronic configuration of dubnium is [Rn]5f^{14}6d^{3}7s^2. Theoretical calculations predicted that relativistic effects may stabilize of

the $7s_{1/2}$ orbitals resulting in the presence of trivalent Db(III), something not observed with the lighter homologues [Pershina1993; Pyykkö1988; Schädel2003]. Schädel *et al.* investigated the complexation of dubnium by unbuffered α-hydroxyisobutyric acid (α-HIB) and its elution to determine the most stable oxidation state of dubnium [Schädel1992]. In these experiments, the dubnium was loaded onto a strongly acid cation exchange resin (Aminex A6, particle size 17.5 ± 2 μm) in 0.5 M α-HIB. Under these conditions, tetravalent and trivalent activities are strongly retained on the column while pentavalent activities are eluted. The dubnium activity was observed to be eluted within 4 s, indicating that the most stable oxidation state in aqueous solution is +5 [Schädel1992].

Paulus *et al.* investigated the chemical behavior of dubnium using reversed-phase anion exchange chromatography, Aliquat 336 (an aliphatic amine) and pure HCl. In these extractions, the elution sequence Pa > Nb ≥ Db > Ta was observed [Paulus1998; Paulus1999]. This is different from the sequence observed from the mixed HCl/HF studies done in [Kratz1989; Zimmermann1993], suggesting that with the addition of HF to the solutions, the complexation behavior of group V elements can no longer be attributed to the pure chloride complexes [Paulus1998; Paulus1999].

The most recent experiments on dubnium were performed by Trubert *et al.*, investigating the behavior of dubnium in fluoride media [Trubert1998; Trubert2002]. These experiments employed three successive ion exchange columns. The first column used cation exchange to provide purification from the actinide activities. On the second column, an anion exchange column was used to isolate dubnium and an additional cation exchange resin was used to retain the long-lived decay produces of ^{262}Db (3.24-hr ^{254}Fm).

After one hour, the third column was stripped and the decay of ^{254}Fm was detected using boron-implanted silicon detectors. The activity of ^{262}Db was indirectly assigned based on the detected number of ^{254}Fm decays. These experiments showed that dubnium forms negatively charged complexes in HF solutions like its homologues.

While these initial experiments showed that dubnium behaved liked a group V element, the used of mixed acid solutions made further interpretation of the results difficult. To better elucidate the chemical properties of dubnium, it is necessary to use pure acid solutions.

1.7   Liquid-Liquid Extraction

Due to the low production rates of transactinides, chemical systems in which the element of interest undergoes the same reaction multiple times are preferred. Liquid-liquid, or solvent extraction, is one such method and was chosen for the experiments in this dissertation. Liquid-liquid extraction refers to a technique in which a solute is distributed between two immiscible liquids. Generally, the two liquids consist of an aqueous phase/solution and an organic extractant. Due to variations in the strength of the interaction of the solute molecules with those of the extractant, different solutes will have different solubilities in different liquids. This uneven solubility allows for the extraction of part, or all, of the solute from the aqueous phase to the extractant. After equilibrium has been reached in the system, the distribution of the solute between the two phases can be shown as:

$$D = \frac{[A]_{org}}{[A]_{aq}}$$ (1.15)

where D is the distribution ratio and the concentration of the solute in the organic and aqueous phases are $[A]_{org}$ and $[A]_{aq}$, respectively. The percent of solute extracted (%E) can then be determined as

$$\%E = \frac{100 \cdot D}{1 + D} \tag{1.16}$$

1.7.1   Complex Formation in Solution

When in contact with a liquid, the solute and solvent particles interact. If the solvent is water, then hydration takes place. Successive hydrolysis reactions can be written as:

$$M(H_2O)_{n-i} + \cdot (H_2O) \leftrightarrow M(H_2O)_n \tag{1.17}$$

where n is the coordination number. For group V elements, n = 6. In the case of complexation occurring between the metal and an acidic ligand, HL, the equation becomes:

$$M + HL \leftrightarrow ML + H \tag{1.18}$$

In a mixture of water and acid, these two processes, complex formation and hydrolysis, compete with each other. The competition can be described by the following equation [Pershina1998b]:

$$M(H_2O)_{\circ}^{+} + OH^- + L^- \leftrightarrow \tag{1.19}$$

$$M O (OH) \quad (H_2O) L^{(\ - \ - \ )+} + (\quad \circ + \ - \ )H_2O$$
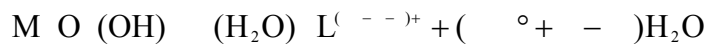
This competition leads to a plethora of possible complexes in solution and is discussed in more detail in Chap. 4.1.1 and 4.2.1.

1.7.2 Organophosphorus Extractants

Many substances can be added to the solvents that will form a complex with the metal that is soluble in the organic phase. Specifically, organophosphorus compounds can complex with metal complexes and extract them into the organic phase. The results presented in this dissertation concentrate on the use of two organophosphorus compounds: bis(2-ethylhexyl) hydrogen phosphate (HDEHP, Fig. 1.5a) and bis(2-ethylhexyl) hydrogen phosphite (BEHP, Fig. 1.5b). In addition, the extraction of relatively-long lived niobium from 2-ethylhexyl hydrogen-2-ethylhexyl phosphonate (DEHPA, Fig. 1.5c) and diisooctyldithiophosphinic acid (DiOPA, Fig. 1.5d) was investigated.
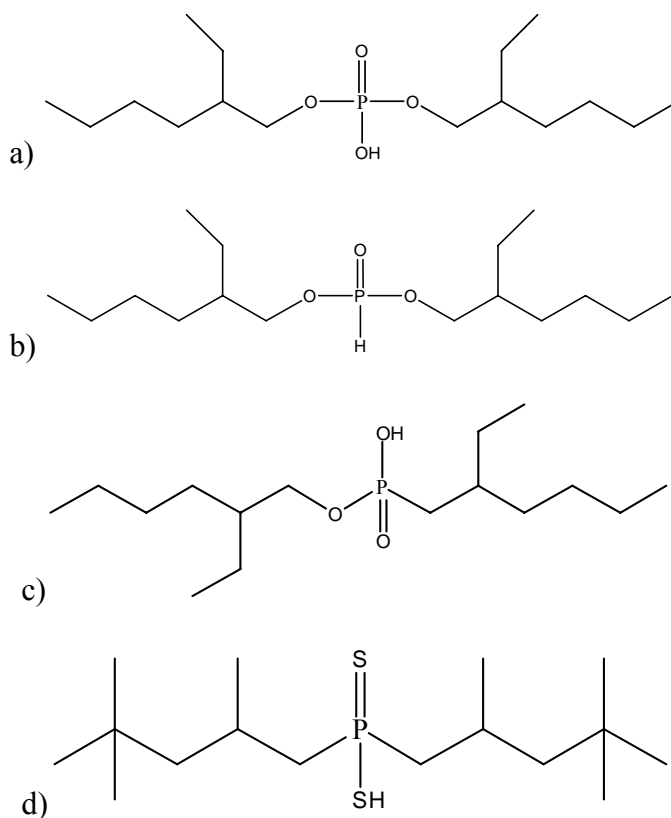
Fig. 1.5: Chemical structure of a) bis(2-ethylhexyl) hydrogen phosphate (HDEHP) and b) bis(2-ethylhexyl) hydrogen phosphite (BEHP) c) 2-ethylhexyl hydrogen-2-ethylhexyl phosphonate (DEHPA) and d) diisooctyldithiophosphinic acid (DiOPA).

In organic media, two linear acids may form a dimer. The partial neutralization of the hydrophilic groups leads to increased solubility of the acid in the organic solvent and only dissolves sparingly in the aqueous phase. BEHP is not an acid and is not known to dimerize in solution. However, HDEHP, DEHPA and DiOPA have a tendency to form dimers which can be represented by [Rydberg2004]:

$$2HA_{org} \leftrightarrow H_2A_{2(org)} \tag{1.20}$$

These dimeric acids may then form monobasic complexes with metal ions.

1.7.3 *Extraction Mechanisms*

The complexes formed in aqueous, acidic media can be extracted into the organic phase by one of four main processes [Rydberg2004]:

i)   Extraction of coordinatively saturated metal chelate type complexes:

$$M^{z+}_{(aq)} + zHA_{(org)} \leftrightarrow MA_{z(org)} + zH^+_{(aq)} \tag{1.21}$$
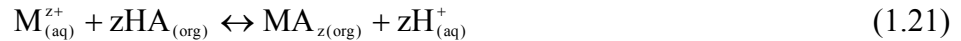
In this mechanism, a metal ion, M^{z+}, is complexed by zA^- ligands to form neutral MA_z. This neutral, coordinatively saturated metal complex is then extracted directly into the organic phase.

ii)   Extraction of metal complexes as adducts according to the general equation:

$$M^{z+} + zA^- + bB \leftrightarrow MA_zB_b \tag{1.22}$$

In this mechanism, a neutral, coordinatively saturated metal complex is formed in the aqueous phase. This complex is then extracted by a neutral ligand into the organic phase in the form of a neutral, metal adduct.

iii)   Metal extraction by liquid anion exchangers (amines):

$$M^{z+}_{(aq)} + nL^-_{(aq)} + pA^+L^-_{(org)} \leftrightarrow (A^+)_p ML^{-p}_{n(org)} + pL^-_{(aq)} \tag{1.23}$$

In this mechanism, an anionic metal complex is formed in the aqueous phase. This anionic complex is then extracted into the organic phase by the cationic ligand.

i) Other extractable metal complexes, i.e., monovalent metals that form extractable complexes with large organic monobasic anions or monovalent inorganic anions that form extractable complexes with large organic cations.

$$M^{+}_{(aq)} + A^{-}_{(org)} \leftrightarrow KA_{(org)} \tag{1.24}$$

In this mechanism, the metal forms cationic complexes in aqueous solution. These complexes are then extracted into the organic phase by anionic ligands.

Organophosphorus compounds preferentially extract via the mechanisms represented by eqns. (1.22) and (1.24).

1.8   Scope of Chemistry Experiments

Previous transactinide experiments with the chloride, bromide and fluoride complexes of dubnium (see Chap 1.5 for a summary) have shown that dubnium is a member of group V and exhibits chemical behavior that is more similar to niobium and protactinium (Pa) than to tantalum. However, the experiments were usually performed in mixed acid media and/or under conditions under which equilibrium was not assured, making interpretation of the results difficult. It is preferable to concentrate on chemical systems that demonstrate selectivity between the members of one group of the periodic table, yield information regarding complex formation and reach equilibrium within a known time.

1.8.1   *Requirements for Transactinide Chemistry*

Systems that are suitable for studying transactinide elements must fulfill three main requirements. First, transactinide elements are produced solely through the use of nuclear reactions, typically with cross sections on the order of nano- to picobarns. For dubnium, this yields only a few atoms per hour, requiring one atom-at-a-time chemistry as the dubnium atom will only interact with atoms of its surroundings and not with other dubnium atoms. To obtain reproducible results, it is necessary to choose systems in which the dubnium atom undergoes the same chemical reaction multiple times. Liquid-liquid extraction is an example of such a system and has been used successfully to study transactinides [Schädel2003].   Second, a large excess of un-reacted beam, fission fragments and transfer products from reactions with the target or target backing are also created in the nuclear reactions in addition to the few atoms of interest. To study differences in chemical behavior of the transactinide and its homologues, the use of a physical preseparator to separate the element of interest from the transfer products and un-reacted beam is required prior to the chemistry set-up. Third, ^{262}Db, with a half-life of 34 s, is the longest lived isotope of dubnium that has been confirmed in independent experiments. It is therefore mandatory for the system to reach equilibrium within 10 seconds, to ensure that chemistry is completed before a majority of the dubnium atoms have decayed.

In this dissertation, the extraction of niobium and tantalum, the lighter homologues of dubnium, from HCl and mixed HCl/LiCl solutions was studied for a variety of acid concentrations and organic extractants. The goal of the experiments was to find a system under which niobium and tantalum exhibited different chemical

behavior, and that the differences in chemical behavior gave indications as to complex formation and speciation. Initially, experiments were performed using long-lived isotopes of niobium and tantalum. However, in order to best replicate conditions under which dubnium will be studied, on-line experiments using short-lived accelerator-produced isotopes of niobium and tantalum were also performed.

2   Experimental

Part I: Cold Fusion Production and Decay of Neutron Deficient Isotopes of Dubnium

2.1   The Berkeley Gas-filled Separator (BGS)

The experiments described in this dissertation were performed at LBNL using the Berkeley Gas-filled Separator (BGS), which has been described extensively before [Düllmann2006; Folden III2004a; Gregorich2003; Gregorich2005; Loveland2002]. The BGS employs a series of three magnets to provide physical separation of complete-fusion-evaporation products of nuclear reactions from unreacted beam, transfer reaction products and other unwanted reaction products. In these experiments, beams of $^{51}V^{11+}$, $^{50}Ti^{12+}$ and $^{18}O^{4+}$ were accelerated by the LBNL 88-Inch Cyclotron. The beam then passed through a series of focusing magnets and a collimater prior to the BGS. At the entrance to the BGS, the beam passed through a 45-$\mu g/cm^2$ thick carbon (C) window that serves to separate the vacuum of the beam line from the 67-Pa helium (He) gas inside the BGS.

2.1.1 Targets

After passing through the carbon window, the beam traverses through ~1 cm of He fill gas before encountering the target. The BGS is designed for the use of two different types of targets, rotating and stationary, both of which were used in this work.

The rotating targets consisted of nine arc-shaped targets on the periphery of a 14-inch diameter wheel; a ^{238}U target wheel is shown in Fig. 2.1 for example. These targets were rotated at ~10 s^{-1}, which reduced the heat load on any one spot and allowed for the use of high intensity beams (0.3 to 0.8 particle-μA in this work). In these experiments, rotating targets of ~470-μg/cm^2 metallic lead (98.4% ^{208}Pb, 1.1% ^{207}Pb and 0.5% ^{206}Pb) and ~441-μg/cm^2 ^{209}Bi were used. Both targets were deposited on a 35-μg/cm^2 ^{nat}C backing. This backing supported the target during production and was placed upstream of the targets during irradiations. The ^{208}Pb target was also covered with 5 – 10 μg/cm^2 ^{nat}C to decrease losses of target material due to sputtering and allow for radiative cooling.

The lighter homologues of dubnium (niobium and tantalum) were produced in nuclear reactions using stationary targets, as these reactions had much higher production rates and thus required lower intensity beams. These targets consisted of 20-mm diameter foils on a telescoping arm that allowed for quick switching between different target types. Targets of 586-μg/cm^2 self-supporting ^{124}Sn and 384-μg/cm^2 ^{74}Se, deposited on 40-μg/cm^2 C and covered with 5-μg/cm^2 Au were used. Since the targets were stationary, the heat load on the irradiated section was increased. Thus, maximum beam intensities were limited to 25 – 75 particle-nA.

Fig. 2.1: Sample target wheel.

2.1.2   Magnets

In addition to the atoms of interest, a large excess of un-reacted beam, fission fragments and transfer products from reactions with the target or target backing are also created in the nuclear reactions. Separation of the wanted from the unwanted reaction products was achieved in the BGS using the principle of magnetic rigidity. When charged particles encounter a magnetic field perpendicular to the direction of motion, they will curve according to the Lorentz force vector. In scaler terms this is $F = qvB$ where q is the charge on the particle, v is the velocity of the particle and B is the magnetic field. The Lorentz force must also be equal to the centripetal force on the particle, $F = mv^2/\rho$, where m is the mass of the particle and ρ is the radius of curvature of motion. Solving these two equations for magnetic rigidity, the products of field strength and

radius, gives $B\rho = mv/q$. The radius of curvature in the BGS is fixed by design. Thus, by varying the magnetic field, different magnetic rigidities can be selected.

To achieve separation, the BGS employs three magnets: quadrupole (Q1), gradient field dipole (M1) and flat field dipole (M2). A schematic of the BGS is shown in Fig. 2.2 and a picture of the BGS as seen from the target box is shown in Fig. 2.3. The quadrupole magnet is located directly downstream of the target and serves to vertically focus the reaction products at the expense of horizontal focusing. The increased vertical focusing results in an increased acceptance cone to 45 msr of 4π. However, as the only focusing magnet is directly after the target, the image at the focal plane has a large horizontal and vertical distribution. To achieve maximum acceptance in the BGS, the vertical spread of the entrance cone is over focused beyond Q1. This results in a magnification of the initial vertical image by a factor of -7. In the horizontal plane a two-centimeter distance corresponds to 1% difference in magnetic rigidity.
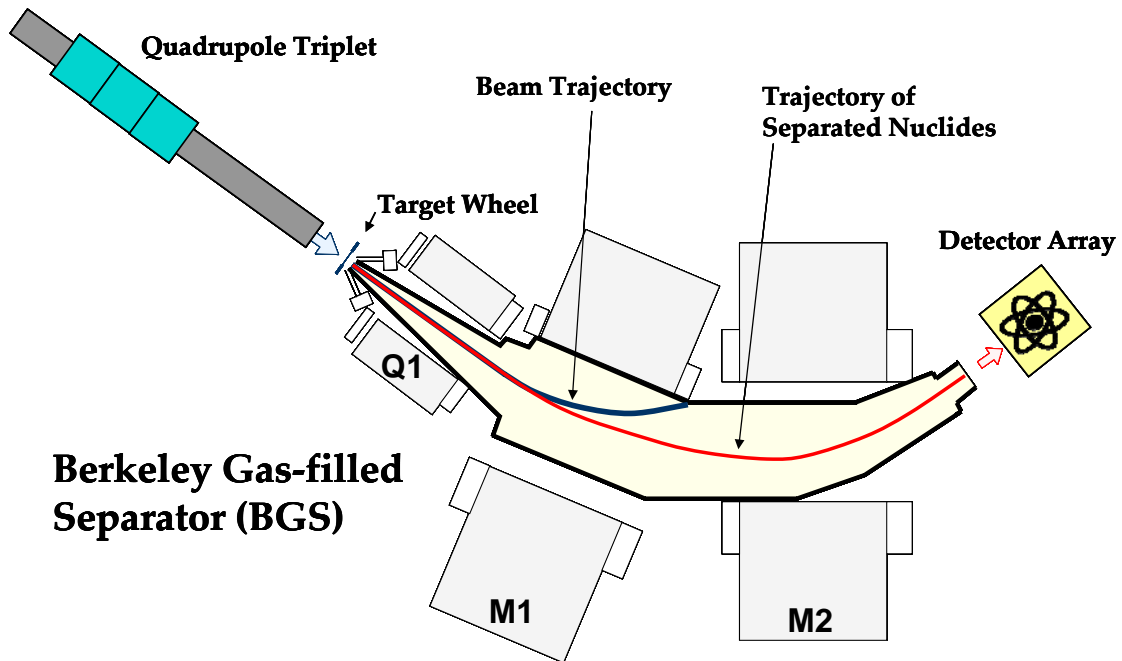
Fig. 2.2: Schematic of the BGS. The blue line shows the path of the beam while the red line indicates the path of the separated EVRs.

After being focused by the quadrupole magnet, beam and reaction products enter the gradient-field dipole and then the flat-field dipole magnets. The actual separation of beam and unwanted reaction products from wanted reaction products occurs in the dipole magnets based on their differing magnetic rigidities in 0.5-torr He gas.
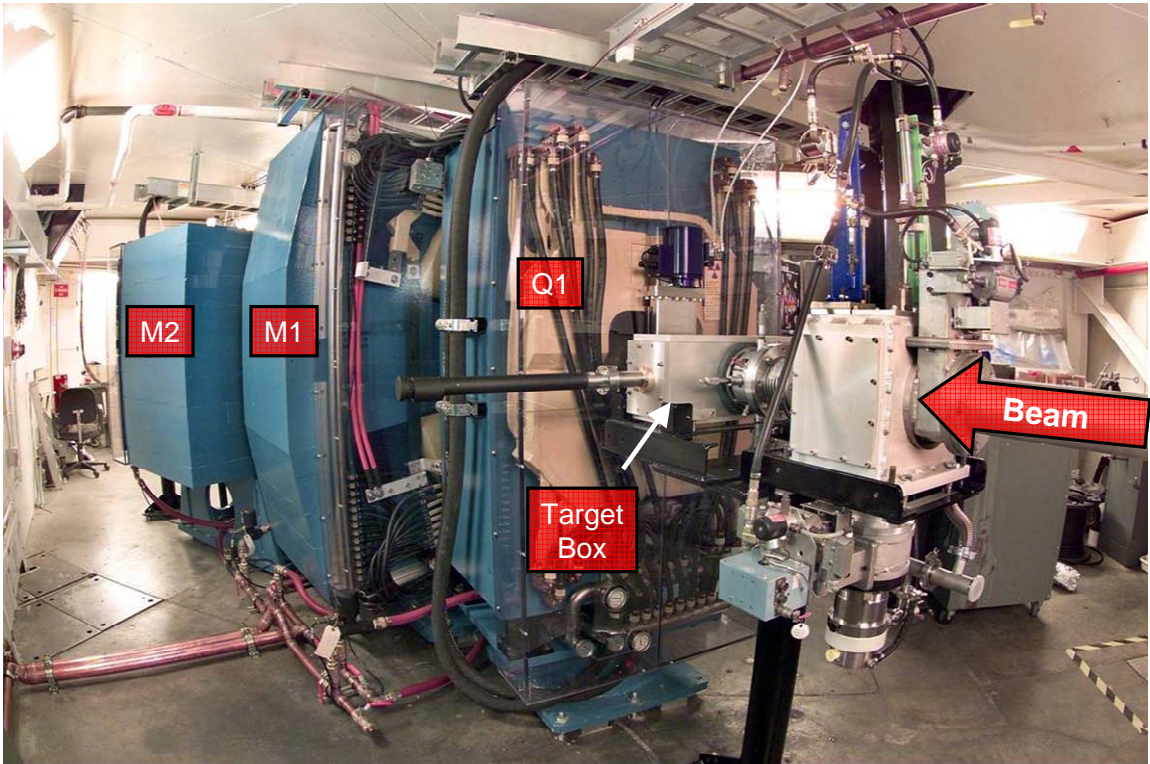
Fig. 2.3: Picture of the Berkeley Gas-Filled Separator (BGS). The beamline, target chamber and magnets have been labeled for clarity.

2.1.2.1 Magnetic Rigidities in Helium

The magnetic rigidity of heavy ions passing through dilute He gas has been measured by Ghiorso *et al*. [Ghiorso1988]. This study showed a general trend of $\bar{q} \propto v Z^{1/3}$, where $\bar{q}$ is the average charge, v is the ion velocity and Z is the atomic number of the ion. However, as can be observed in Fig. 2.4, there are significant

deviations from the trend due to electronic shell effects of the stripped ions. Gregorich *et al.* measured the magnetic rigidity of ions with Z = 99 – 111 in the BGS. Together with data from [Ghiorso1988], they made a global fit to the average charge in He gas, after including a sinusoidal correction for the shell structure of the stripped ion [Gregorich2005]. The sinusoidal correction is based on an estimate of the number of electrons, Z-(mx+b) remaining on the ion. It has an amplitude, d, of approximately half of a charge unit and a period of 32, the length of the sixth and seventh rows of the periodic table. There is an ascending node, f, at about halfway through the 5d electron shell:
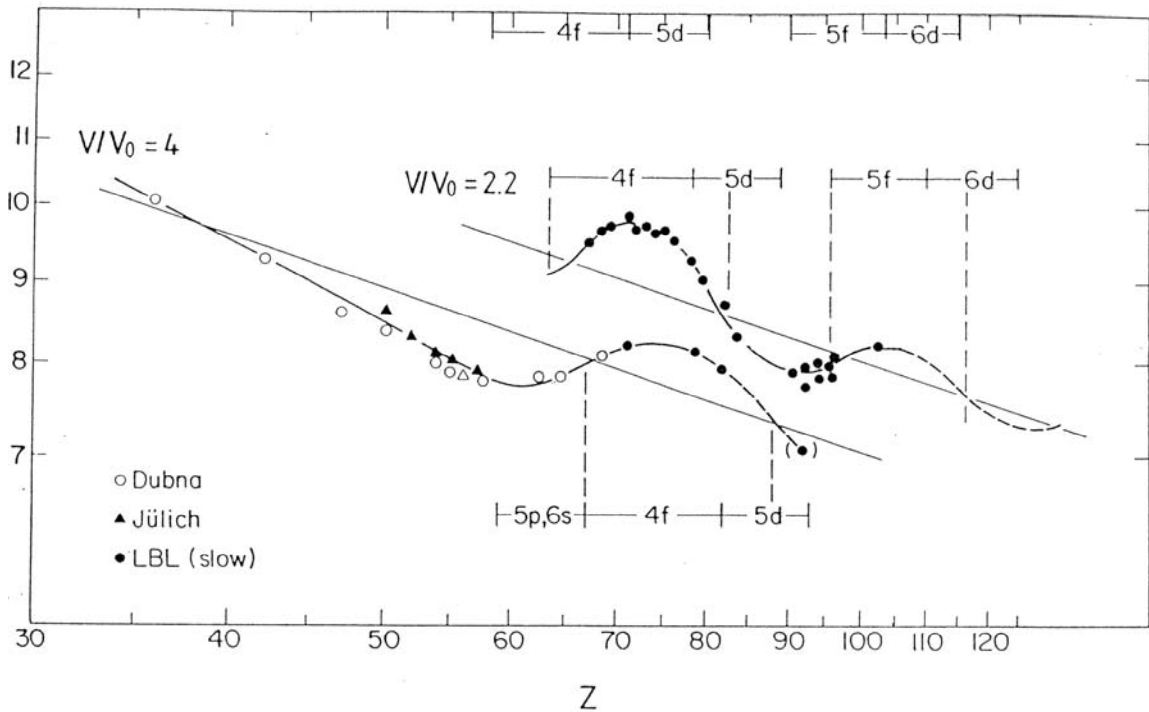
Fig. 2.4: Experimental values for Bρ/A as a function of the atomic number, Z, of the ions. The straight lines are fits to the data points to show the trend of $\sim Z^{-\frac{1}{3}}$ and are meant to guide the eye only (adapted from [Ghiorso1988]).

$$\bar{q} = mx + b + d \cdot \sin\left\{\frac{2\pi}{32}[Z - (mx + b) - f]\right\} \tag{2.1}$$

$$x \equiv \frac{\upsilon}{\upsilon_0} Z^{\frac{1}{3}} \qquad \text{for } Z >\approx 45$$

where $\upsilon_0 = 2.1866 \times 10^6$ m/s is the Bohr velocity and $mx + b$ shows the linear $\upsilon Z^{\frac{1}{3}}$ trend. A best fit to the data was obtained when $m = 0.641$, $b = -0.235$, $d = 0.517$ and $f = 74.647$ [Gregorich2005]. Fig. 2.5 shows the fit to the data after subtracting the sinusoidal correction from the average charge state.
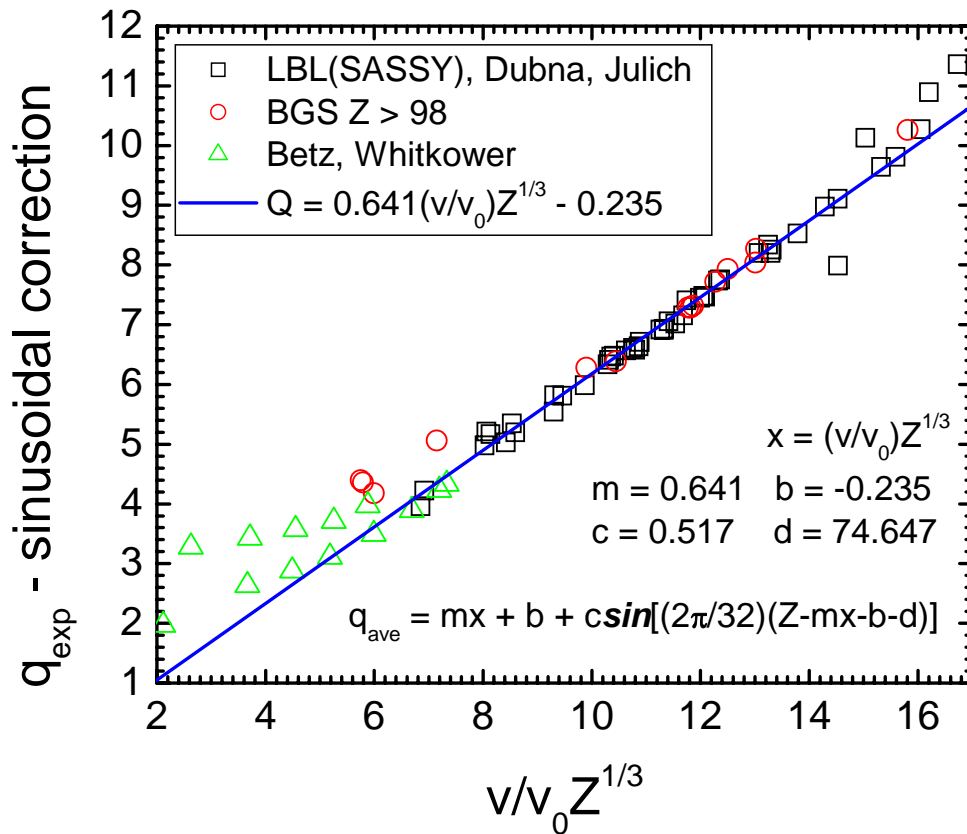
Fig. 2.5: Average charges of heavy ions passing through dilute He gas. The y-axis shows the experimental average charges, with the sinusoidal correction for the electronic shell structure of the stripped ions removed. The best fit is indicated by the solid blue line (adapted from [Gregorich2005])

The field produced in the BGS is set by the expected mean charge state, $\overline{q}$, of the reaction products of interest. The following equations give the currents as a function of the magnetic rigidity of the reaction products and the desired ratio R = I(M2)/I(M1). R was determined experimentally to be 1.69.

$$I(Q1) = (795 A T^{-1} m^{-1}) B\rho \qquad (2.2)$$

$$I(M1) = \frac{B\rho}{0.002467 + 0.002016R} A \cdot T^{-1} \cdot m^{-1} \qquad (2.3)$$

$$I(M2) = \frac{B\rho}{\dfrac{0.002467}{R} + 0.002016} A \cdot T^{-1} \cdot m^{-1} \qquad (2.4)$$

2.1.3   Focal Plane Detector

After separation in the BGS, the recoils passed through a multi-wire proportional counter (MWPC) and were implanted into a focal plane detector (FPD). The MWPC was located ~23 cm upstream of the FPD and consisted of two 0.9-μm thick Mylar windows isolating an isobutane fill gas from the He of the BGS. The isobutane was held at a pressure of 0.5 kPa above the BGS pressure. An EVR passing through the MWPC (biased at +400-500 V) initiated a process of charge multiplication that was collected by electrodes at the top, bottom, left and right sides of the MWPC. A signal in the MWPC started the time-to-amplitude (TAC) converter that was stopped with a signal in the FPD. This TAC signal between the MWPC and the FPD allowed for differentiation between implantation events and decays within the FPD.

The FPD was comprised of an implantation detector and an upstream detector [Folden III2004b; Gregorich2005]. This is shown in Fig. 2.6. The implantation detector consisted of three silicon cards, each containing 16 vertical strips that allowed for

36

determination of the horizontal position. Energy was calibrated using a four-point α source containing ^{148}Gd, ^{239}Pu, ^{241}Am and ^{244}Cm. The α lines had a FWHM of 70 keV. The vertical position was determined by resistive charge division of the charges collected at the top and bottom of each strip [Alberi1976]. Position resolutions were calculated using standard error propagation methods and are nearly proportional to 1/Energy. At the 1σ level, position resolutions were 0.24 – 0.35 mm over 9.4 – 7.0 MeV.
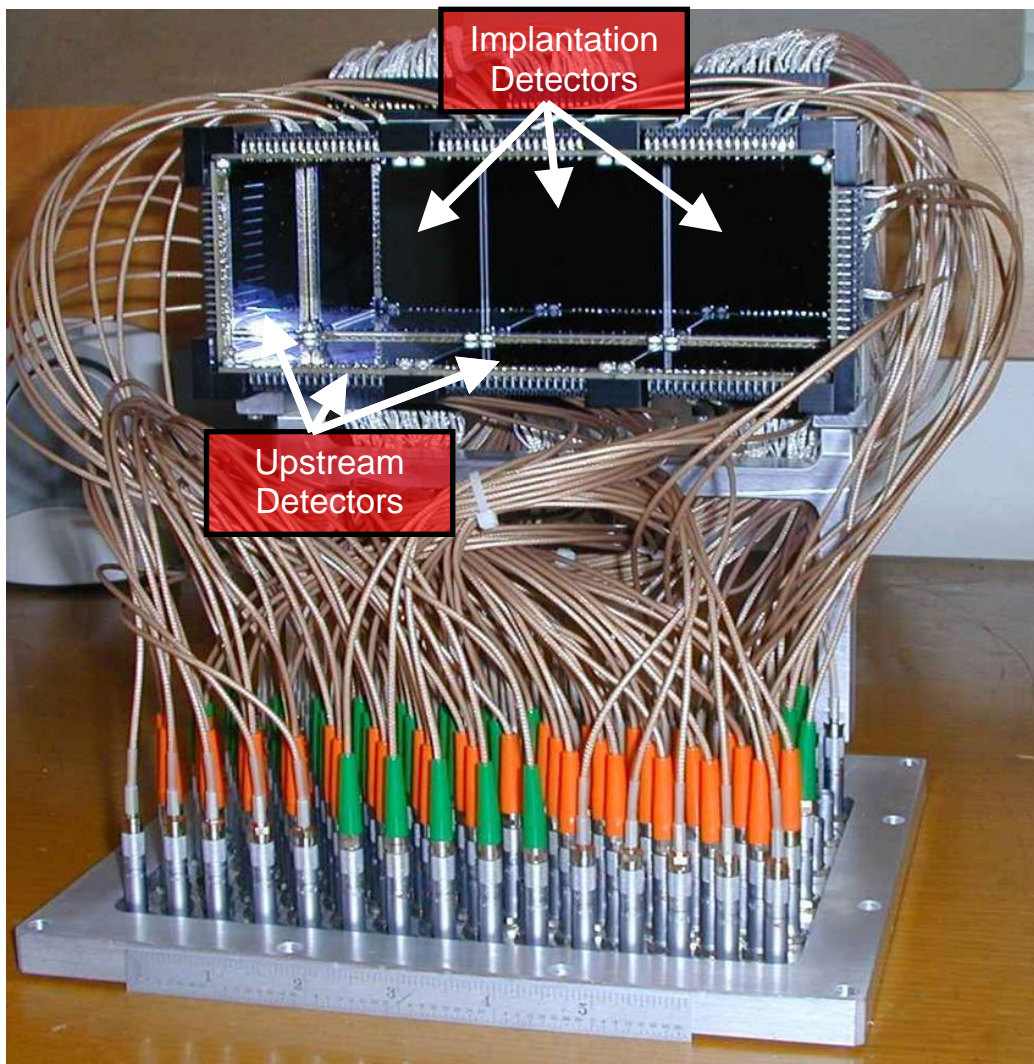
Fig. 2.6: Focal Plane Detector. The implantation detectors and sample upstream detectors are labeled for clarity.

To discriminate decay-like events (events anti-coincident with a signal from the MWPC) from signals due to light and low-ionizing particles, which deposit a similar amount of energy in the FPD, three silicon cards were mounted directly behind the implantation detector. A signal in any of the 'punch-through' detector strips indicates light and low-ionizing particles.

Eight additional silicon cards were mounted perpendicular to, and upstream of, the implantation detector. These 'upstream' detectors allowed for greater efficiency in detecting α particles and spontaneous fission (SF) fragments escaping from the implantation detector. The efficiency for detecting α particles was ~76% of 4π: 51% of all α particles deposit their full energy in the implantation detector. An additional 25% of α particles lose a fraction of their energy in the focal plane detector and hit an upstream detector. Their full energy can thus be reconstructed by summing the signals in both the implantation and upstream detectors [hereafter, all events depositing their full energy in the FPD (implantation detector only or split between the implantation and upstream detectors) are referred to as "full energy α's"]. Of the remaining 24% of all α particles, 16% escape out of the front of the detector box at an angle nearly normal to the focal plane, depositing less than 300 keV in the focal plane detector. As the deposited energy necessary to trigger the Multi-Branch System (MBS) data acquisition system [Essel2000] ranges from 200 keV at the top and bottom of the strips to 500 keV at the center, no information was recorded for ~16% of α-decays. Finally, about 8% of all α particles escape out of the front of the detector box but lose sufficient energy to trigger the data acquisition system (hereafter, such events are referred to as "escape α's").

2.1.4   Cross Section Measurements and Rutherford Scattered

Particles

The cross section, σ, of a reaction is a function of the beam intensity, *I*, and target

thickness, *N*, and the rate, *R*, at which reaction products appear [Krane1988]:

$$\sigma = \frac{R}{I \cdot N} \qquad (2.5)$$

For the reactions in this dissertation, *I·N* was measured by the detection of

Rutherford-scattered particles that are produced when the beam encounters the high

charge of the target nucleus. The Rutherford-scattered particles were detected by two

PIN diode detectors located at ±27° from the beam axis. To reduce damage due to

radiation, the particles were first attenuated by passing through four wire grids with a

total scaledown factor of (1348 ± 20) [Folden III2004a] and then a 0.188-in diameter

circular collimator. The distance between the detectors and target was 292 mm.

Since the Rutherford detectors were held at a fixed angle with regard to the beam,

the differential Rutherford scattering cross section, $d\sigma/d\omega$, must be taken into account.

For reactions in which the mass of the projectile, A_p, is less than the mass of the target,

A_t, $d\sigma/d\omega$ can be approximated by [Segrè1977]:

$$\frac{d\sigma}{d\varpi} = \left(\frac{e^2 Z_p Z_t}{2 \cdot \mathrm{ELab}} \right)^2 \sin(\theta)^{-4} \frac{\left[\cos(\theta) + \left(1 + \frac{A_p^2}{A_t^2} \sin(\theta)^2 \right)^{0.5} \right]^2}{\left(1 - \frac{A_p^2}{A_t^2} \sin(\theta)^2 \right)^{0.5}} \qquad (2.6)$$

where Z_p and Z_t are the atomic number of the projectile and target, respectively,

and θ is the laboratory frame angle of the Rutherford detectors.

For a given irradiation, the number of Rutherford-scattered particles observed, N_{Robs}, $d\sigma/d\omega$, and the solid angle subtended by the Rutherford detectors, Ω, can be used to determine the luminosity, $Nt\phi t$, or number of events expected per unit cross section, of the experiment:

$$Nt\phi t = \frac{N_{Robs} \cdot scaledown}{\frac{d\sigma}{d\varpi} \cdot \Omega} \qquad (2.7)$$

The actual cross section for a specific energy must take into account the efficiencies for detecting events, ε_{det}, the efficiency of the BGS, ε_{BGS}, the number of events observed, N_{obs} and the luminosity of the experiment:

$$\sigma = \frac{N_{obs}}{\varepsilon_{BGS} \cdot \varepsilon_{det} \cdot Nt\phi t} \qquad (2.8)$$

2.1.5　Systematic Uncertainties in Cross Sections

Systematic uncertainties in the measured cross sections at the BGS are the result of five main contributions:

i)　　An uncertainty 10% has been estimated for the transport of EVRs to the focal plane detector for the ^{48}Ca + $^{206\text{-}208}Pb$ reactions by a comparison of the size and shape of the modeled and experimental focal plane position distributions [Gregorich2005].

ii)　　the angle of the Rutherford monitor detectors is known within 0.2° with respect to the beam direction. This results in a 3% uncertainty in the Rutherford cross section, corresponding to a 3% error in the EVR cross sections.

iii)　　the uncertainty in the solid angle subtended by the collimators placed in front of the monitor detectors is dominant ed by the uncertainty in the size of the

opening and is estimated to contribute 4% to the systematic error in cross

sections.

iv)   between the target and the Rutherford monitor detectors are a series of screens

that attenuate the scattered particles. In the ^{207}Pb(^{48}Ca,2n)^{253}No reaction, the

ratio of ^{253}No EVRs in the focal plane detector to the Rutherford scattered ^{48}Ca

ions was measured with and without the attenuation screens. The uncertainty in

the attenuation factor was determined to be 5%.

v)   the systematic uncertainty in the absolute energy from the 88-Inch Cyclotron is

~1%, resulting in energy uncertainties of 0.6 - 0.8 MeV and Rutherford

scattering cross section uncertainties of 2%.

As the Rutherford detectors monitor the product of beam intensity and target thickness,

no additional error is added as a result in variations in beam intensity or target thickness.

Standard error propagation of the seven systematic contributions results in a systematic

error of ~12%.

Part II: Development of Extraction Systems for Group V Elements

2.2   Off-Line Studies

2.2.1   Production and Separation of Long-Lived Radionuclides

2.2.1.1   Separation of ^{95}Nb

Carrier-free ^{95}Zr ($t_{\frac{1}{2}}$ = 64.02 d, 100% β^-) was obtained from Isotope Products as ^{95}Zr oxalate in 0.5 M oxalic acid (500 µCi in 5 mL). The decay product of ^{95}Zr is ^{95}Nb ($t_{\frac{1}{2}}$ = 34.975 d, 100% β^-), resulting in the production of carrier-free ^{95}Nb.

To separate the ^{95}Nb from the ^{95}Zr parent, 2 mL of the solution were placed in a centrifuge cone. To this, 1 mL lanthanum nitrate [La(NO$_3$)$_3$] solution (10 mg/mL lanthanum) and ~250 µL ammonia (NH$_3$) were added, allowing for co-precipitation of the lanthanum, niobium and zirconium. The sample was then centrifuged for 10 min and the resulting supernatant was removed. This supernatant was then assayed for radioactivity. If radioactivity was found, the precipitation step was repeated. The precipitant was then washed with 2 mL H$_2$O before being re-dissolved in 12 M HCl.

The lanthanum, zirconium and niobium were separated using a Dowex AG 1x8 anionic exchange resin (20 – 50 mesh). The column was ~65 mm high and 4-5 mm wide and had a free column volume (FCV) of 10 drops. This column was rinsed with H$_2$O until neutral and then equilibrated with ~3.5 mL 12 M HCl. The HCl solution containing lanthanum, zirconium and niobium was then added onto the column and washed with three FCV's of 12 M HCl. The ^{95}Zr and ^{95}Nb were then eluted using two elutions with

2 M HCl, the first having a volume of 3 mL and the second 2 mL. The column was then washed with 3 mL H_2O to elute the remaining activity. All fractions were collected and assayed using high purity germanium γ-ray detectors (HPGe).

The separated ^{95}Nb was evaporated to dryness and then re-dissolved in 12 M HCl. After assaying the solution using a HPGe, it was estimated that the amount of ^{95}Nb present in the samples was 10^{-10} M. A 10^{-6} M niobium tracer solution was also made by evaporating the ^{95}Nb tracer to dryness and then re-dissolving the ^{95}Nb in a mixture of 12 M HCl and 10^{-6} M $NbCl_5$.

2.2.1.2   Production and Preparation of ^{182}Ta

^{182}Ta ($t_{1/2}$ = 114.43 d, 100% β-) was produced through neutron irradiation of ^{nat}Ta (99.988% ^{181}Ta) powder at Oregon State University. The cross section for the reaction ^{181}Ta(n,γ)^{182}Ta is ~20.5 b for thermal neutrons [Sears1992]. Given an average neutron flux of 7 x 10^{-14} cm^2s^{-1} [Loveland2005], after a 12 hr period of irradiation, 6.2 x 10^{-4} % of the sample would be in the form of activated ^{182}Ta, while the remainder would be ^{nat}Ta.

After irradiation, the tantalum powder was dissolved in 2 mL of concentrated hydrofluoric acid (HF). From this solution, 100 - 150 μL aliquots were periodically taken and evaporated to dryness. The resulting residue was then dissolved in ~50 μL of saturated boric acid [$B(OH)_3$] to destroy the remaining fluoride. The $B(OH)_3$ solution was evaporated to dryness and re-dissolved in 12 M HCl. This solution was then evaporated to dryness an additional time and re-dissolved in 12 M HCl. It was estimated that the concentration of tantalum in the solution was 10^{-6} M, based on irradiation time and HPGe assays of the solution.

2.2.2   Extraction Procedure

For the off-line chemistry, four milliliters of organic phase was contacted with four milliliters of aqueous phase in a 15 mL plastic centrifuge vial (VWR). 10 – 20 µL of tracer containing either ^{95}Zr/^{95}Nb or ^{182}Ta in concentrated HCl was added to the solution. The phases were mixed using a vortex mixer for 10 - 90 seconds and then centrifuged. Three milliliters each of the organic phase and of the aqueous phase were removed and both samples were counted using the same HPGe. Five parallel experiments were performed for each acid concentration or mixing time. Extraction yields were determined using:

$$E(\%) = \frac{[Me]_{org}}{[Me]_{org} + [Me]_{aq}} \times 100 \qquad (2.9)$$

where E(%) is the percentage of the metal ions in the organic phase and $[Me]_{org}$ and $[Me]_{aq}$ refer to the concentration of metal in the organic and aqueous phases, respectively. Relative metal concentrations in each phase were determined by the γ-ray activity in each sample. Final values for the extraction yield at each set of conditions were determined by taking a weighted mean of the values for the five samples. The error was determined from the statistical counting uncertainty using standard error propagation techniques and the results are reported at the one sigma level. Due to the long half-lives of the isotopes (>30 days) and the comparatively short counting times (<12 hours), no correction of the data due to decay loss was required.

2.3   *On-Line Studies*

2.3.1   Production and Pre-separation of Short-Lived Isotopes

On-line experiments were performed at the 88-Inch Cyclotron at LBNL. Short-lived ^{170}Ta ($T_{1/2}$ = 6.76 m) was produced in ^{124}Sn(^{51}V,5n) reaction. The ^{74}Se(^{18}O,p3n) reaction was used for the production of ^{88g}Nb ($T_{1/2}$ = 14.5 m). Laboratory-frame center-of-target beam energies were 215.0 MeV for ^{51}V^{11+} and 68.9 MeV for ^{18}O^{4+}.

The ^{51}V or ^{18}O beam passed through a (40-45)-μg/cm^2 carbon vacuum window at the entrance to the BGS and a negligible amount of helium gas before entering the target. For the production of ^{88g}Nb, a target of 384-μg/cm^2 ^{74}Se, deposited on 40-μg/cm^2 C and covered with 5-μg/cm^2 Au, was used. The typical beam intensity of the ^{18}O^{4+} projectiles was 75 particle·nA. A 20-mm diameter self-supporting 586-μg/cm^2 ^{124}Sn target was used for the production of ^{170}Ta, with typical ^{51}V^{11+} beam intensities of 25 particle·nA. The niobium and tantalum EVRs recoiling out of the target were separated in the BGS from the beam and almost all unwanted reaction products based upon their differing magnetic rigidities in the 67-Pa He of the BGS [Gregorich2000; Ninov1998]. The magnetic rigidity for the niobium and tantalum EVRs were estimated as previously described [Gregorich2005] and experimentally determined to be 0.95 and 1.59 T·m, respectively.
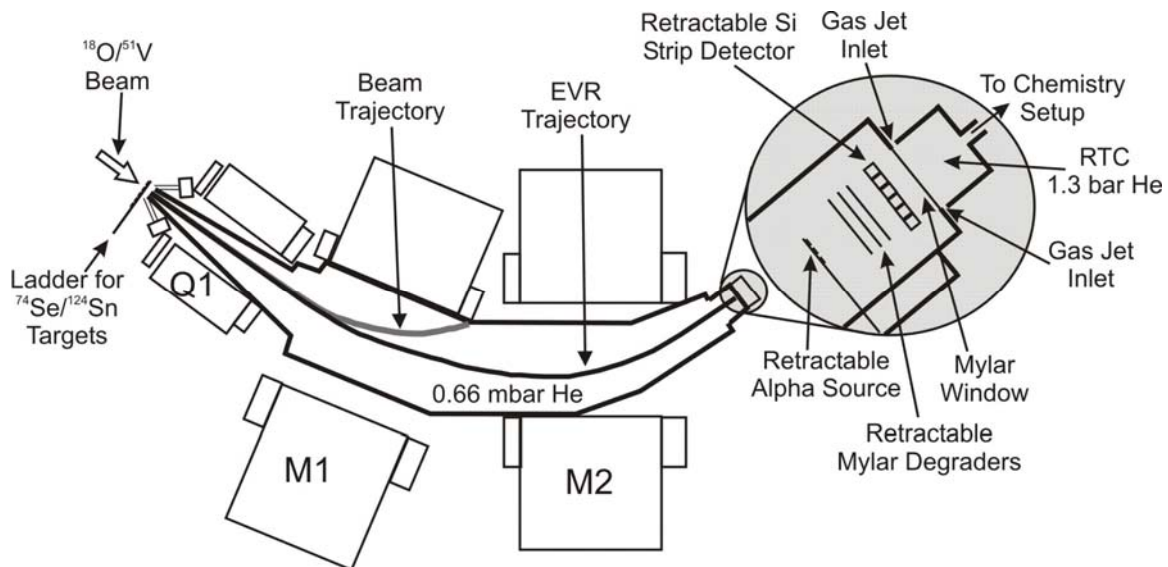
Fig. 2.7: Schematic of the BGS at LBNL in the configuration required for chemistry experiments with preseparation. Modified from [Düllmann2005].
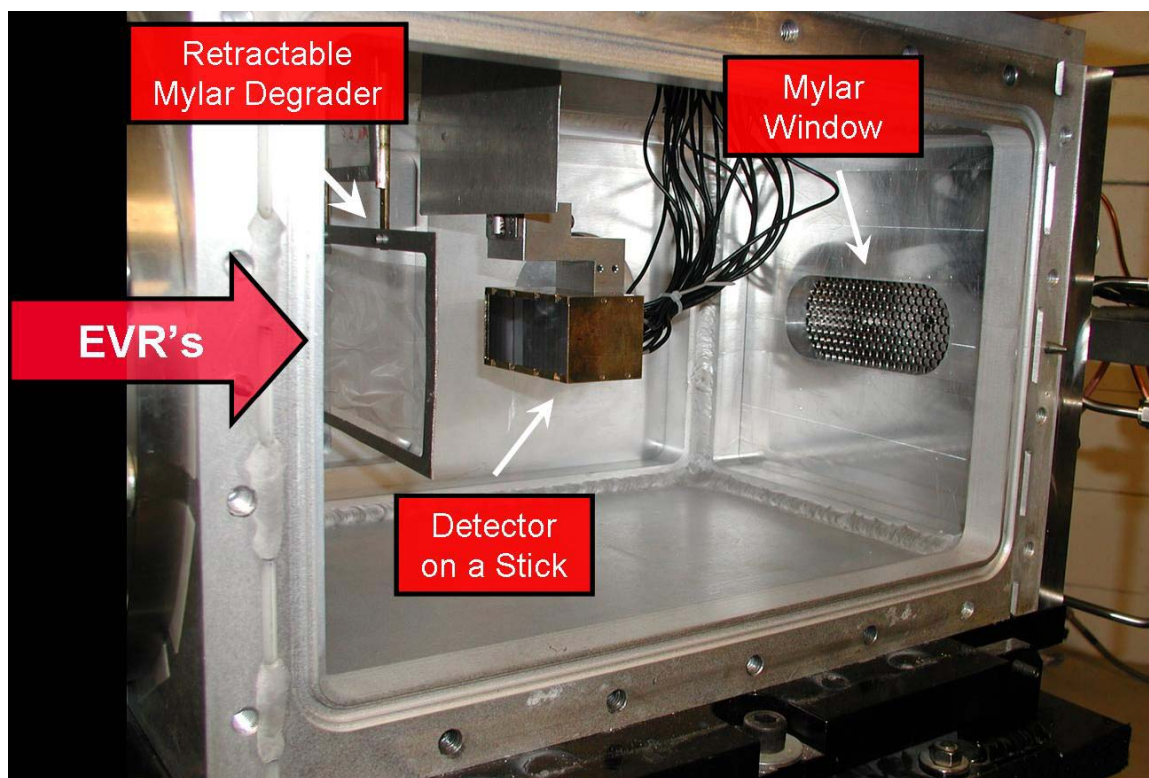
Fig. 2.8: View of the inside of the detection chamber after modification allowing for use of the RTC.

2.3.2   The Recoil Transfer Chamber (RTC)

For the chemistry experiments, the MWPC and FPD used in Chap. 2.1.3 was removed and replaced by a Recoil Transfer Chamber (RTC) [Kirbach1999]. Fig. 2.7 contains a schematic of the modified experimental setup. The inside of the detection chamber, with the FPD removed and the RTC attached, is shown in Fig. 2.8. The figure shows the placement of the mylar degraders and the mylar window at the entrance to the RTC that serves to separate the 67-Pa He in the BGS from the 1.3 bar He in the RTC. Also included in the figure is the retractable detector-on-a-stick (DoS) that allows for centering of the EVR's. The DoS consists of two silicon chips, identical to those used for the FPD (as described in Chap. 2.1.3). The position of EVRs recoiling into the RTC can be determined by placing the DoS in front of the RTC window. A view of the RCT from the outside is shown in Fig. 2.9.
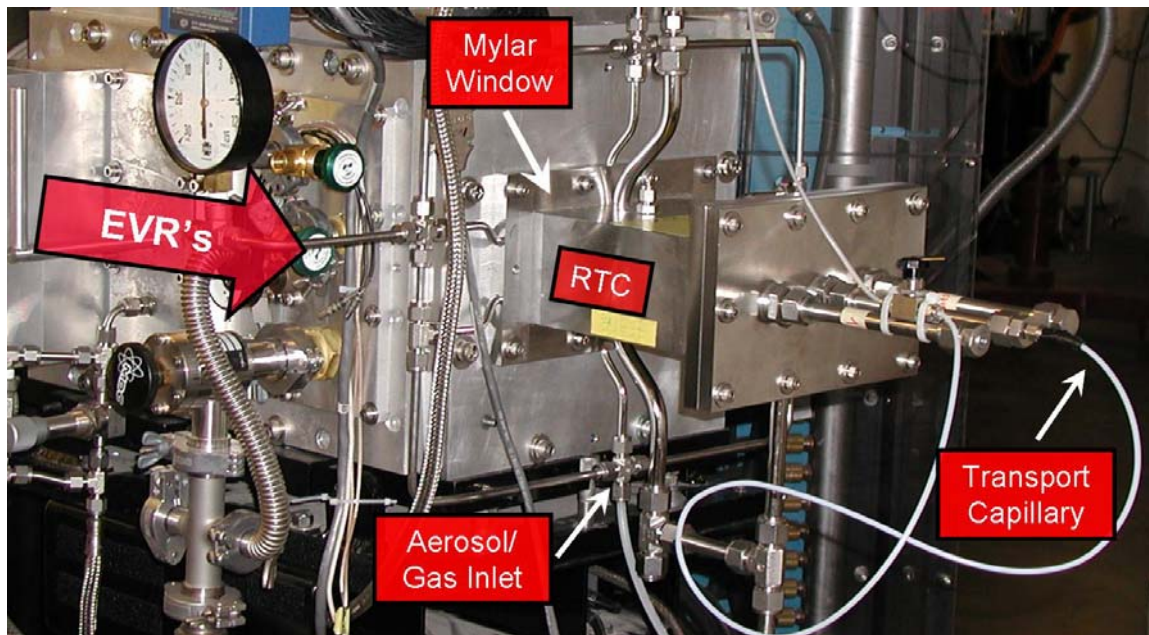
Fig. 2.9: View of the RTC from the outside.

After traveling through the BGS, the recoiling atoms were slowed down by passing through a 3.3-µm Mylar window at the entrance to the 40-mm-deep RTC [Kirbach2002; Kirbach1999]. The EVRs were then thermalized in approximately 1.3 bar of helium gas in the RTC. Due to the larger momentum of the ^{51}V beam, the tantalum EVRs have a larger kinetic energy than the niobium EVRs. To account for this, the tantalum EVRs were degraded by passing through an additional 6.0-µm thick retractable Mylar foil prior the RTC window, to ensure that they were thermalized in the RTC.

2.3.3   Chemistry Procedure

Helium gas at flow rates of 1.6 - 1.8 L/min was seeded with KCl aerosols prior to entering the RTC. The KCl aerosol particles were produced in an oven at a temperature of 650 ºC. After thermalization in the RTC, the EVRs were captured on the aerosols and transported through a 2-mm i.d. and ~20 meter long stainless steel capillary to the chemistry setup. The transport efficiency of the gas-jet system was determined to be ~70% in separate experiments [Düllmann2005].

The aerosol particles containing the EVRs were deposited on small platinum foils at the exit of the gas-jet capillary using the apparatus shown in Fig. 2.10. At the collection apparatus, the helium stream seeded with the KCl aerosols emerges into a broad cone into vacuum via supersonic expansion. The aerosols are slower than the helium and emerge in a narrower cone, allowing them to deposit on the platinum foils.
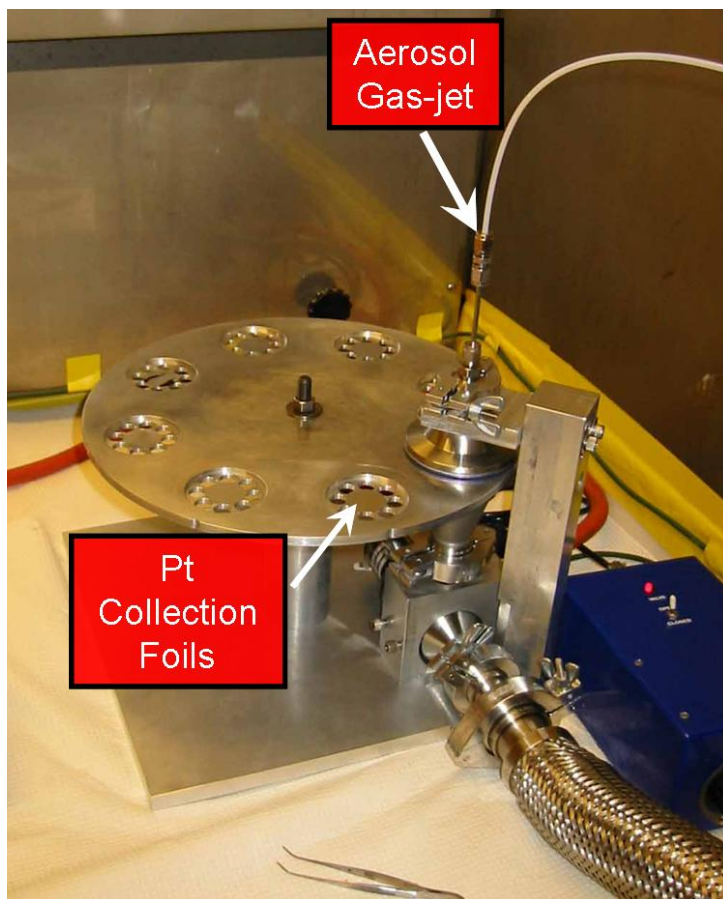
Fig. 2.10: Apparatus for collecting aerosol particles.

The aerosols were allowed to collect for 10 minutes and then the collected KCl was dissolved in 100 μL of HCl or solutions of HCl and lithium chloride (LiCl). The solution was then transferred to a centrifuge cone containing an additional 3900 μL of the same acid solution. The amount of niobium and tantalum transferred into the 4000 μL aqueous phase from the aerosol residue was determined to be ~10^{-18} moles, giving a metal concentration of 10^{-16} M in the aqueous phase prior to mixing. An equal volume of 0.01 M HDEHP or 0.01 M BEHP in chloroform was added to the aqueous solution and the two phases were mixed for up to 90 s using a vortex mixer. The samples were centrifuged for 20 seconds and a 3 mL aliquot of each phase was removed for assay.

49

To minimize the effect of variations in sample geometry and detector efficiency, both aliquots were assayed using the same HPGe γ-ray detector. The first sample measured was usually the aliquot containing the smaller fraction of niobium or tantalum to minimize statistical error due to decay. Each aliquot was counted for 4 minutes with a 15 seconds interval allotted for changing the samples. Due to the short half-lives of the nuclides, the data obtained from the second aliquot measured had to be corrected for decay. Five experiments were performed for each acid concentration or mixing time. Extraction yields were also determined using eqn 2.9. Relative metal concentrations in each phase were determined by the γ-ray activity in each sample. Final values for the extraction yield at each set of conditions were determined by taking a weighted mean of the values for the five samples. The error was determined from the statistical counting uncertainty using standard error propagation techniques and the results are reported at the one sigma level.

To determine the role that adsorption to the surface of the vial played, the yield of niobium and tantalum for each trial was normalized based upon the integrated beam current. The yield values were then corrected for the volume of the aliquot that was counted and the decay of the isotopes during chemistry and measurement of the two samples. These values were compared to a series of trials in which the aerosol was dissolved directly into 3.0 mL of an aqueous phase and subsequently counted, without chemistry being performed. The amount niobium or tantalum observed in each sample comprised ≥95% of the expected activity.

2.4   *Materials*

Bis(2-ethylhexyl) hydrogen phosphate (HDEHP, 97%) bis(2-ethylhexyl) hydrogen phosphite (BEHP, 96%), 2-ethylhexyl hydrogen-2-ethylhexyl phosphonate (DEHPA, 96%) were purchased from Aldrich Chemical Company and used as received. Chloroform (ACS reagent, ≥99.8%) was obtained from Sigma-Aldrich, Inc. Diisooctyldithiophosphinic acid (DiOPA, ~85%) and lithium chloride anhydrous (Ultra >99.0%) was purchased from Fluka. The hydrochloric acid (puriss.) used for the preparation of solutions was obtained from Fluka and assayed at 37%. To determine the concentration of the acid solutions prepared from the stock HCl, aliquots of each solution were taken and bromothymol blue was added to each aliquot. The solutions were titrated with a standardized solution of 0.98 N sodium hydroxide (A.C.S. reagent grade sodium hydroxide in ASTM reagent grade I water) purchased from Aldrich Chemical Company. Actual concentrations of the HCl solutions used in both the on- and off-line chemistry experiments were the same and were determined to be 1.0, 2.9, 5.8, 8.8 and 11.1 M.

3   Production of ^{258,257}Db in the ^{208}Pb(^{51}V,x*n*)$^{259-x}$Db and ^{209}Bi(^{50}Ti,x*n*)$^{259-x}$Db Reactions

3.1   *Previous Work*

3.1.1   GSI ^{209}Bi(^{50}Ti,x*n*)$^{259-x}$Db

The ^{209}Bi(^{50}Ti,x*n*)$^{259-x}$Db reaction was initially investigated in 1985 by Heßberger *et al.* to produce the first atoms of ^{258}Db and ^{257}Db [Heßberger1985]. These experiments measured 1*n* and 2*n* excitation functions with maximum cross sections of 2.9±0.3 and 2.1±0.8 nb at excitation energies of 8.9 MeV and 16.9 MeV, respectively. More recent experiments by the same group concluded that the maximum cross sections for ^{258}Db and ^{257}Db via the same reaction are closer to 4.3±0.4 nb and 2.4±0.3 nb at excitation energies of 15.8 MeV and 22.3 MeV, respectively [Heßberger2001]. These excitation energies are more reasonable than those published in [Heßberger1985] as the threshold for the evaporation of 1 and 2 neutrons occurs at 7.8 and 15.7 MeV, respectively. In addition, the neutron leaves with some kinetic energy (usually 1 – 2 MeV). As such, the peak of the excitation function is several MeV above the threshold for neutron emission. The excitation functions measured in [Heßberger2001] are shown in Fig. 3.1. The relatively

high production rate allowed for the detailed study of the decay properties of the [258]Db and [257]Db, including the various decay modes, decay energies, and half-lives.
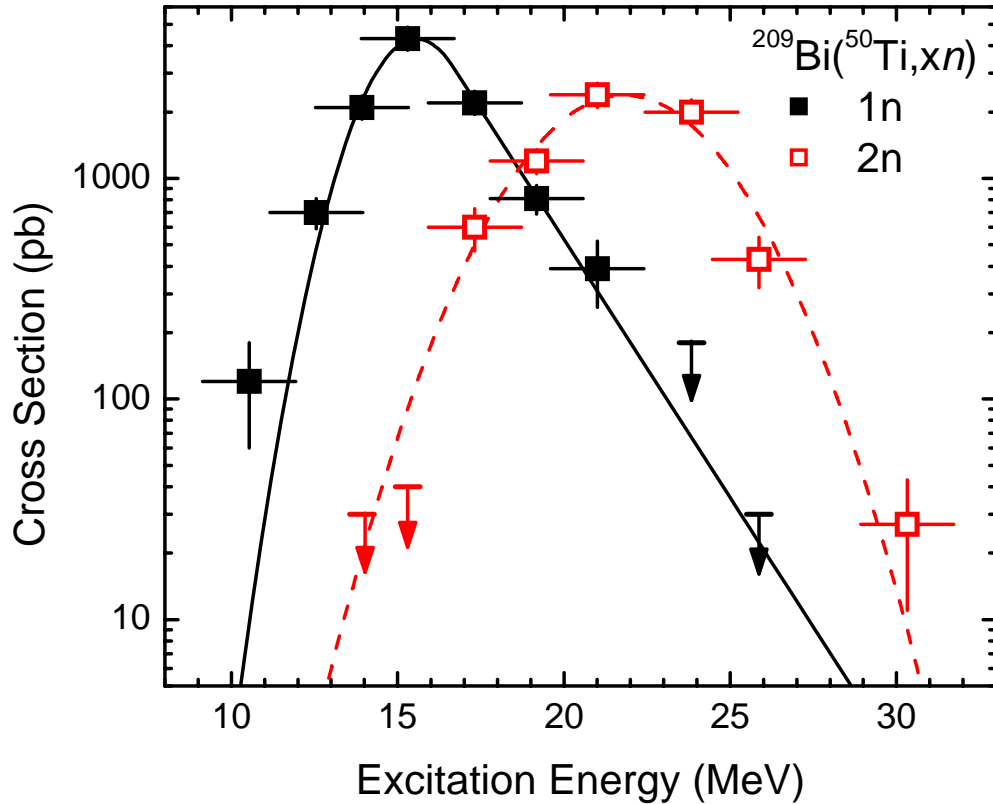
Fig. 3.1: Excitation functions obtained at GSI for the 1*n* and 2*n* exit channels of the [209]Bi([50]Ti,x*n*) reaction [Heßberger2001]. Error bars in the horizontal direction represent the spread of excitation energies through the target. Vertical error bars (shown when larger than symbols) indicate the uncertainty in cross sections due to counting statistics. The lines are Gaussian on the low energy side smoothly joined to an exponential on the high energy side and fit to the data according to the procedure described in Chap. 1.3.2 and [Dragojević2008; Gregorich2007].

3.1.2   LBNL [209]Bi([50]Ti,x*n*)[259-x]Db

The [209]Bi([50]Ti,x*n*)[259-x]Db reaction was first investigated at LBNL by J. B. Patin at the compound nucleus excitation energies of 15.0 and 17.0 MeV [Patin2002]. An upper

limit of 0.33 nb was obtained at 15.0 MeV. Ten EVR-α correlations were observed at 17.0 MeV. These correlations were assigned to the decay of ^{258}Db based on the half-life obtained from the Maximum Likelihood Decay Fits by the Simplex Method (MLDS [Gregorich1991]) code fitted to the lifetimes of the 10 correlations, leading to the conclusion that no events of ^{257}Db were observed. From these observations, a cross section of $3.1^{+1.5}_{-1.3}$ nb was determined for the 1*n* exit channel and an upper limit of 0.25 nb for the 2*n* exit channel [Patin2002].

3.1.3   LBNL ^{208}Pb(^{51}V,2*n*)^{257}Db

J. B. Patin also investigated the 2*n* exit channel of the ^{208}Pb(^{51}V,2*n*)^{257}Db reaction at an excitation energy of 24.9 MeV [Patin2002]. During this reaction, ten EVR-α and five EVR-α-α correlations were observed. From these data, the cross section was determined to be $1.4^{+0.7}_{-0.6}$ nb.

3.2   Rationale for New Experiments

To test the FBD model (as discussed in Chap. 1.3.1), the 1*n* excitation functions of coupled reaction pairs have been studied [Folden III2004b; Folden III2006; Nelson2008]. In these coupled reaction pairs, identical compound nuclei of heavy element isotopes are produced using targets and projectiles with a difference of one in their atomic number. By producing the same compound nucleus, the last term in FBD, $\frac{\Gamma_n}{\Gamma_{tot}}P_<$, is identical for the two reactions (ignoring small differences in angular momentum), allowing for the investigation of the product of σ_{cap} and P_{CN}. The more

asymmetric target-projectile combinations have smaller repulsive Coulomb forces, which are expected to result in larger cross sections because of the larger σ_{cap}.

This dissertation contains the measurement of the $1n$ and $2n$ excitation functions for the ^{208}Pb(^{51}V,xn)$^{259-x}$Db reaction. The $1n$ excitation function for the complementary reaction, ^{209}Bi(^{50}Ti,n)^{258}Db, was re-measured using the a detection setup that was identical to the one used for the ^{208}Pb(^{51}V,xn)$^{259-x}$Db reaction.

3.3   *Experimental Conditions*

Beams of ^{51}V^{11+} and ^{50}Ti^{12+} were accelerated to energies of $4.7 - 5.1$ MeV/nucleon in the Lawrence Berkeley National Laboratory's (LBNL) 88-Inch Cyclotron. Typical beam intensities were 0.3 to 0.8 particle-μA [(1.8-5.0)·10^{12} s^{-1}]. At the entrance to the BGS [Gregorich2003; Gregorich2005; Loveland2002], the beam passed through a 45-μg/cm^2 thick ^{nat}C window that serves to separate the vacuum of the beam line from the 67-Pa helium gas inside the BGS. Nine arc-shaped target segments were mounted on the circumference of a 35.6-cm-diameter wheel which was rotating at ~600 rpm and was located approximately one centimeter downstream of the entrance window. For the irradiations with ^{51}V, each target segment consisted of ~470-μg/cm^2 metallic lead (98.4% ^{208}Pb, 1.1% ^{207}Pb and 0.5% ^{206}Pb) deposited on a 35-μg/cm^2 ^{nat}C backing and covered with 5-10 μg/cm^2 ^{nat}C. The energy thickness of the lead layer on each target segment was approximately 4.5 MeV. Targets consisting of ~441-μg/cm^2 ^{209}Bi on a 35-μg/cm^2 ^{nat}C backing were irradiated with ^{50}Ti and had an energy thickness of ~3.9 MeV. Energy losses of ^{51}V through ^{nat}C and ^{208}Pb and of ^{50}Ti through ^{nat}C and ^{209}Bi were calculated with SRIM2006.02 [Ziegler2004].

Systematic uncertainty in the absolute energy from the 88-Inch Cyclotron is estimated to be ~1% [Gregorich2005]. Two PIN diode detectors located at $\pm 27°$ from the beam axis monitored the product of target thickness and beam intensity on-line by the detection of Rutherford-scattered particles. Analysis of the pulse heights of the Rutherford-scattered projectiles provided relative energies to within 0.1% for the various ^{51}V and ^{50}Ti beam energies. These resulted in ^{51}V center-of-target (COT) beam energies of 236.1, 239.7, 244.1, 247.2, 250.8 and 255.0 MeV, while the ^{50}Ti COT beam energies were 229.5, 231.8, 233.6, 236.0 and 238.4 MeV. Compound nucleus excitation energies were calculated using these beam energies with the experimental mass defects for ^{51}V, ^{50}Ti, ^{208}Pb and ^{209}Bi [Audi2003] and the Thomas-Fermi mass defects for the compound nucleus [Myers1994]. The resulting ranges of compound nucleus excitation energies within the ^{208}Pb targets were 13.1 ± 1.8, 16.0 ± 1.8, 19.5 ± 1.8, 22.0 ± 1.8, 24.9 ± 1.8 and 28.3 ± 1.8 MeV. The ranges of compound nucleus excitation energies within the ^{209}Bi targets were 13.1 ± 1.6, 15.0 ± 1.6, 16.4 ± 1.6, 18.3 ± 1.6 and 20.6 ± 1.6 MeV.

Dubnium compound nucleus EVRs are formed with the momentum of the projectile and recoil from the target. These EVRs were separated from the beam and other unwanted reaction products in the BGS based upon their differing magnetic rigidities in helium gas. Magnetic rigidities of the dubnium EVRs were estimated as previously described ([Gregorich2005], Chap. 2.1.2.1). The efficiency for collecting dubnium EVRs at the BGS focal plane was modeled using a Monte Carlo simulation of the EVR trajectories in the BGS, as described in [Gregorich2003; Gregorich2005], and resulted in energy dependent efficiencies, ε_{BGS}, of $53 - 58\%$ and $66 - 70\%$ for the ^{208}Pb(^{51}V,xn) and ^{209}Bi(^{50}Ti,xn) reactions, respectively. Between the ^{208}Pb(^{51}V,xn) and

the ^{209}Bi(^{50}Ti,xn) experiments, a collimator upstream of the target was modified to decrease the vertical and increase the horizontal extension of the beam spot on the target wheel. The vertical magnification of reaction products in the BGS is a factor of -7. By decreasing the height of the collimator, the vertical distribution of the reaction products is smaller at the focal plane, and this resulted in an increased ε_{BGS} for the ^{209}Bi(^{50}Ti,xn) reaction.

After separation in the BGS, the dubnium recoils passed through the MWPC and were implanted into the FPD. As discussed in Chap. 2.1.3, the efficiency for detecting α particles was ~76% of 4π. Of the remaining 24% of all α particles, no information was recorded for ~16% of α-decays. Finally, about 8% of all α particles escape out of the front of the detector box but lose sufficient energy to trigger the data acquisition.

3.4   *Known Decay Properties*

The known decay properties of ^{258,257}Db and their daughters are shown in Fig. 3.2. Due to similarities in α-particle energies and lifetimes of ^{258,257}Db and their daughters, the rate of random escape-like events and the probability of not observing α particles, stringent rules were used to assign events to ^{258}Db or ^{257}Db. Assignment of a decay chain to ^{258}Db was made based on the observation of an EVR [$10.0 \leq E(MeV) \leq 30.0$, prompt TOF signal between MWPC and FPD, anti-coincident with punch-through and upstream detectors] correlated in position (same strip, $\pm 3\sigma$ vertical position) and time to either:

i) ^{258}Db-like α particles [$8.8 \leq E(MeV) \leq 9.4$, < 25 s]   followed by time- and position-correlated α particles of ^{254}Lr [$8.3 \leq E(MeV) \leq 8.6$, < 75 s].
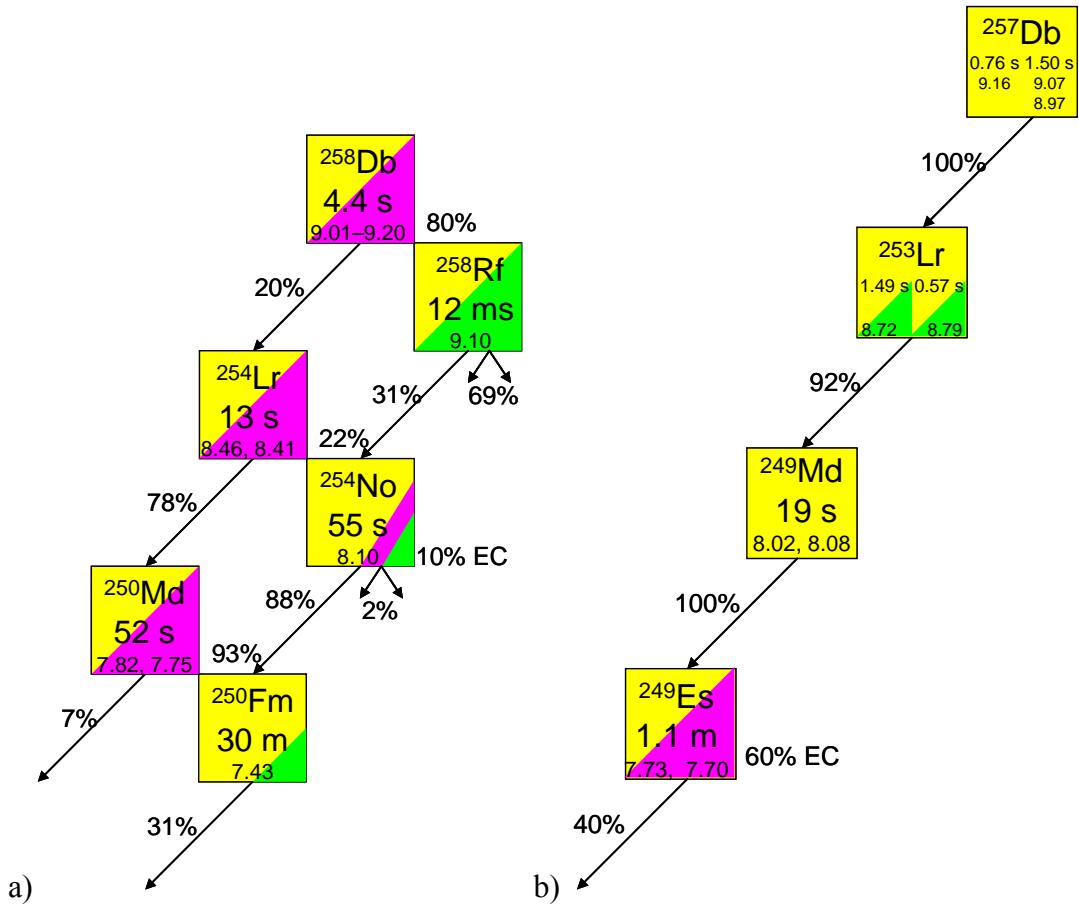
Fig. 3.2: Decay schemes for a) ^{258}Db and b)^{257}Db. Data was compiled from [Audi2003; Gates2008a; Heßberger2001]

ii) ^{258}Db-like α particles [$8.9 \leq E(MeV) \leq 9.4$, <25 s] followed by time- and position-correlated α particles of both ^{254}No [$8.0 \leq E(MeV) \leq 8.2$, < 325 s] and ^{250}Fm [$7.3 \leq E(MeV) \leq 7.6$, < 2 hr].

iii) ^{254}Lr-like α particles [$8.3 \leq E(MeV) \leq 8.6$, < 100 s] followed by time- and position-correlated α particles of ^{250}Md [$7.6 \leq E(MeV) \leq 8.0$, < 300 s]. In this case, the decay of ^{258}Db was assumed to go unobserved.

The α-decay of the electron capture (EC) daughter of ^{258}Db has recently been observed [Gates2008a]; however, due to similar decay properties, α-decay of ^{258}Db cannot be distinguished from α-decay of ^{258}Rf in chains that proceed through ^{254}No. At beam energies below the 2n exit channel threshold of 14.3 MeV, an EVR correlated in time (< 25 s) and position (same strip, ±3σ vertical position) to a spontaneous fission (SF) was also assigned to the decay of ^{258}Db. The detection of ^{250}Fm in case (iii) was also not required at beam energies below the 2n exit channel threshold.

^{257}Db was identified by the observation of an EVR [$10.0 \leq E(MeV) \leq 30.0$, anti-coincident with punch-through and upstream detectors, prompt TOF signal between MWPC and focal plane detector] followed by a time and position (same strip, ±3σ vertical position) correlated

i) ^{257}Db-like α particle [$8.8 \leq E(MeV) \leq 9.4$, < 10 s] followed by a time- and position-correlated α or SF decay of ^{253}Lr [$8.6 \leq E_\alpha(MeV) \leq 8.9$ or $100 \leq E_{SF}(MeV) \leq 300$, < 10 s].

ii) ^{257}Db-like α particle [$8.8 \leq E(MeV) \leq 9.4$, < 10 s] followed by time- and position-correlated α particles of both ^{249}Md [$7.9 \leq E(MeV) \leq 8.2$, < 325 s] and ^{245}Es [$7.3 \leq E(MeV) \leq 7.6$, < 500 s].

iii) ^{253}Lr-like α particle [$8.6 \leq E_\alpha(MeV) \leq 8.9$, < 20 s] followed by the time- and position-correlated decay of either ^{249}Md [$7.9 \leq E(MeV) \leq 8.2$, < 150 s] or ^{245}Es [$7.6 \leq E(MeV) \leq 7.8$, < 500 s]. The decay of ^{257}Db was assumed to go unobserved in this case.

Events identified as α particles were required to be anti-coincident with the MWPC and punch-through detectors, in the same strip as and within a vertical position of ±3σ of the EVR.

To minimize the contribution of random correlation of unrelated events, a fast beam-shutoff scheme was employed. Upon the detection of an EVR-like event followed by a position- (same strip, ±3 mm vertical position) and time-correlated (< 180 s) α-like event [$8.0 \leq E(MeV) \leq 10.0$], the beam was shut off for 240 s to allow for detection of additional α- or SF-like events under nearly background-free conditions. This fast 'shutoff' mode was employed for all energies of both reactions except the 236.1 and 244.1 MeV [51]V irradiations.

3.5 Results

The spectrum of all focal plane events with $6 < E(MeV) < 20$ in the low-gain analogue-to-digital converters (ADCs) (anti-coincident with the MWPC and punch-through detector) is presented in Fig. 3.3a. The spectrum of all α-like events initiating a beam shutoff is contained in Fig. 3.3b, while Fig 3.3c shows all α-like events occurring during the beam shutoff and correlated in time (<240 s) and position (same strip, ±3σ vertical position) to the α-like event initiating beam shutoff. Fig. 3.3d shows all α-like events occurring during the beam off that were *not* correlated in time (<240 s) and position (same strip, ±3σ vertical position) to the α-like event initiating beam shutoff.
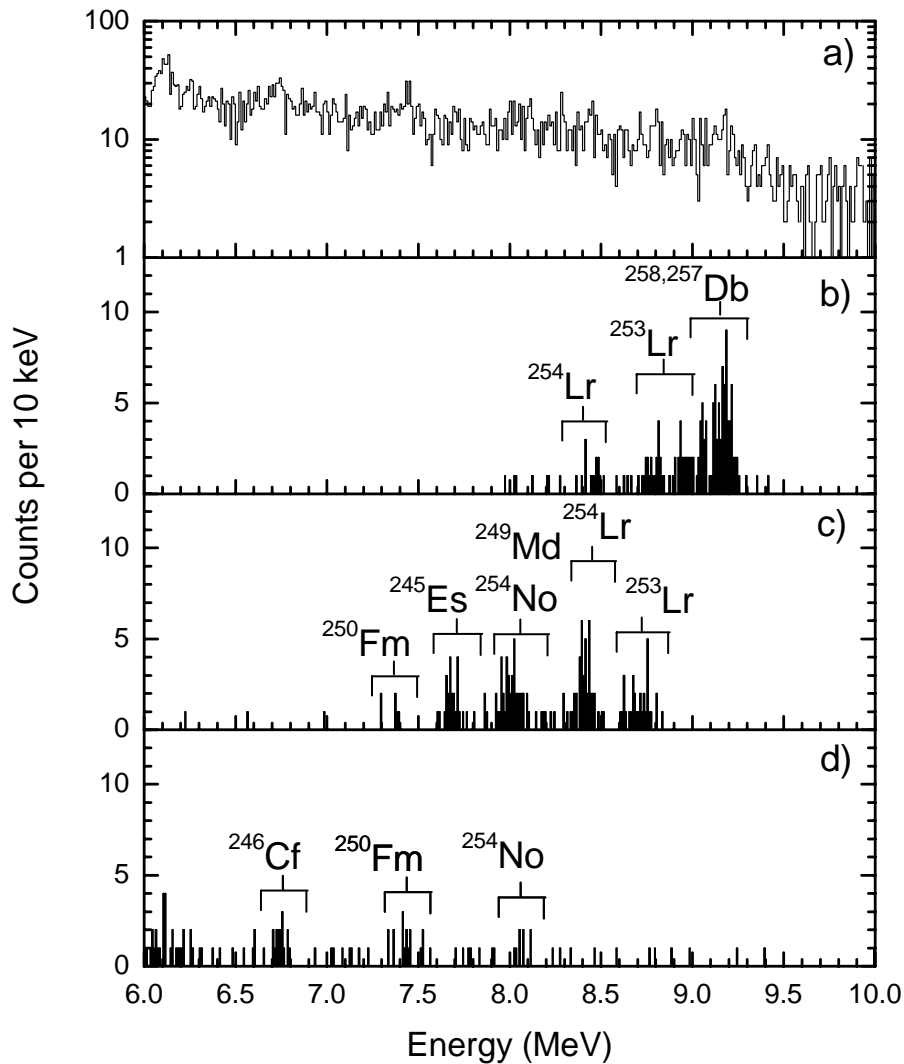
Fig. 3.3: Particle spectra recorded in the focal plane detector for: a) all events from the low-gain spectra anti-coincident with the MWPC and punch-through detectors; b) all α-like events initiating a beam shutoff c) all α-like events occurring during the beam off and correlated within 3σ and 240 s to the α-like event initiating shutoff; d) all α-like events occurring during the beam off that were *not* correlated within 3σ and 240 s to the α-like event initiating beam shutoff. The peaks at 7.4 and 6.7 MeV are due to ^{250}Fm and ^{246}Cf α-particles that are correlated to earlier beam shutoff events. The peak at 8.1 is due to ^{254}No α-decays that are preceded by ^{258}Db α-decays in which the α-particle escaped the front of the detector and imparted only a portion of its energy, thus not triggering a beam shutoff. These decays are long-lived enough to be recorded in subsequent beam shutoffs due to the high rate of Db-like events.

3.5.1   Observed 1n Decay Properties

^{258}Db

Sixty-eight α-decay chains observed in the two reactions were attributed to the decay of ^{258}Db. An additional 9 EVR-SF correlations were observed at the lowest two ^{50}Ti beam energies. These events were attributed to decay of ^{258}Rf, the electron capture (EC) of ^{258}Db, as the excitation energy of the compound nucleus was at least 2 MeV below the threshold for the 2n exit channel. The half-life measured from the 77 observed decays of ^{258}Db is $4.2^{+0.4}_{-0.3}$ s, in good agreement with the literature value of $4.4^{+0.9}_{-0.6}$ s [Heßberger1985].

The observed full energy α-decays constituted 4 α-lines with energies of 9.20 ± 0.03, 9.12 ± 0.03, 9.05 ± 0.03 and 8.84 ± 0.04 MeV, in order of decreasing intensity. The three lowest energy lines were all observed to occur with a relative intensity $i_{\mathrm{rel}} \approx 0.15$, while the highest energy α-line, 9.20 ± 0.03, was observed with $i_{\mathrm{rel}} \approx 0.55$. These lines are in agreement with those observed previously by Heßberger *et al.* [Heßberger1985].

^{254}Lr

Forty-nine full energy α-decays followed the α-decay of ^{258}Db and were attributed to the decay of ^{254}Lr during the experiments. The half-life measured from these decays is $17.8^{+1.9}_{-1.6}$ s, slightly longer than the literature value of 13^{+3}_{-2} s [Heßberger1985]. Two α-lines were observed for ^{254}Lr: 8.43 ± 0.03 and

8.48 ± 0.03 MeV. These are in agreement with the accepted values of 8.41 ± 0.02 and 8.46 ± 0.02 MeV [Heßberger1985].

^{254}No

Seventeen full energy α-decays of ^{254}No were observed during the irradiations. As this isotope can be produced in either EC of ^{254}Lr or α-decay of ^{258}Rf, no half-life information was calculated. However, two α-lines were observed for this isotope: 8.07 ± 0.03 and 8.11 ± 0.03 MeV, both values in agreement with the accepted value of 8.09 MeV [Firestone1996].

^{50}Md

The ^{258}Db decay chains were observed to pass through ^{250}Md six times. From these six α-decay events, a half-life of $24.7^{+9.5}_{-5.4}$ s was obtained for ^{250}Md. This value is shorter than the accepted value of 52 s [Audi2003], possibly due to low statistics. ^{250}Md is known to have 2 α-lines: 7.75 and 7.83 MeV [Firestone1996]. In this work, lines were observed at 7.76 ± 0.03 and 7.86 ± 0.03 MeV, in agreement with the accepted values.

^{250}Fm

Thirty-two full energy α-decays of ^{250}Fm, the great-granddaughter of ^{258}Db, were observed. The measured half-life of ^{250}Fm based on these α-decays is $28.4^{+3.9}_{-3.0}$ min, in agreement with the accepted value of 30 min [Audi2003].   One α-line at 7.44 ± 0.03 MeV was observed, as compared to the accepted value of 7.43 ± 0.02 MeV [Firestone1996].

3.5.2　Observed 2*n* Decay Properties

^{257}Db

Forty-eight decay chains observed during the two reactions were attributed to the α-decay of ^{257}Db.　Two isomers are known for ^{257}Db [Heßberger2001]:

^{257g}Db: $t_{1/2} = 1.50^{+0.19}_{-0.15}$ s, $E_\alpha = 9.074 \pm 0.020$ and 8.967 ± 0.020 MeV

^{257m}Db: $t_{1/2} = 0.76^{+0.15}_{-0.11}$ s, $E_\alpha = 9.163 \pm 0.020$ MeV

α-lines were observed at 9.18 ± 0.03, 9.08 ± 0.03 and 8.94 ± 0.03 MeV.　Decays contributing to the 9.18 ± 0.03 MeV α-line were assigned to ^{257m}Db, while the other decays were assigned to ^{257g}Db. The resulting half-lives of the ground and metastable states of ^{257}Db are $1.82^{+0.27}_{-0.21}$ s and $0.58^{+0.13}_{-0.09}$ s are, respectively, in agreement with literature data [Audi2003; Heßberger2001].

^{253}Lr

Forty-four of the forty-eight ^{257}Db α-decays were followed by the detection of a full energy α-decay of ^{253}Lr and one by the SF of ^{253}Lr. ^{253}Lr is also known to have two isomers with differing α-decay energies and life-times [Heßberger2001]:

^{253g}Lr: $t_{1/2} = 0.57^{+0.07}_{-0.06}$ s, $E_\alpha = 8.794 \pm 0.010$ MeV

^{253m}Lr: $t_{1/2} = 1.49^{+0.30}_{-0.21}$ s, $E_\alpha = 8.722 \pm 0.010$ MeV

α-lines were observed at 8.79 ± 0.03 and 8.73 ± 0.03 MeV.　The α-decays contributing to the 8.79 ± 0.03 MeV α-line were assigned to ^{253g}Lr, while the α-decays at 8.73 ± 0.03 MeV were assigned to ^{253m}Lr. The resulting half-lives of the ground and metastable states of ^{253}Lr are $0.80^{+0.19}_{-0.13}$ s and $1.60^{+0.24}_{-0.18}$ s, in agreement with literature data [Audi2003; Heßberger2001].

^{249}Md

Twenty-four full energy α-decays of ^{249}Md were observed in the ^{257}Db α-decay chains. The half-life measured for ^{249}Md based on these decays is $23.8^{+3.8}_{-2.9}$ s, consistent with the accepted value of 24 s [Audi2003]. The α-decays corresponded to an α-particle energy of 8.03 ± 0.03 MeV, consistent with the accepted value of 8.03 MeV [Firestone1996].

^{245}Es

A further fourteen α-decays were attributed to the decay of ^{245}Es, the great-granddaughter of ^{257}Db. The half-life measured for ^{245}Es based on these α-decays is $0.92^{+0.20}_{-0.14}$ min, consistent with the accepted value of 1.1 min [Audi2003]. α-lines were observed at 7.75 ± 0.03 and 7.70 ± 0.03 MeV, in agreement with the accepted values of 7.730 and 7.699 MeV.

3.5.3 Random Rates

EVR-α-α (EVR-α-SF) random rates were calculated by taking the observed number of EVRs and multiplying by the probability of observing two α's (correlated α-SF) within the required time and position windows. The rate of EVR-like events in the focal plane detector was 0.3 s^{-1}, while the rate of α-like events was 9×10^{-3} s^{-1}. Seventy-one high energy (> 100 MeV) events were observed during the irradiation. Identification of a ^{258,257}Db α-decay chain required the detection of an EVR, followed by an α-like event in the same strip within $\pm 3\sigma$ and 25 s and then an additional α-like event within $\pm 3\sigma$ and 325 s. 0.05 random correlations of this type were expected during the irradiation; thus, it is unlikely that any of the α-decay chains are of random origin.

Identification of ^{257}Db through EVR-α-SF correlations required detection of time and position correlated EVR, α, and SF. The probability of randomly observing a decay chain fitting the prescribed parameters is 2×10^{-5}.

Random rates for EVR-SF correlations were calculated by taking the observed number of SF events and multiplying by the probability of observing an EVR preceding the SF within the predefined time and position windows. EVR-SF correlations were assigned to the decay of ^{258}Db at the lowest ^{51}V beam energy and the two lowest ^{50}Ti beam energies, where the excitation energy of the compound nucleus was below the threshold for the 2n exit channel. During the irradiations at these energies, 16 SF-like events $[100 < E(MeV) < 300]$ were observed. The probability of any one of these SF events correlating to an EVR within 25 s and a position window of $\pm 3\sigma$, within the same strip, is 0.3, making it unlikely that more than one of the ten observed EVR-SF correlations is of random origin.

3.5.4 ^{208}Pb(^{51}V,xn)$^{259-x}$Db Excitation Functions

Fig. 3.4 shows excitation functions of the 1n and 2n exit channels of the ^{208}Pb(^{51}V,xn) reaction. Horizontal error bars represent the range of beam energies covered inside the target, while vertical error bars represent the uncertainties due to counting statistics and are presented at the 1σ level [Schmidt2000]. Table 3.1 contains more detailed information regarding beam and excitation energies, number of events observed and cross sections for the reactions. A fit to the 1n data indicates that the excitation function has a maximum cross section of 2160 ± 530 pb at 15.2 ± 0.9 MeV.

The maximum cross section of the 2*n* exit channel occurs at 23.4 ± 1.0 MeV and is

1980 ± 300 pb, nearly equal to that of the 1*n* exit channel.
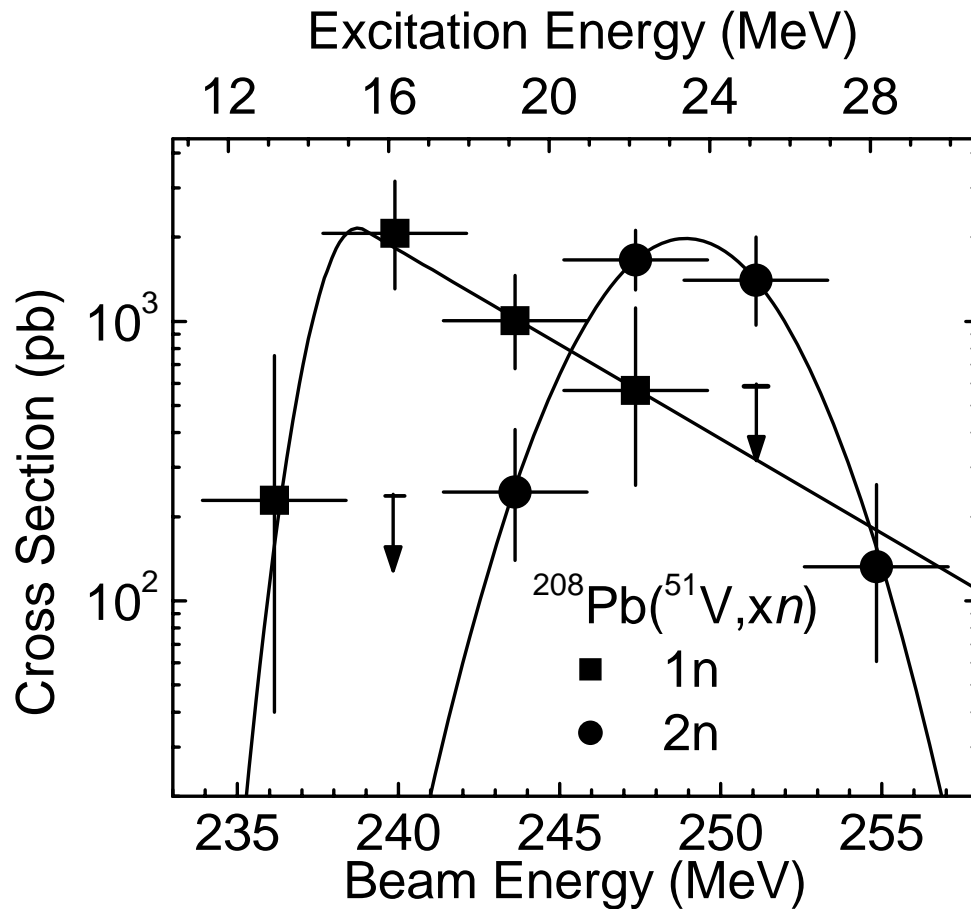
Fig. 3.4: 1*n* and 2*n* excitation functions for the ^{208}Pb(^{51}V,x*n*)$^{259\text{-}x}$Db reactions. Horizontal error bars represent the range of beam energies inside the target. Vertical error bars are uncertainties due to counting statistics. Downward arrows are upper limit cross sections calculated at the 1σ level. The lines are fits to the data using the procedure described in Chap. 1.3.2 and [Dragojević2008; Gregorich2007].

Table 3.1: Experimental conditions and results for the ^{208}Pb(^{51}V,xn)$^{259\text{-}x}$Db reaction

Beam energy (MeV)	Excitation energy (MeV)	ε_{BGS}	Observed number of 1n events	1n cross section (pb)	Observed number of 2n events	2n cross section (pb)
236.1	13.1	0.64	1	230^{+520}_{-190}	0	<180
239.7	16.0	0.65	7	2070^{+1100}_{-760}	0	<240
244.1	19.5	0.66	9	1000^{+460}_{-330}	5	250^{+170}_{-110}
247.2	22.0	0.67	3	570^{+550}_{-310}	20	1660^{+450}_{-370}
250.8	24.9	0.68	0	<590	10	1400^{+600}_{-430}
255.0	28.3	0.69	0	<180	3	130^{+130}_{-70}

3.5.5 ^{209}Bi(^{50}Ti,xn)$^{259\text{-}x}$Db Excitation Functions

The 1n excitation function for the ^{209}Bi(^{50}Ti,xn) reaction, as well as the 2n cross sections at the two highest ^{50}Ti beam energies, are shown in Fig. 3.5. More detailed information regarding beam and excitation energies, number of events observed and cross sections for the reactions is contained in Table 3.2. The maximum cross section of 5910 ± 810 pb occurs at an excitation energy of 16.2 ± 0.6 MeV for the 1n exit channel. These results are slightly higher than the previous value of 4300 ± 400 pb at 15.8 ± 0.1 MeV obtained by Heßberger *et al.* [Heßberger2001]. In [Heßberger2001] a value of 2400 ± 300 pb is given as the maximum of the 2n cross section, approximately half that of the 1n exit channel.

Fig. 3.5 also includes the 1n excitation function measured by Heßberger *et al.* in [Heßberger2007; Heßberger2001]. Based on the differences between the ^{209}Bi(^{50}Ti,1n) excitation function measured in this work and in [Heßberger2007; Heßberger2001], an energy discrepancy of several MeV may exist between beam energies reported in the two experiments.
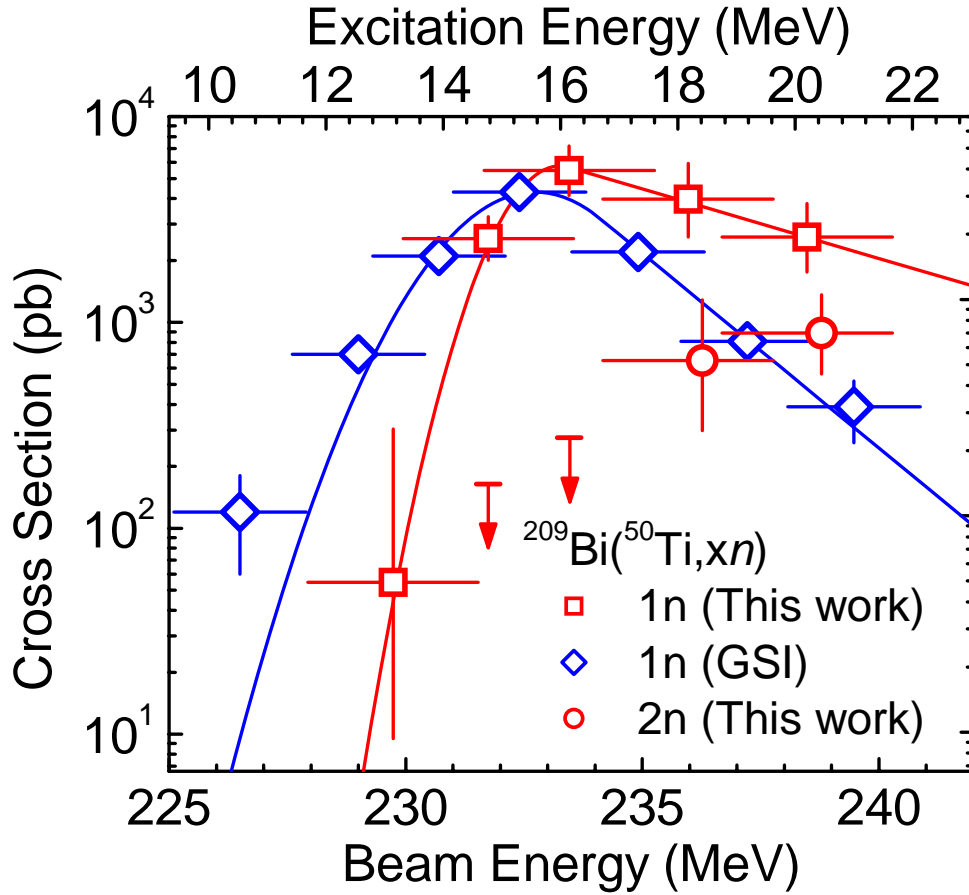
Fig. 3.5: Excitation functions for the ^{209}Bi(^{50}Ti,n)^{258}Db reaction as measured by LBNL (this work) and GSI ([Heßberger2007; Heßberger2001]). A partial excitation function measured at LBNL for the 2n exit channel is also included. Horizontal error bars represent the range of beam energies inside the target. Vertical error bars are uncertainties due to counting statistics. Downward pointing arrows are upper limit cross sections calculated at the 1σ level. The lines are a Gaussian smoothly joined up to an exponential on the high energy side best fitting the 1n data using the procedure described in Chap. 1.3.2 and [Dragojević2008; Gregorich2007].

Table 3.2: Experimental conditions and results for the ^{209}Bi(^{50}Ti,xn)$^{259-x}$Db reaction

Beam energy (MeV)	Excitation energy (MeV)	ε_{BGS}	Observed number of 1n events	1n cross section (pb)	Observed number of 2n events	2n cross section (pb)
229.5	13.1	0.80	1	55^{+250}_{-45}	0	<140
231.8	15.0	0.81	23	2550^{+720}_{-550}	0	<160
233.6	16.4	0.82	16	5480^{+1730}_{-1370}	0	<280
236.0	18.3	0.83	8	3360^{+1940}_{-1370}	3	650^{+630}_{-350}
238.4	20.3	0.84	9	2600^{+1190}_{-850}	7	890^{+463}_{-330}

3.6   *Discussion*

3.6.1   Comparison of 1*n* Excitation Functions

A comparison of the excitation functions for the 1*n* exit channels of the ^{208}Pb(^{51}V,x*n*) and ^{209}Bi(^{50}Ti,x*n*) reactions is shown in Fig. 3.6. The maximum cross section for the ^{209}Bi(^{50}Ti,x*n*) reaction is 2.7 ± 1.1 times larger than the maximum ^{208}Pb(^{51}V,x*n*) cross section. According to the FBD model, location of the maximum of the 1*n* excitation function is a result of competition between two factors that vary with energy: the reaction channel for single neutron emission, $\sigma_{cap} \times P_{CN} \times \dfrac{\Gamma_n}{\Gamma_t}$, and losses in EVR formation due to second chance fission or neutron emission, $P_<$. The reaction channel for single neutron emission increases with increasing bombarding energy, however, $P_<$ decreases with increasing energy once the threshold for second chance fission or neutron emission has been reached [Świątecki2003; Świątecki2005]. Since the threshold for $P_<$ depends on the compound nucleus and not the method of formation, the energy at which the maximum cross sections of the 1*n* exit channels is located is expected to be similar for the two reactions. This is in agreement with our result that the maximum cross sections occur at excitation energies of 15.2 ± 0.7 and 16.2 ± 0.6 MeV, for the ^{208}Pb(^{51}V,x*n*) and ^{209}Bi(^{50}Ti,x*n*) reactions, respectively.
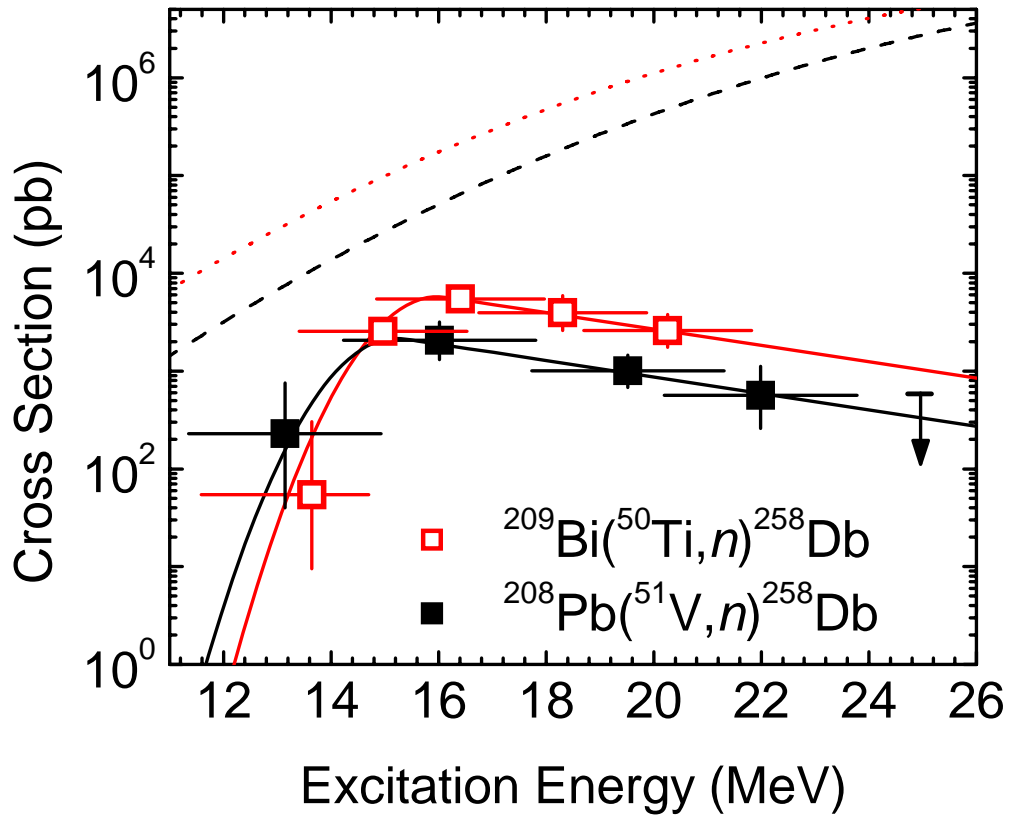
Fig. 3.6: Comparison of the $1n$ excitation functions for the ^{208}Pb(^{51}V,n) and ^{209}Bi(^{50}Ti,n) reactions. Horizontal error bars represent the range of beam energies inside the target. Vertical error bars are uncertainties due to counting statistics. Downward pointing arrows are upper limit cross sections calculated at the 1σ level. The solid lines are Gaussians smoothly joined to exponentials on the high energy side using the procedure described in Chap. 1.3.2 and [Gregorich2007]. The lines are $\sigma_{cap} \times 10^{-4}$ for the ^{208}Pb(^{51}V,n) (dashed) and ^{209}Bi(^{50}Ti,n) (dotted) reactions.

For two reactions that produce the same compound nucleus, losses in EVR formation due to $\frac{\Gamma_n}{\Gamma_t}P_<$ are almost identical, and losses due to P_{CN} are expected to be similar at a given excitation energy [Świątecki2003; Świątecki2005]. Prior to forming a compound nucleus, the nuclei must first overcome a barrier formed from their mutual

Coulomb + nuclear potential [Świątecki2005]. The barrier heights as calculated using eqn. (5) in [Świątecki2005] are 251.9 MeV and 242.4 MeV in laboratory frame for the ^{208}Pb(^{51}V,n) and ^{209}Bi(^{50}Ti,n) reactions, respectively. These correspond to respective excitation energies of 25.8 and 23.4 MeV. The effect of this difference in σ_{cap} as a function of energy is shown in Fig. 4. Comparison of the excitation functions at low energies is hindered by counting statistics, as only one event was observed for each reaction. Above the peak, the ^{208}Pb(^{51}V,n) reaction has consistently lower cross sections than the ^{209}Bi(^{50}Ti,n) reaction, an effect mirrored in the ratio of calculated σ_{cap} values for the two reactions. Thus, differences in experimental ^{208}Pb(^{51}V,n) and ^{209}Bi(^{50}Ti,n) cross sections are mainly due to the difference in capture cross sections for the two reactions.

3.6.2   *Comparison of 2n Excitation Functions*

Fig. 3.7 shows a comparison of the excitation functions for the ^{208}Pb(^{51}V,2n) (this work) and ^{209}Bi(^{50}Ti,2n) [Heßberger2007; Heßberger2001] reactions and includes σ_{cap} as a function of energy. Due to possible energy discrepancies between the two laboratories, direct comparison of the 2n cross sections is difficult. However, over the energy range of the excitation functions, σ_{cap} is larger for the ^{209}Bi(^{50}Ti,2n), again due to the lower height of the barrier in relation to the excitation energy of the compound nucleus. From this, the maximum cross section for the ^{209}Bi(^{50}Ti,2n) should be larger than that of the ^{208}Pb(^{51}V,2n) reaction; however, the maximum cross section of the two reactions is identical within the error bars.
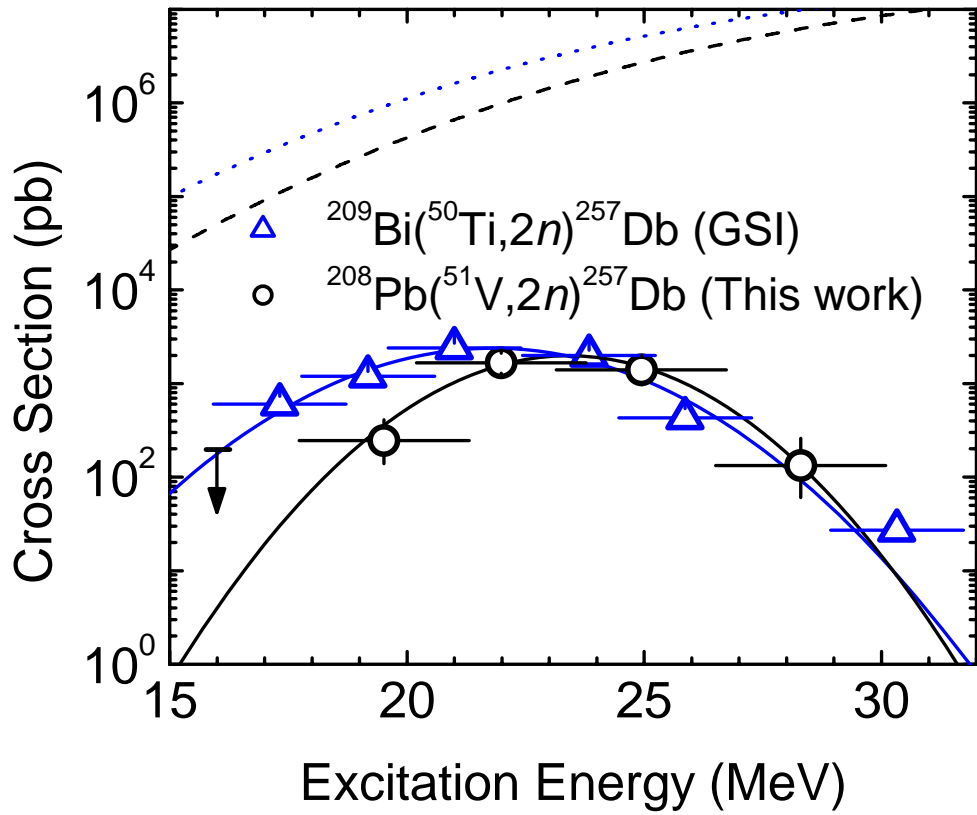
Fig. 3.7: Comparison of the 2n excitation functions for the ^{208}Pb(^{51}V,2n) (this work) and ^{209}Bi(^{50}Ti,2n) [Heßberger2007; Heßberger2001] reactions. Horizontal error bars represent the range of beam energies inside the target. Vertical error bars are uncertainties due to counting statistics. Downward pointing arrows are upper limit cross sections calculated at the 1σ level. The solid lines are fits to the data using the procedure described in Chap. 1.3.2 and [Gregorich2007]. The broken lines are $\sigma_{cap} \times 10^{-4}$ for the ^{208}Pb(^{51}V,n) (dashed) and ^{209}Bi(^{50}Ti,n) (dotted) reactions.

4   Off-Line Extractions

4.1   *Extraction of Niobium and Tantalum from HCl Solutions*

4.1.1   Hydrolysis and Complex Formation of Niobium and Tantalum in HCl Solutions

Understanding the chemistry of niobium and tantalum is hindered by the competition between hydrolysis and complex formation (see Chap 1.6.1). For example, niobium and tantalum form chlorocomplexes of the same type, MCl_6^-, in the absence of water. With the addition of water, the elements begin to hydrolyze in dissimilar ways [Pershina1998a; Pershina1998b], leading to differences in complex formation and in extraction behavior. Understanding these differences is hindered not only by the plethora of species formed, but also by the tendency of niobium and tantalum to form polynuclear complexes when semi-macroscopic amounts of the metal are present.

4.1.1.1   Niobium

Several experiments have been conducted previously to ascertain information regarding complex formation of niobium in HCl solutions. Electrodialysis experiments were performed on niobium in HCl solutions by Nabivantes *et al.* [Nabivanets1964].

Their results indicated that niobium is present as cationic polymers at <5 M HCl. Below 2 M HCl, the formation of colloids was determined after a decrease in niobium migration to the cathode was observed. At >5 M HCl, the formation of anionic chloro-complexes becomes predominant and the formation of cationic species ceases above 8 M HCl.

Kim *et al.* investigated the anion exchange of niobium, tantalum and protactinium in solutions of mixed HCl-HF media [Kim1973]. They varied the HCl concentration from 0.01 – 12 M and the HF concentration from 0.01 – 22 M. The studies were performed using semi-macroscopic quantities of niobium and tantalum formed via the neutron activation of ^{nat}Nb and ^{nat}Ta. From their results, they determined that the niobium species change from polymeric cationic complexes based on $Nb(OH)_2Cl_2^+$ and $NbOCl_2^+$ at low HCl concentrations to neutral complexes like $Nb(OH)_2Cl_3$ around 3 – 6 M HCl [Kim1973].

Spectroscopic studies of niobium in HCl solutions were performed by Kanzelmeyer *et al.* [Kanzelmeyer1953; Kanzelmeyer1956]. In these studies, the HCl concentration was varied from 1.0 – 11.8 M and the effect of the HCl concentration on an absorbance peak at 281 mμ was observed. The 281 mμ peak appears at 6 HCl and increases with increasing HCl concentration [Kanzelmeyer1953]. To determine what complex was being formed at >6 M HCl, the unknown niobium absorbance spectrum was compared to an absorbance spectrum from (C₂H₅)₄NNb(OH)₂Cl₄. Both spectra showed identical peaks at 281 mμ, leading to the conclusion that at 6 – 9 M HCl, the predominant specie in solution is $Nb(OH)_2Cl_4^-$ [Kanzelmeyer1953; Kanzelmeyer1956]. Sabatini *et al.* also performed spectroscopic studies on niobium in HCl solutions. They investigated the infared spectra of niobium at high HCl concentrations. From this they

determined that $Nb(OH)_2Cl_4^-$ is replaced by $NbOCl_4^-$, $NbOCl_5^{2-}$ and $NbCl_6^-$ above 11 M HCl [Sabatini1966]. Davies *et al.* used Raman spectroscopy to study the hexachloro-anions of niobium. Niobium chloride was dissolved in 12.6 HCl. At that concentration, $NbCl_6^-$ was observed in solution [Davies1968].

Campderrós *et al.* performed studies on the facilitated transport of niobium with tri-butyl phosphate (TBP) through membranes [Campderrós2000]. They observed that the highest niobium transport yields were observed at 6 – 9 M HCl. At high HCl concentrations, they conclude that TBP may either form an ionic association with anionic complexes, or ionic association with cationic complexes. As such, Campderrós *et al.* suggest the formation of $Nb(OH)_2Cl_4^-$ around 6 M HCl and the formation of cationic $HNbOCl_3^+$ if the H^+ concentration is raised above 8 M HCl.

4.1.1.2   Tantalum

Less is known about the speciation of tantalum than of niobium. When tantalum is present in solution in semi-macroscopic amounts, the formation of polynuclear species in the form of $(TaO_{>1}Cl_{<3}nCl)_x$ hinders its extraction [Schäfer1959]. In addition, Campderrós *et al.* studied the facilitated transport of tantalum with TPB through membranes in the presence of HCl solution. They observed transport of tantalum at low HCl concentration. From this, they suggested that $Ta(OH)Cl_4$ exists at low HCl concentrations and can be extracted by tributyl phosphate [Campderrós2000].

Nabivanets *et al.* have also performed electrodialysis experiments on tantalum in HCl solutions [Nabivanets1962]. They observed the formation of colloidal tantalum at >8 M HCl when the tantalum concentration was 10^{-3} M. Below 0.5 M HCl, tantalum was

observed to exist as colloids. Polymeric cationic forms of tantalum predominant ed the solutions from 0.5 – 4 M HCl. The conversion of cationic forms of tantalum into anionic forms was seen at 6 – 7 M HCl. These experiments show that tantalum begins to form anionic species at acid concentrations approximately 1 M higher than those seen for niobium [Nabivanets1964; Nabivantes1962]. This would suggest the formation of $Ta(OH)_2Cl_4^-$ at >6 M HCl, $TaOCl_4^-$ at medium HCl concentrations and $TaCl_6^-$ above 12 M HCl [Pershina1998b].

4.1.2 Rationale for New Experiments

The known (and postulated) complexes of niobium and tantalum in solution as a function of HCl concentration are summarized in Table 4.1. Several discrepancies exist among the complexes postulated for niobium by different works. For example, in [Nabivanets1964], no cationic complexes were observed above 8 M HCl. At this same acid concentration, [Campderrós2000] postulated that $HNbOCl_3^+$ may exist. In addition, [Kim1973] observed neutral complexes akin to $Nb(OH)_2Cl_3$ at acid concentrations where [Nabivanets1964] concluded that cationic polymers are the dominant species. Even less is known regarding speciation of tantalum. Accurate interpretation of the results of these studies is hindered by the formation of polymeric and colloidal species due to the high (semi-macroscopic) concentrations of niobium and tantalum used in the experiments. The use of microscopic (<10^{-15} M) concentrations of niobium and tantalum prevents the formation of polymeric and colloidal species. Investigations of this simplified system aids in the understanding of complex formation of the group V elements.

77

Table 4.1: Predominant complexes of Nb(V) and Ta(V) in solution as a function of HCl concentration

HCl [M]	Nb	Reference	Ta	Reference
< 0.5			colloid	[Nabivanets1962]
< 2	colloid	[Nabivanets1964]		
< 3	polymeric cationic complexes based on $Nb(OH)_2Cl_2^+$ $NbOCl_2^+$	[Kim1973]	$Ta(OH)Cl_4$	[Campderrós2000]
< 4			polymeric cations	[Nabivanets1962]
3 – 6	$Nb(OH)_2Cl_3$	[Kim1973]		
< 5	cationic polymers	[Nabivanets1964]		
> 5	anionic-chlorocomplexes	[Nabivanets1964]		
> 6	$Nb(OH)_2Cl_4^-$	[Kanzelmeyer1953; Kanzelmeyer1956]	anionic $Ta(OH)_2Cl_4^-$	[Nabivanets1962; Pershina1998b]
> 8	no cationic complexes	[Nabivanets1964]	$TaOCl_4^-$	[Pershina1998b]
8	$HNbOCl_3^+$	[Campderrós2000]		
11	$NbOCl_4^-$ $NbOCl_5^{2-}$ $NbCl_6^-$	[Sabatini1966]		
> 12	$NbCl_6^-$	[Davies1968]	$TaCl_6^-$	[Pershina1998b]

Based upon previous experiments [Davies1968; Kanzelmeyer1956; Kim1973; Nabivanets1962; Nabivanets1964; Sabatini1966], V. Pershina has postulated that, in HCl, the change from cationic to anionic species occurs between 5 and 7 M HCl for niobium and between 6 and 8 M HCl for tantalum as shown in Fig. 4.1 [Pershina1998b]. Well-defined chemical systems that probe the region where the complexes formed by the

group V elements change from cationic to anionic can be used to study and evaluate complex formation of the group V transactinide element, dubnium.
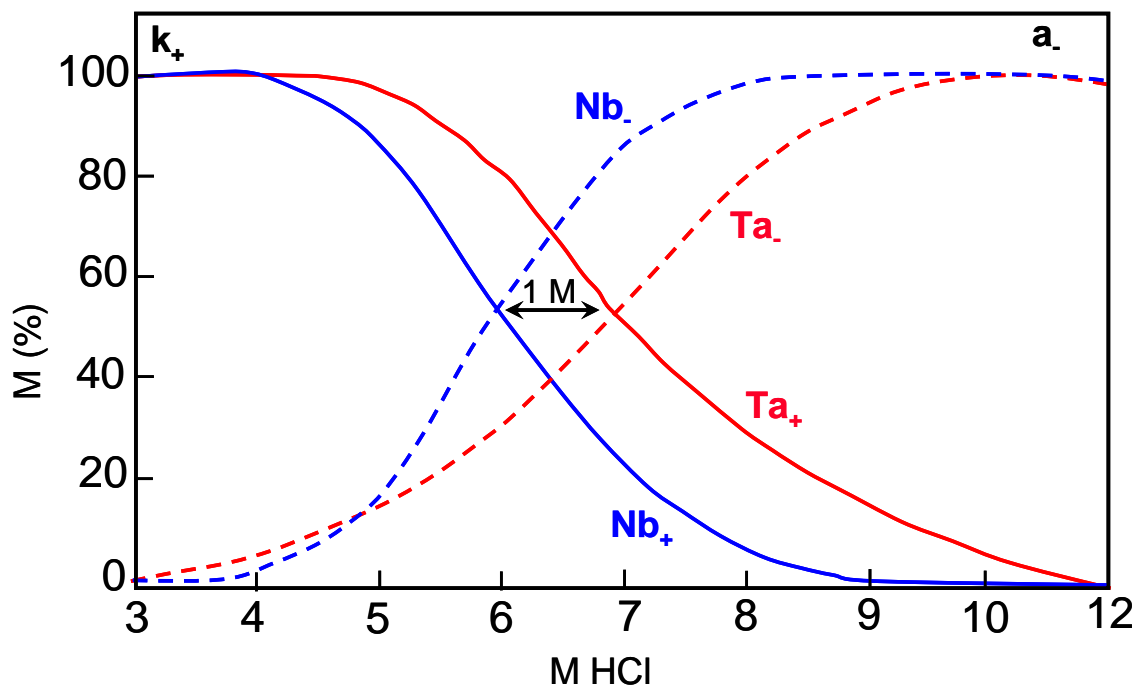
Fig. 4.1: Distribution of ionized niobium and tantalum species between the cationic (k_+) and anionic (a_-) forms in HCl solutions (adapted from [Pershina1998b]).

For this dissertation, the extraction of niobium and tantalum by four different organophosphorus complexes was studied off-line as a function of HCl concentration using trace (10^{-10} M) and semi-macroscopic (10^{-6} M) concentrations of niobium and tantalum. These results were then used to determine appropriate systems for the study of microscopic quantities of niobium and tantalum for potential transactinide experiments. The aqueous phases consisted of 1 - 11 M HCl. For the organic phases, the ligands bis-2-ethylhexyl hydrogen phosphate (HDEHP, see Fig. 1.5a), bis-2-ethylhexyl hydrogen

phosphate (BEHP, see Fig. 1.5b), 2-ethylhexyl hydrogen-2-ethylhexyl phosphonate (DEHPA, see Fig. 1.5c) and diisooctyldithiophosphinic acid (DiOPA, see Fig. 1.5d) were investigated. All organic phases consisted of 0.01 M ligand in $CHCl_3$.

The liquid-liquid extraction of niobium and tantalum from HDEHP has been previously investigated using toluene and carbon tetrachloride (CCl_4) as solvents and semi-macroscopic metal quantities. Kimura *et al.* extracted niobium and tantalum from HCl into solutions of 50% HDEHP in toluene. They observed a decrease in niobium extraction with increasing HCl concentration while the tantalum extraction yield remained constant over the concentrations studied (0.01 – 1 M HCl) [Kimura1960; Kimura1961]. Das *et al.* performed similar experiments, extracting niobium and tantalum from HCl solutions into 0.01 M HDEHP in chloroform [Das1981]. In their studies, a decrease in tantalum extraction yield (98.5 – 49.5%) was observed as the HCl concentration was increased from 0.8 to 5.6 M. In contrast, the niobium extraction yield was observed to increase from 18.6 to 32.2%.

4.1.3   Kinetics

Extraction yields as a function of phase contact time were studied for all systems. Mixing times of 10 – 60 s were used for the investigation of niobium, while tantalum was studied over times ranging from 10 – 90 s. The results for the extraction of niobium are shown in Fig. 4.2 (HDEHP), Fig. 4.3 (BEHP), Fig. 4.4 (DEHPA) and Fig. 4.5 (DiOPA). For extraction by HDEHP, DEHPA and DiOPA, equilibrium was reached within 30 s at acid concentrations ≤6 M. At 9 M HCl, equilibrium was reached within 20 s when niobium was extracted by HDEHP and DEHPA, but not until 30 s when extracted by DiOPA. All three ligands reached equilibrium within 10 s at 11 M HCl. For the other

remaining ligand, BEHP, equilibrium was reached within 10 s regardless of acid concentration.
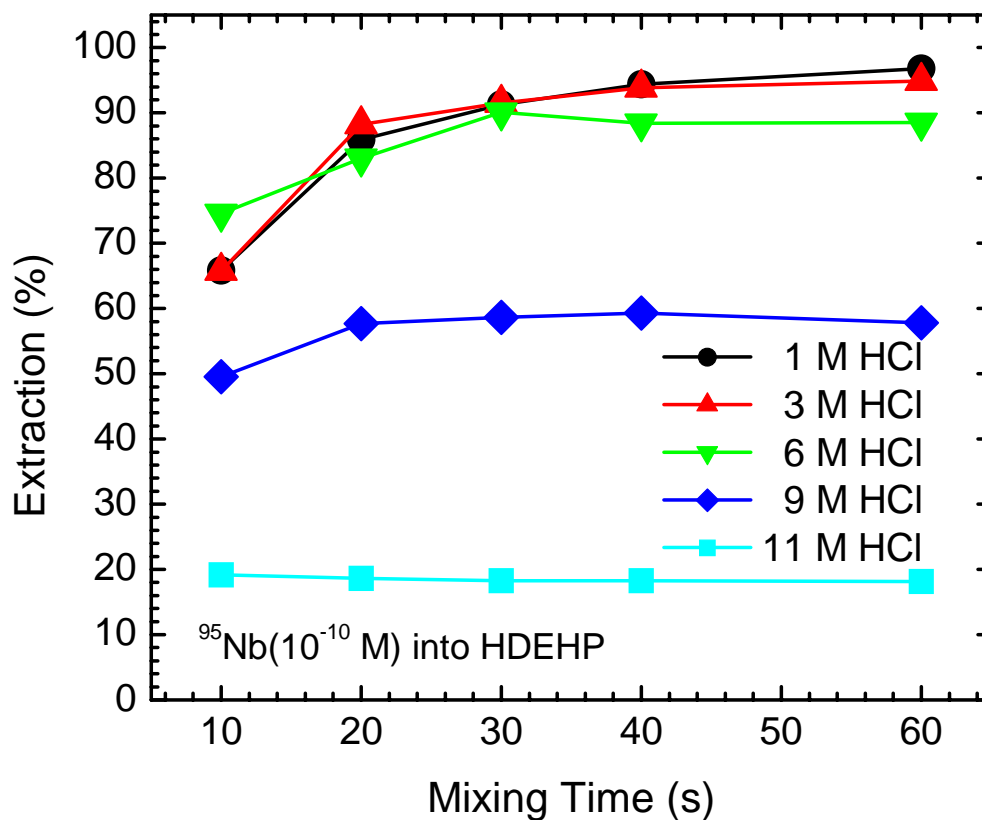
Fig. 4.2: Extraction of ^{95}Nb (10^{-10} M) from solutions of 1 (●), 3 (▲), 6 (▼), 9 (♦) or 11 (■) M HCl by 0.01 M HDEHP in CHCl$_3$ as a function of mixing. Error bars are smaller than the symbols.
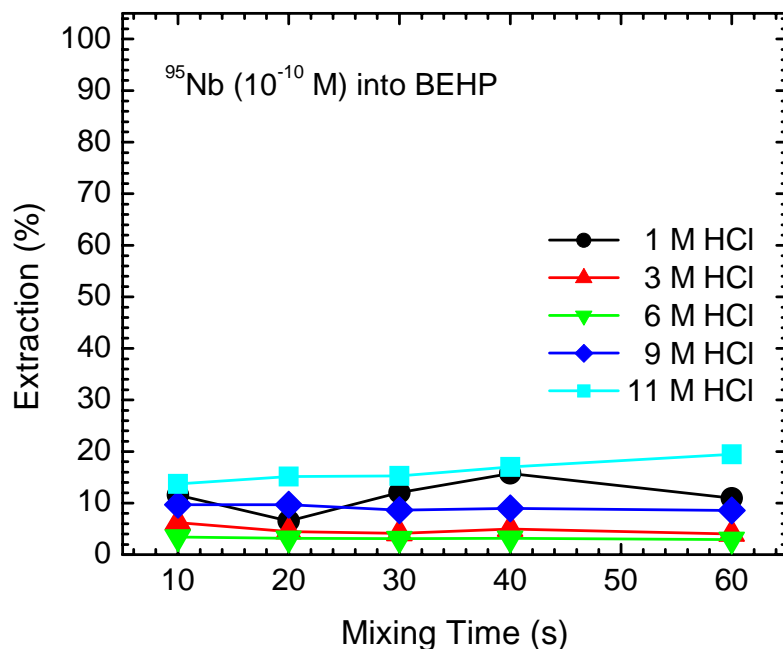
Fig. 4.3: Extraction of ^{95}Nb (10^{-10} M) from solutions of 1 (●), 3 (▲), 6 (▼), 9 (◆) or 11 (■) M HCl by 0.01 M BEHP in CHCl$_3$ as a function of mixing. Error bars are smaller than the symbols.
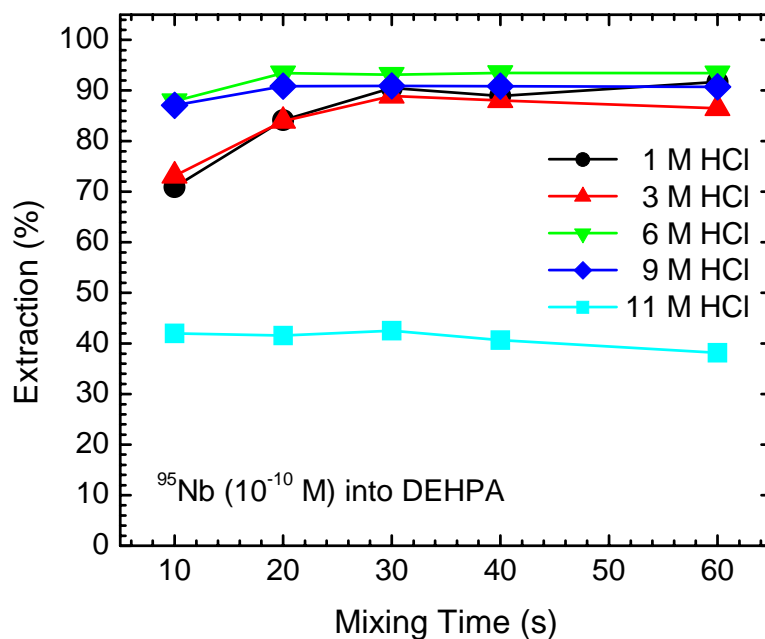
Fig. 4.4: Extraction of ^{95}Nb (10^{-10} M) from solutions of 1 (●), 3 (▲), 6 (▼), 9 (◆) or 11 (■) M HCl by 0.01 M DEHPA in CHCl$_3$ as a function of mixing. Error bars are smaller than the symbols.
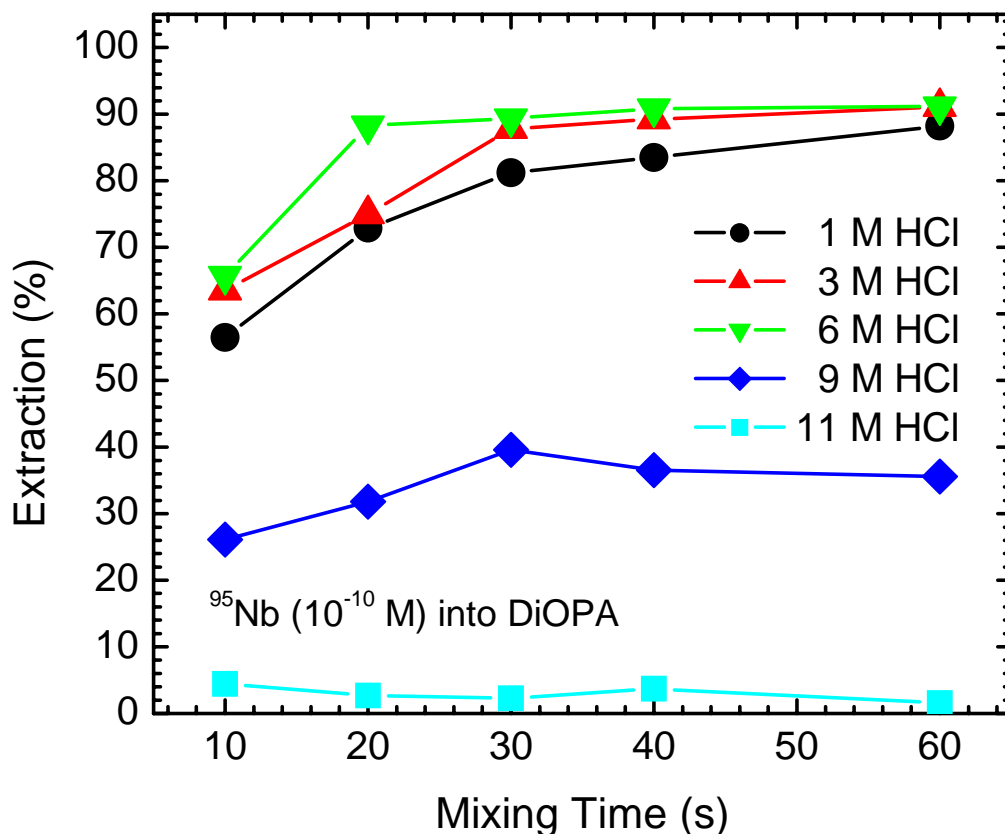
Fig. 4.5: Extraction of ^{95}Nb (10^{-10} M) from solutions of 1 (●), 3 (▲), 6 (▼), 9 (♦) or 11 (■) M HCl by 0.01 M DiOPA in CHCl$_3$ as a function of mixing. Error bars are smaller than the symbols.

Tantalum was extracted from HCl solutions by HDEHP (Fig. 4.6) and BEHP (Fig. 4.7) as a function of phase contact time. In the HDEHP system, equilibrium was only observed at 1 M HCl and was reached in <60 s. Above 1 M HCl, equilibrium was not seen within the maximum mixing time of 90 s. Samples were not mixed beyond 90 s, as experiments with short-lived isotopes are limited to 90 s by the short lifetimes of those isotopes. When tantalum was extracted by BEHP, equilibrium was observed at >3 M HCl within 10 s, but not at 1 or 3 M HCl.

Based on these results, mixing times of 60 s for niobium and 90 s for tantalum were chosen for comparisons of extraction experiments.
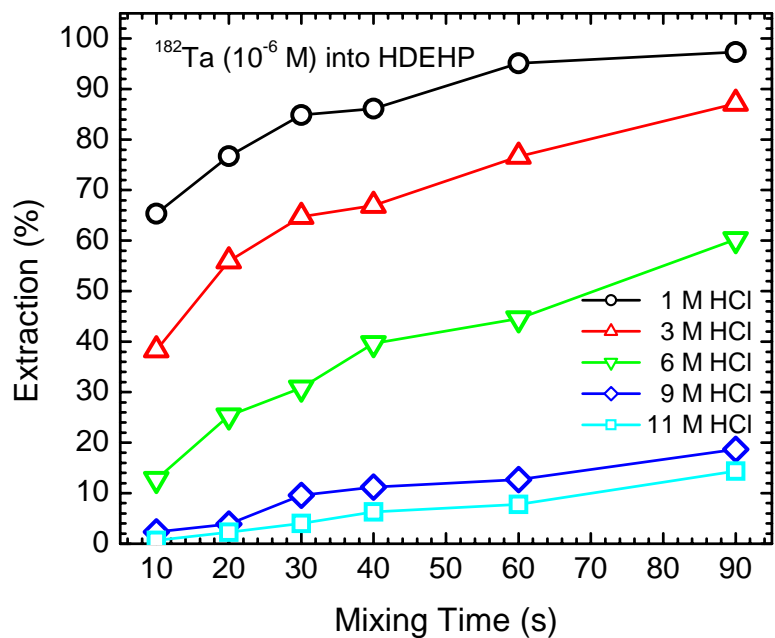
Fig. 4.6: Extraction of tantalum (10^{-6} M) from solutions of 1 ($\circ$), 3 ($\triangle$), 6 ($\triangledown$), 9 ($\diamond$) or 11 ($\square$) M HCl by 0.01 M HDEHP in $CHCl_3$ as a function of mixing time. Error bars are smaller than the symbols.

Fig. 4.7: Extraction of tantalum (10^{-6} M) from solutions of 1 ($\circ$), 3 ($\triangle$), 6 ($\triangledown$), 9 ($\diamond$) or 11 ($\square$) M HCl by 0.01 M BEHP in $CHCl_3$ as a function of mixing time. Error bars are smaller than the symbols.

4.1.4   Niobium

The extraction of ^{95}Nb (10^{-10} M) from HCl solutions by HDEHP, BEHP, DEHPA and DiOPA was studied as a function of HCl concentration. Results are shown in Fig. 4.8. The three ligands that extract cationic species, (HDEHP, DEHPA and DiOPA) show very similar extraction behavior. For both HDEHP and DiOPA, high extraction yields (>80%) were observed up to 6 M HCl. A decrease in extraction yield was then observed at both 9 and 11 M HCl. For the DEHPA, the other cationic extractor, extraction yields >80% were observed to 9 M HCl, and then the yield decreased at 11 M HCl. These results are consistent with previous experimental data suggesting that the formation of cationic complexes dominant es speciation until ~6 M HCl (see [Pershina1998b] for a summary). The extraction behavior observed in this dissertation is in agreement with the results of [Kimura1960]; which are summarized in Chap. 4.1.2. However, the results of [Das1981], in which a very similar system was investigated (0.01 M HDEHP in CCl$_4$, 1 – 5.6 M HCl) are in disagreement with both this work and those in [Kimura1960].
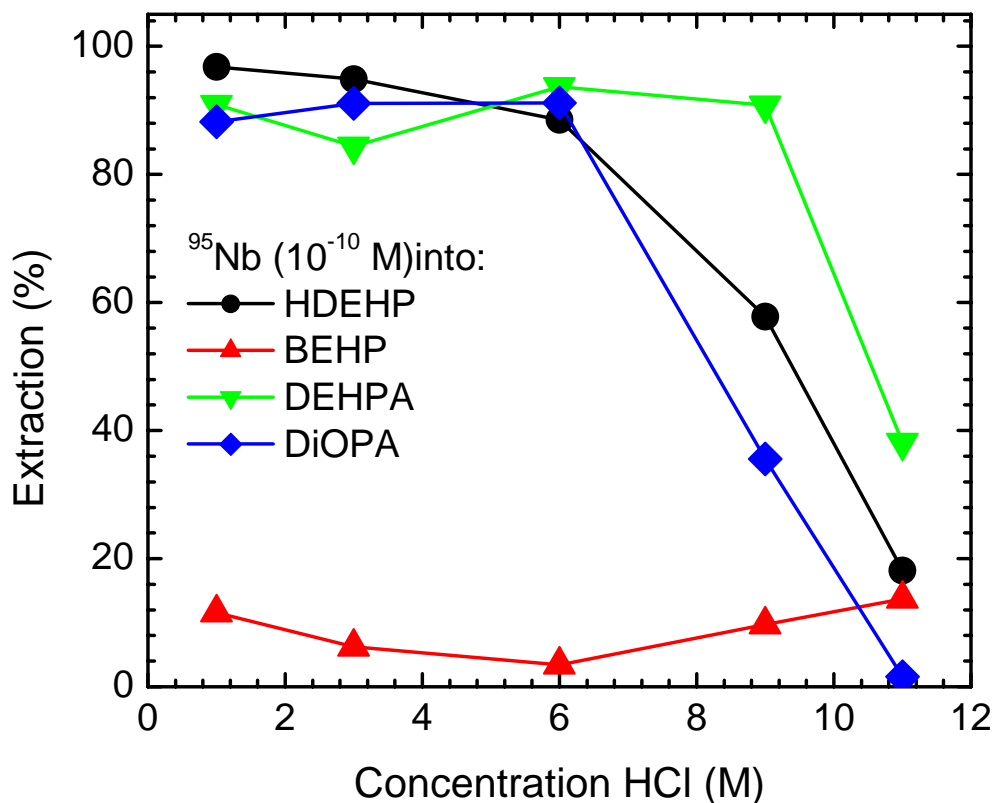
Fig. 4.8: Extraction of ^{95}Nb (10^{-10} M) into solutions of 0.01 M HDEHP (●), BEHP (▲), DEHPA (▼) or DiOPA (♦) in CHCl$_3$ as a function of HCl concentration. Error bars are smaller than the symbols.

The fourth ligand investigated, BEHP, preferentially extracts neutral species in solution. Over the acid range studied, low extraction yields (<20%) of niobium with BEHP were observed. This suggests either the dominant species in solution are not neutral or that the neutral complexes formed are inextractable.

Similar extraction behavior was observed for three of the ligands (HDEHP, DEHPA, DiOPA) investigated with niobium. As such, experiments on both niobium and tantalum were performed using the neutral extractor, BEHP, and only one cation extractor, HDEHP. These two ligands were chosen due to the similarities of their side

chains. Between the two ligands, the only difference is the presence of an acidic –OH
group on HDEHP that is replaced by a –H on BEHP.
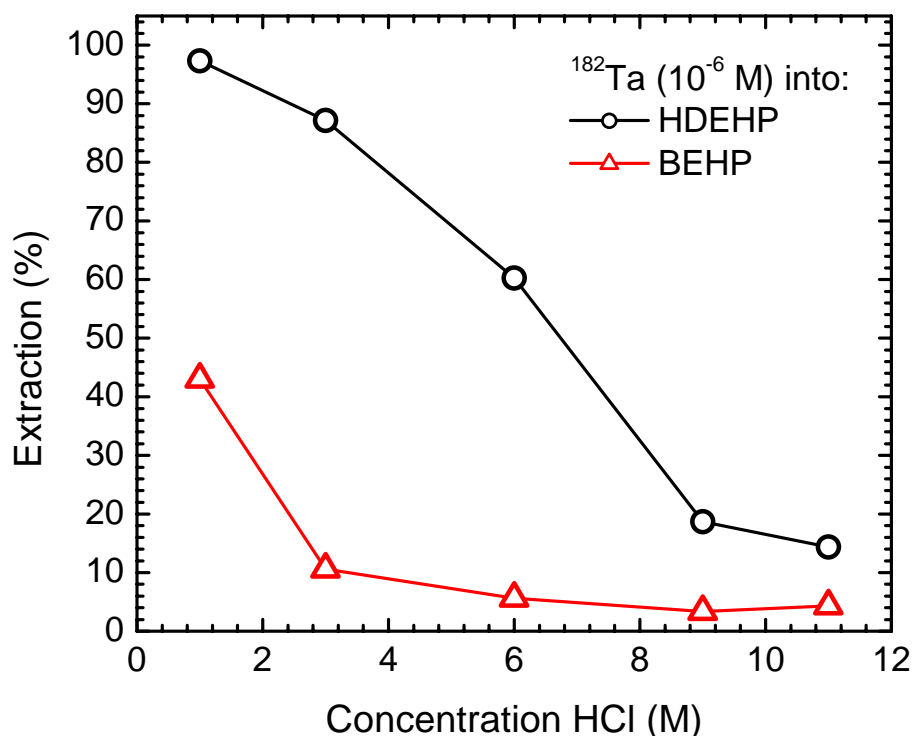
Fig. 4.9: Extraction of ^{182}Ta (10^{-6} M) into solutions of 0.01 M HDEHP ($\circ$), BEHP (Δ) in
CHCl$_3$ as a function of HCl concentration. Error bars are smaller than the symbols.

4.1.5   Tantalum

Fig. 4.9 contains the results of extractions of ^{182}Ta (10^{-6} M) from HCl solutions by
0.01 M HDEHP or BEHP in CHCl$_3$. A decrease in extraction yield with increasing HCl
concentration is observed for both ligands. However, HDEHP extracts significantly more
tantalum than BEHP does for the same acid concentrations. BEHP only extracts >10% of
at 1 M HCl, while HDEHP extracts >90% at this concentration and >10% until 9 M HCl.

The results with HDEHP are consistent with those observed first by Das *et al*. [Das1981] using a similar chemical system (0.01 M HDEHP in CCl$_4$, 1 – 5.6 M HCl) and suggest the formation of inextractable complexes (likely anionic) to become the predominant species in solution at >6 M HCl.

4.2   Extraction of Niobium and Tantalum from HCl/LiCl Extractions

4.2.1   Hydrolysis and Complex Formation of Niobium and Tantalum in HCl/LiCl Solutions

Few studies have been performed on niobium and tantalum in HCl/LiCl solutions. Nabivanets *et al*. used electrodialysis to study the effect of varying the Cl$^-$ concentration at 2.5 M H$^+$ concentrations. They observed no formation of anionic complexes when the Cl$^-$ concentration was increased, indicating that niobium required an increase in both H$^+$ and Cl$^-$ to form anions [Nabivanets1962]. Similar studies were performed with tantalum in which the Cl$^-$ concentration was held at 10.5 M at 0.5 M H$^+$. In these experiments, no formation of anionic complexes was observed, indicating that high concentrations of H$^+$ and Cl$^-$ are required [Nabivanets1964].

Kanzelmeyer *et al*. [Kanzelmeyer1953; Kanzelmeyer1956] performed a series of spectroscopic studies on niobium in mixed HCl/LiCl solutions, in which the Cl$^-$ concentration was held constant at 10.5 M, and the H$^+$ concentration was varied from 0.02 to 9.86 M. From their data, they determined that the predominant species in solution at high H$^+$ and Cl$^-$ concentration is $Nb(OH)_2Cl_4^-$. As the H$^+$ concentration is lowered, insoluble colloids based upon $Nb(OH)_3Cl_2$ are formed via the reaction:

$$Nb(OH)_2 Cl_4^- + H_2O \leftrightarrow Nb(OH)_3 Cl_2 + H^+ + 2Cl^- \tag{4.1}$$
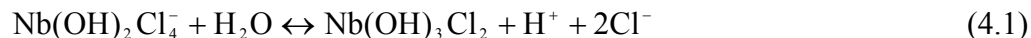
Colloidal $Nb(OH)_3 Cl_2$ then becomes the predominant specie <2 M H^+. Due to the low niobium concentrations used in this work, the formation of colloidal species is prohibited. Instead, the dominant specie at low H^+ concentrations is expected to be the monomer $Nb(OH)_3 Cl_2$.

4.2.2 Rationale for New Experiments

The extractions of niobium and tantalum from HCl solutions provided separation of the elements, however, equilibrium was not reached until 30 s for niobium and or within 90 s for tantalum under some conditions. For eventual experiments with dubnium, it is necessary for the system to reach equilibrium within 10 s. As such, the effect of the H^+ and Cl⁻ concentrations on the extraction and equilibrium for niobium and tantalum were investigated.

4.2.3 Kinetics

The extraction of niobium from HCl solutions by HDEHP required up to 30 s before equilibrium was reached. As such, a new series of experiments was begun to investigate the impact of the H^+ and Cl⁻ on the equilibrium as a function of time. For these experiments, the mixing time of the samples was varied from $10 - 60$ s. In addition, the H^+ concentration was varied from $1 - 11$ M while the Cl⁻ concentration was held constant at 12 M; see Fig. 4.10 for extractions by HDEHP and Fig. 4.11 for extractions by BEHP. A similar set of experiments were performed in which the Cl⁻ concentration was varied from $1 - 11$ M while the H^+ concentration was held constant at 0.5 M. Extractions by HDEHP are shown in Fig. 4.12. For the systems investigated

using HDEHP, equilibrium was observed to occur within 10 s under all H^+ and Cl^- conditions studied. For extractions of niobium by BEHP, equilibrium was reached within 20 s at 1 M H^+; while at all other concentrations it was reached within 10 s.
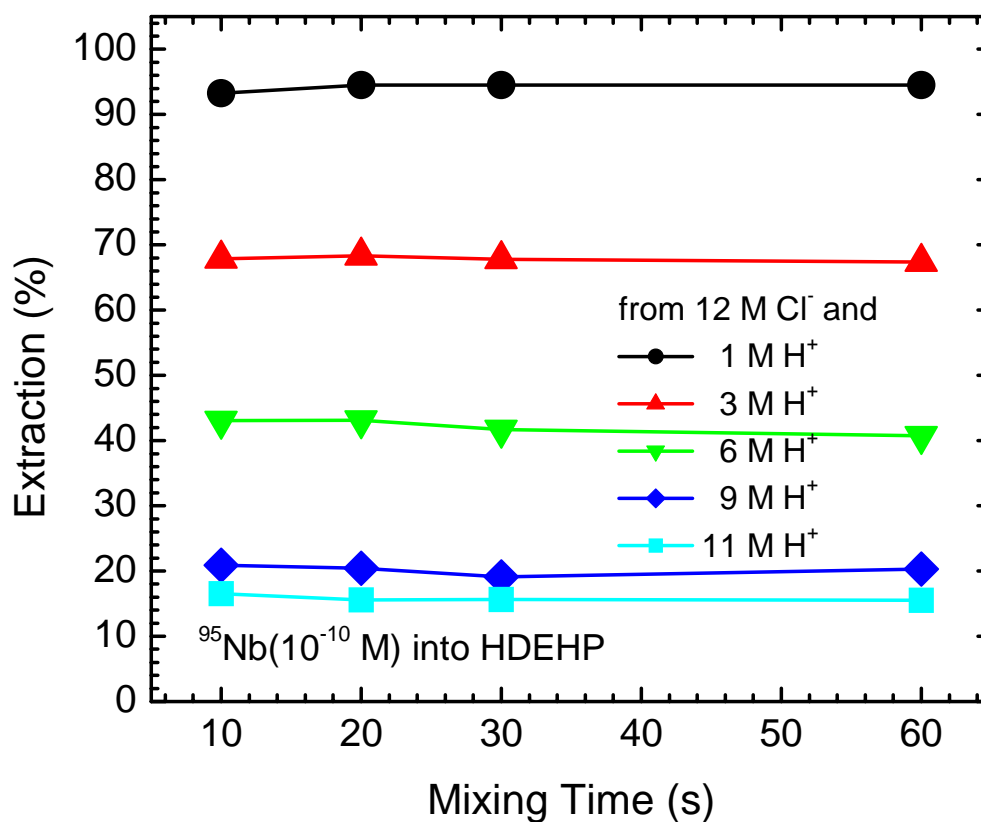
Fig. 4.10: Extraction of ^{95}Nb (10^{-10} M) from solutions of 12 M Cl^- and 1 (●), 3 (▲), 6 (▼), 9 (♦) or 11 (■) M H^+ by 0.01 M HDEHP in CHCl$_3$ as a function of mixing. Error bars are smaller than the symbols.
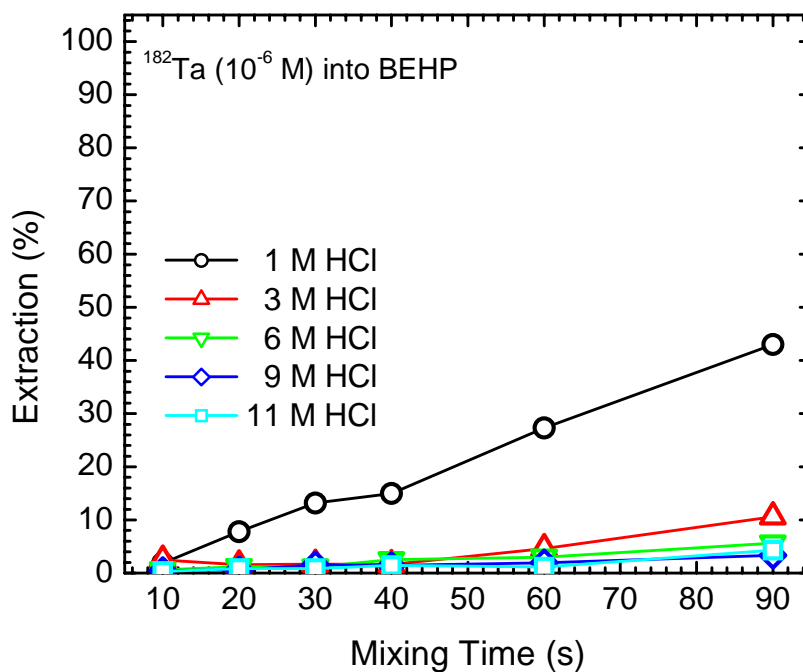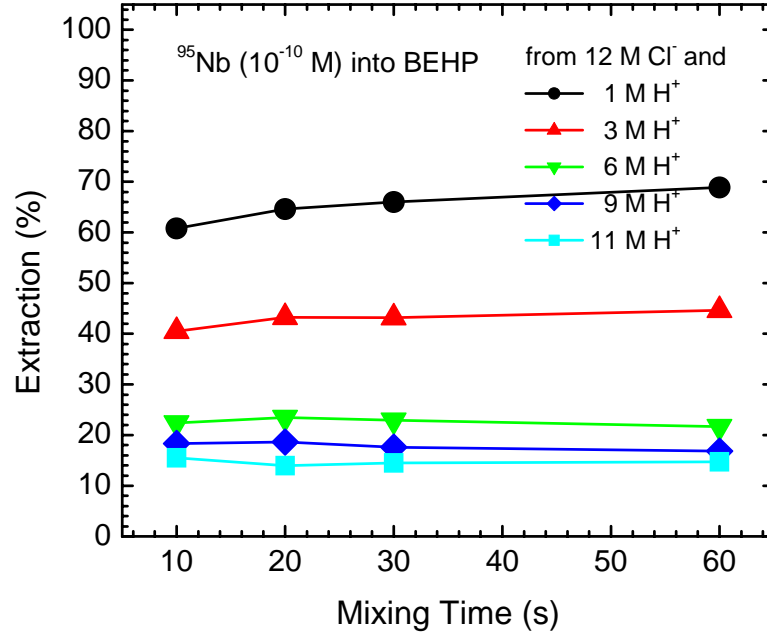
Fig. 4.11: Extraction of ^{95}Nb (10^{-10} M) from solutions of 12 M Cl$^-$ and 1 (●), 3 (▲), 6 (▼), 9 (♦) or 11 (■) M H$^+$ by 0.01 M BEHP in CHCl$_3$ as a function of mixing. Error bars are smaller than the symbols.
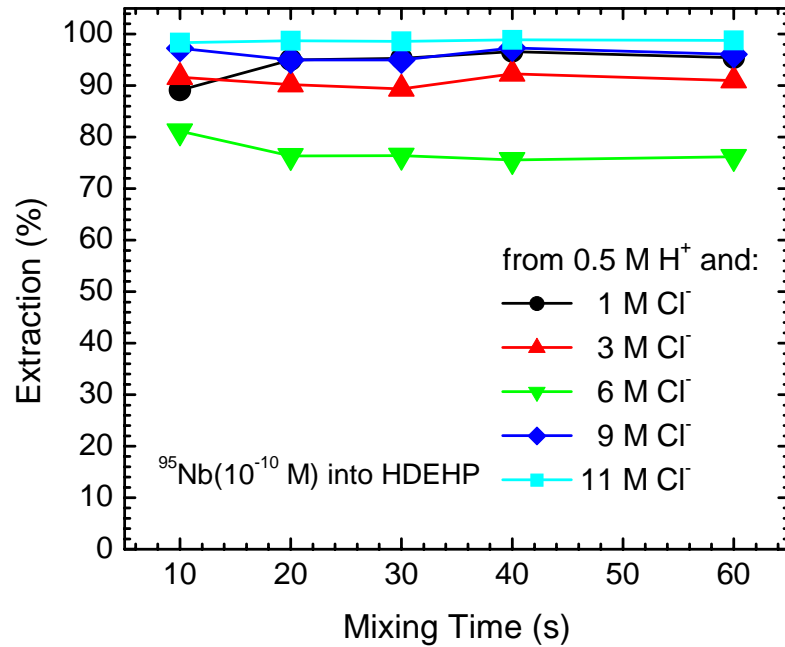
Fig. 4.12: Extraction of ^{95}Nb (10^{-10} M) from solutions of 0.5 M H$^+$ and 1 (●), 3 (▲), 6 (▼), 9 (♦) or 11 (■) M Cl$^-$ by 0.01 M HDEHP in CHCl$_3$ as a function of mixing. Error bars are smaller than the symbols.

The extraction of tantalum by HDEHP was also investigated as a function of mixing time. Only one set of experiments was performed, for which the H^+ concentration was held constant at 0.5 M and the Cl^- concentration was varied from 1 - 11 M, and the results are shown in Fig. 4.13. For all concentrations of Cl^-, equilibrium was reached within 30 s.

Both the extraction of niobium and tantalum showed that when the ratio of Cl^- to H^+ is >1, then the system reaches equilibrium in less time than when in pure HCl media. Based on the results from the kinetics experiments, the extraction of niobium and tantalum by HDEHP and BEHP was compared after 60 s of mixing, ensuring that equilibrium had been reached for all H^+ and Cl^- concentrations.
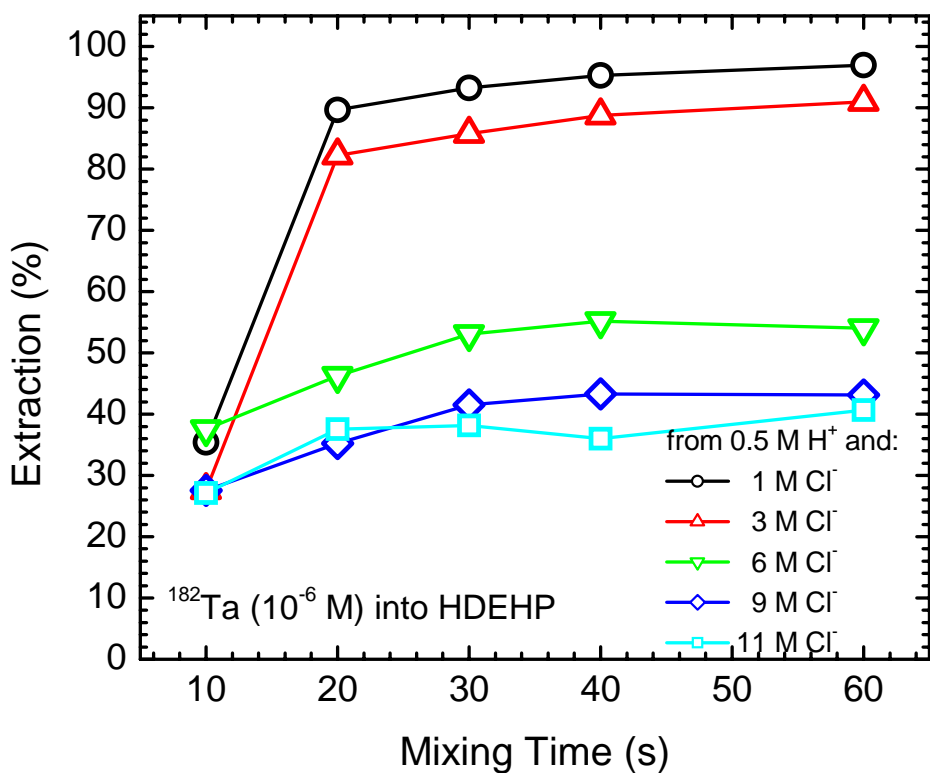
Fig. 4.13: Extraction of tantalum (10^{-6} M) from solutions of 1 (○), 3 (△), 6 (▽), 9 (◊) or 11 (□) M Cl^- and 0.5 M H^+ by 0.01 M HDEHP in $CHCl_3$ as a function of mixing time. Error bars are smaller than the symbols.

4.2.4 Niobium

The effect of varying the HCl, H^+ (at $12\,M\,Cl^-$) and Cl^- (at $0.5\,M\,H^+$) concentrations on the extraction of niobium by HDEHP and BEHP was investigated. Fig. 4.14 contains the results of the extractions by HDEHP. When the Cl^- concentration is varied at low H^+ concentrations, the extraction yield begins to decrease with increasing Cl^- concentration until above $6\,M\,Cl^-$. Above this point, the extraction yield begins to increase. In contrast, the extraction of niobium by HDEHP from solutions in which the H^+ concentration is varied at high Cl^-, decreases as the H^+ concentration is increased and the drop-off is faster than that observed as the HCl concentration was increased. The difference in this behavior is likely due to the effect that the H^+ and Cl^- have on the formation of complexes according to eqn. (1.16) as given earlier:

$$M(H_2O)_{\circ}^{+} + OH^- + L^- \leftrightarrow \tag{1.16}$$

$$M\ O\ (OH)\quad(H_2O)\ L^{(\ -\ -\ )+} + (\quad ^{\circ} +\quad -\quad)H_2O$$
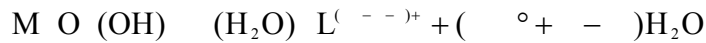
The presence of increased concentrations of H^+ will withdraw OH^- from solution and tend to shift the equilibrium towards the non-extractable hydrolysis products, $M(H_2O)_{w\circ}^{z+}$ or anionic complexes. In contrast, the addition of Cl^- to the system will shift equilibrium towards the formation of extractable cationic oxy- and hydroxychloro species, $M\ O\ (OH)\quad(H_2O)\ L^{(\ -\ -\ )+}$.
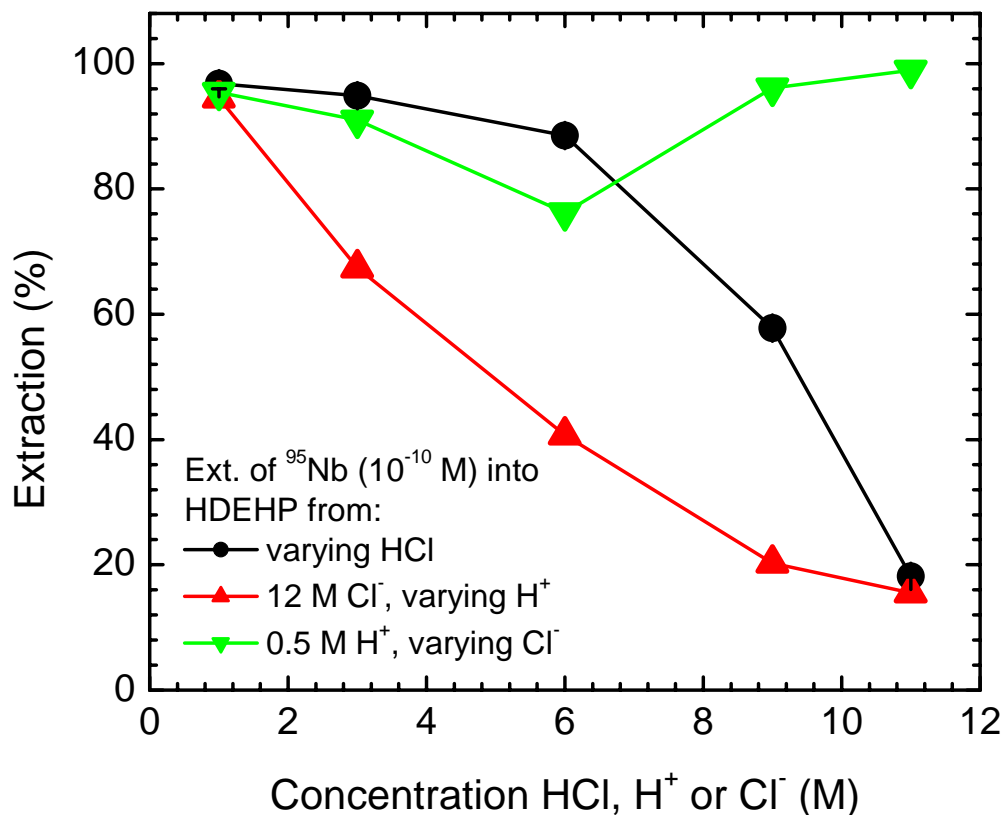
Fig. 4.14: Extraction of ^{95}Nb (10^{-10} M) into solutions of 0.01 M HDEHP from solutions of HCl/LiCl as a function of HCl ($\bullet$), H$^+$ at 12 M Cl$^-$ ($\blacktriangle$) or Cl$^-$ at 0.5 M H$^+$ ($\blacktriangledown$). Error bars are smaller than the symbols.

Results from the extraction of niobium by BEHP are shown in Fig. 4.15. As the H$^+$ concentration is increased, a decrease in extraction yield is observed. Until 11 M H$^+$, the extraction from mixed HCl/LiCl solutions is higher than the extraction from corresponding HCl solutions. This difference may be due to the increased formation of neutral complexes at high Cl$^-$, or due to adduct formation between cationic species, Cl$^-$ and BEHP.
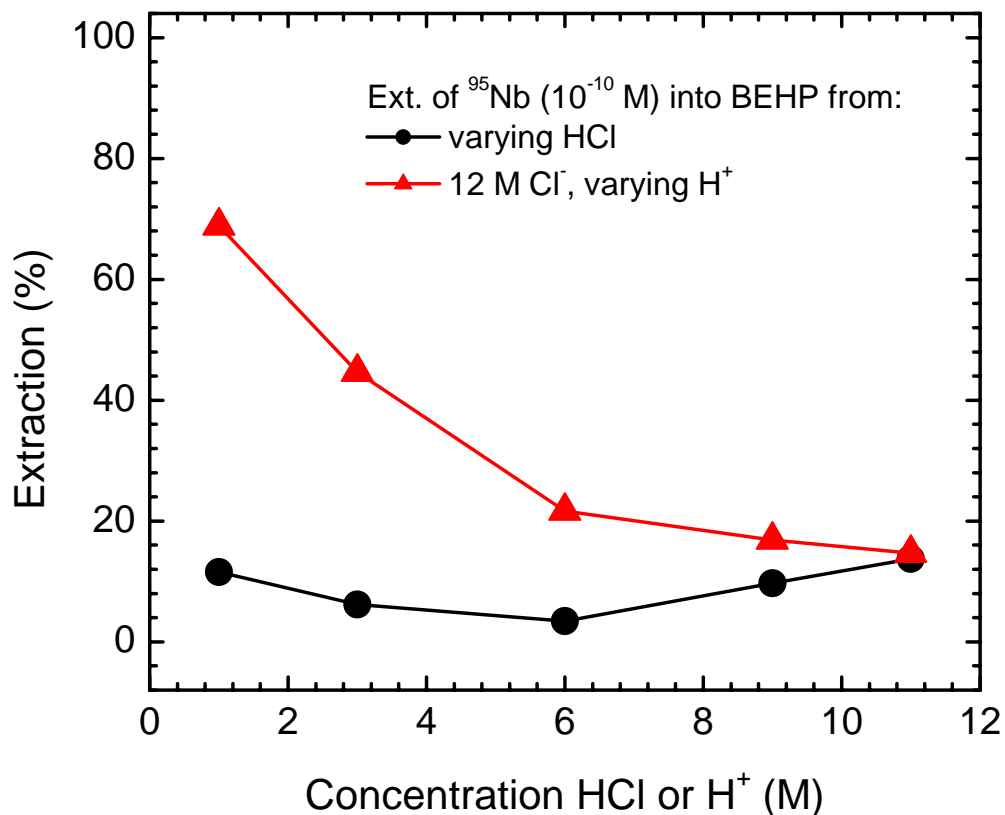
Fig. 4.15: Extraction of ^{95}Nb (10^{-10} M) into solutions of 0.01 M BEHP from solutions of HCl/LiCl as a function of HCl (●), H$^+$ at 12 M Cl$^-$ (▲). Error bars are smaller than the symbols.

4.2.5 Tantalum

The extraction of tantalum by HDEHP from solutions of HCl and HCl/LiCl was investigated as a function of HCl or Cl$^-$ (at 0.5 H$^+$) concentration. Results are shown in Fig. 4.16. Both systems exhibit similar extraction behavior, regardless of differences in H$^+$ concentration for a given Cl$^-$ concentration. A difference in extraction yields is observed at >6 M HCl, where the extraction yields from solutions with low H$^+$ were ~20 % higher than those observed from HCl solutions. This difference is likely due to equilibrium, as the extractions performed as the Cl$^-$ concentration was varied contain

95

results that are at equilibrium, while equilibrium was not observed at high HCl concentrations.
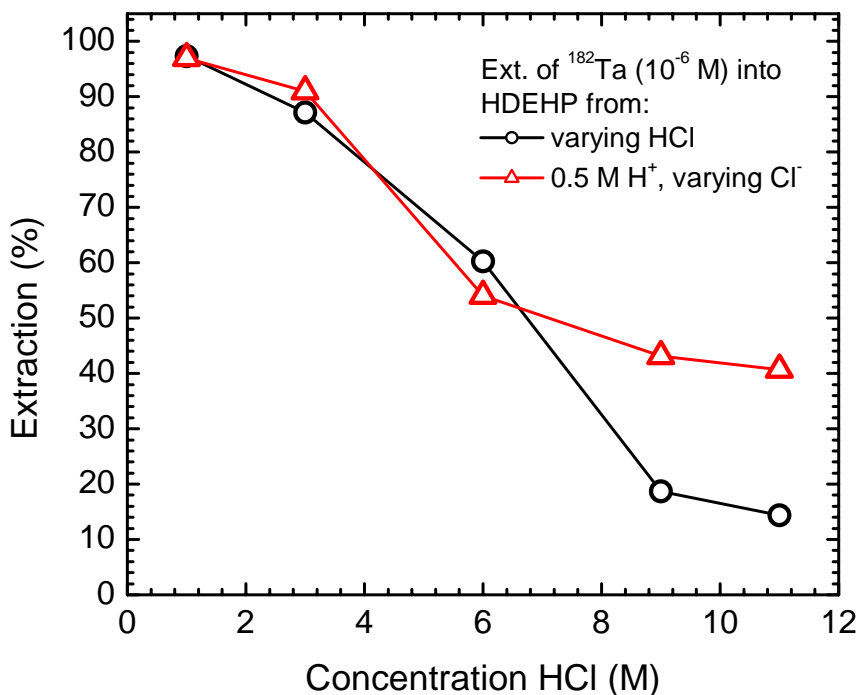
Fig. 4.16: Extraction of ^{182}Ta (10^{-6} M) into solutions of 0.01 M HDEHP from solutions of HCl/LiCl as a function of HCl (●), Cl$^-$ at 0.5 M H$^+$ (▲). Error bars are smaller than the symbols.

4.3   Summary

The off-line studies of the extraction of niobium from HCl solutions indicate the presence of cationic complexes in solution until ~9 M HCl. These species appear to dominant e the solution until ~6 M HCl as evidenced by extraction yields of > 85% when extracted by DiOPA, DEHPA or HDEHP. With increasing acid concentration, the extraction yield decreases, indicating the formation of the unextractable anionic

complexes. Neutral complexes do not appear to play a significant role in niobium chemistry, as evidenced by the low extraction of niobium by BEHP, regardless of HCl concentration. The extraction of tantalum from HCl solutions also indicated that the species in solution shift from cationic to anionic with increasing HCl concentration. However, this change appears to begin at very low HCl concentrations (< 3 M HCl), and anionic species begin to dominant e the solution around 6 M HCl. These acid concentrations are lower than what was observed for the niobium extraction, contrary to what is expected from the experiments summarized in Chap. 4.1.1. The difference may be due to the formation of polymeric and colloidal tantalum species, which would hinder the extraction.

When extractions were performed from solutions in which the H^+ concentration was held at low values while the Cl^- concentration was varied, then both niobium and tantalum showed similar behavior. As the Cl^- concentration was increased, the extraction yield decreased. This suggests that cationic species become less favorable with increasing Cl^- concentration. Since previous studies have shown that anionic complexes are not being formed at low H^+ concentrations, it is assumed that increasing the Cl^- concentration shifts equilibrium to the formation of neutral complexes [Kanzelmeyer1953; Kanzelmeyer1956; Nabivanets1962; Nabivanets1964]. However, the extractions of niobium with BEHP showed decreasing extraction yields with increasing Cl^- concentration, indicating that extractable neutral complexes are not being formed. This paradox requires further investigation, possibly with lower concentrations of niobium and tantalum to decrease any effects that polymerization of the metals has on the results. Equilibrium was observed to occur within 30 s for all the HCl/LiCl systems

97

studied, results that suggest the system is appropriate for application to dubnium chemistry.

Differences in chemical behavior were observed between niobium and tantalum when they were extracted by HDEHP and BEHP from both HCl and HCl/LiCl solutions. However, when in solution, dubnium will not interact with other dubnium atoms. The relatively high concentrations of niobium and tantalum used in the off-line studies will allow for tantalum-tantalum and niobium-niobium interactions. To ensure that these interactions are not overshadowing the chemistry of individual atoms, it is necessary to repeat the experiments on-line, using short-lived accelerator-produced isotopes of niobium and tantalum, as lower metal concentrations can be reached. Also, on-line studies will better replicate the studies with dubnium as formation of species containing O and OH- complexes is slow. In the on-line studies, these species may not have time to form before extraction. The extractions by HDEHP and BEHP from HCl and HCl/LiCl solutions were chosen as candidates for dubnium chemistry. Those studies were repeated on-line and the results are discussed in Chap. 5.

5   On-Line Extractions

The liquid-liquid extraction of cyclotron-produced isotopes of niobium and tantalum from hydrochloric acid media by bis(2-ethylhexyl) hydrogen phosphate (HDEHP) and bis(2-ethylhexyl) hydrogen phosphite (BEHP) was studied as a function of mixing time, acid concentration and H^+ concentration at fixed Cl^-. Fig. 1.5 shows the chemical structures of HDEHP and BEHP. Similar systems have been previously investigated using a variety of solvents and semi-macroscopic quantities of niobium and tantalum (See Chap. 4.1.1 for an overview) [Das1981; Kimura1960; Kimura1961]. However, to best replicate conditions under which dubnium will be studied, it is necessary to use 'carrier-free' trace level amounts ($\leq 10^{-16}$ M) of niobium and tantalum, formed in these nuclear reactions, to avoid the formation of polymeric species. On-line studies using short-lived accelerator-produced niobium and tantalum were performed at LBNL, using the procedures and isotopes as described in Chap. 2.3, to best replicate the experimental conditions present during a transactinide experiment. For these studies, the organic phase was 0.01 M HDEHP or BEHP in $CHCl_3$. Aqueous phases were either 1 – 11 M HCl or mixtures of HCl and LiCl in which the Cl^- concentration was fixed at 12 M and the H^+ concentration was varied from 1 – 11 M.

5.1 Extraction of Niobium and Tantalum from HCl Solutions

5.1.1 Kinetics

Extraction yields as a function of phase contact time were studied for both of the systems. Mixing times of 10 − 60 s were used for the investigation of niobium, while tantalum was studied over times ranging from 10 − 90 s. The results of the kinetics experiments are shown in Fig. 5.1 and 5.2 for the HDEHP system, and in Fig. 5.3 and 5.4 for the BEHP system.
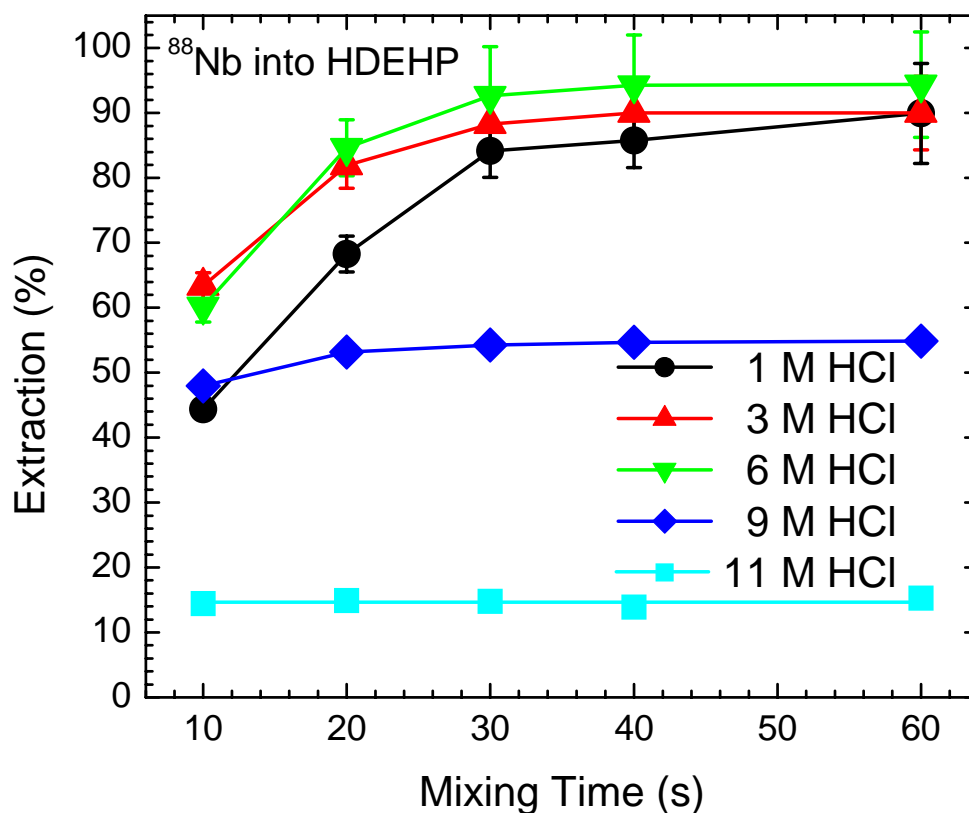
Fig. 5.1: Extraction of niobium from 1 (●), 3 (▲), 6 (▼), 9 (♦) or 11 (■) M HCl by 0.01 M HDEHP in $CHCl_3$ as a function of mixing time. Error bars are shown when larger than the symbol.
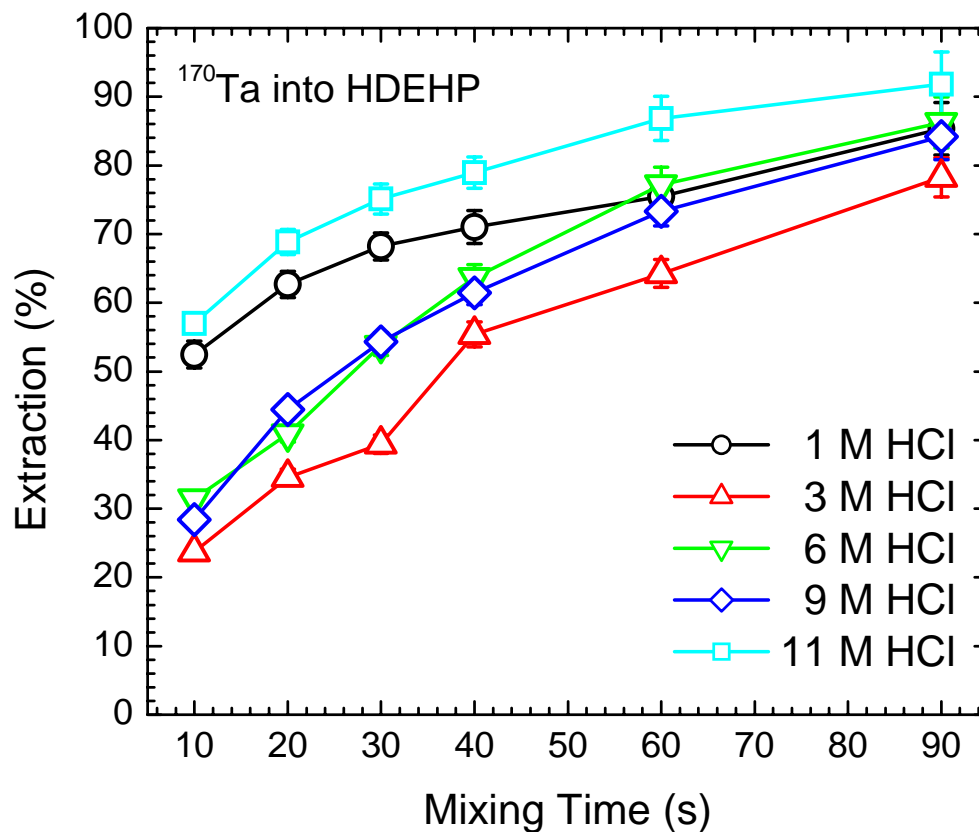
Fig. 5.2: Extraction of tantalum from solutions 1 (○), 3 (△), 6 (▽), 9 (◊) or 11 (□) M HCl by 0.01 M HDEHP in CHCl$_3$ as a function of mixing time. Error bars are shown when larger than the symbols.

Equilibrium in the HDEHP system was not observed for tantalum at any acid concentration up to the maximum 90 s mixing time (See Fig. 5.2). The amount of time needed for equilibrium to be reached in the niobium-HDEHP systems depended upon the acid concentration used (See Fig. 5.1). At 1 – 6 M HCl equilibrium was reached within 30 s, whereas equilibrium was reached within 20 s at 9 M HCl and 10 s at 11 M HCl.
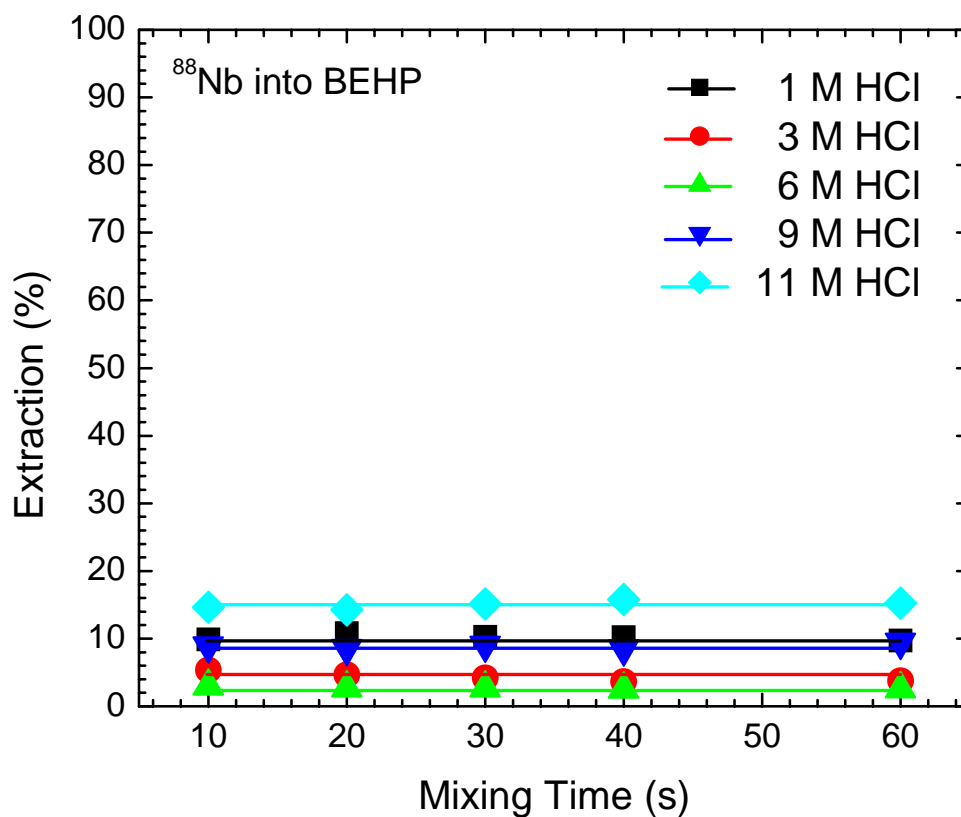
Fig. 5.3: Extraction of niobium from 1 (●), 3 (▲), 6 (▼), 9 (♦) or 11 (■) M HCl by 0.01 M BEHP in CHCl₃ as a function of mixing time. Error bars are smaller than the symbols.

Equilibrium times of <10 s were observed at all acid concentrations when the extraction of niobium with BEHP studied (See Fig. 5.3). For tantalum-BEHP, the amount of time needed to reach equilibrium was dependent upon the acid concentration (See Fig. 5.4). Equilibrium was reached within 40 s at 1, 3 and 6 M HCl, and not observed within 90 s at HCl concentrations of 11 and 9 M.
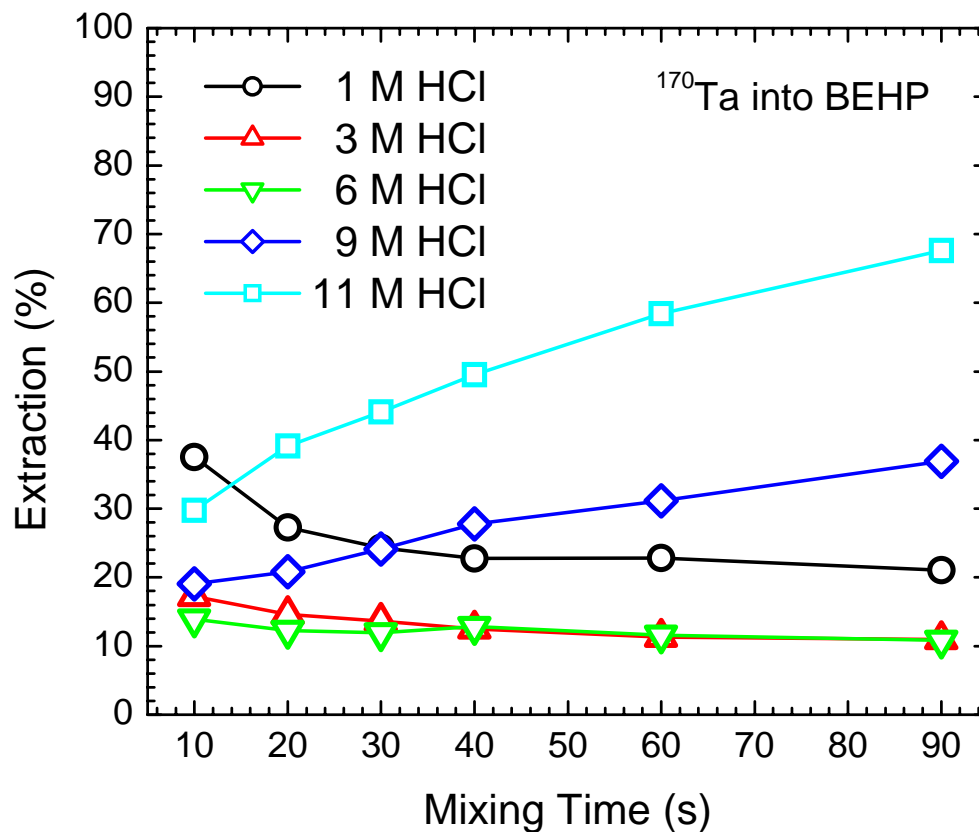
Fig. 5.4: Extraction of tantalum from solutions 1 ($\circ$), 3 ($\triangle$), 6 ($\triangledown$), 9 ($\diamond$) or 11 ($\square$) M HCl by 0.01 M BEHP in $CHCl_3$ as a function of mixing time. Error bars are smaller than the symbols.

Based on these results, a mixing time of 60 s was chosen for experiments with niobium, ensuring equilibrium regardless of acid concentration. A mixing time of 90 s was chosen for the tantalum experiments, as the short half-life of [170]Ta prevented mixing for longer times.

5.1.2   Niobium

The extraction of niobium into 0.01 M HDEHP or 0.01 M BEHP in chloroform was studied over a range of 1-11 M HCl. The results of these experiments are shown in Fig. 5.5. Low extraction yields of niobium by BEHP were observed. The highest yields of (15±1)% and (10±1)% were observed at 11 and 1 M HCl, respectively, while 6 M HCl had the lowest yield of (2.6±0.3)%. For the extractions with HDEHP, the observed yield was greater than 90% for the three lower acid concentrations investigated
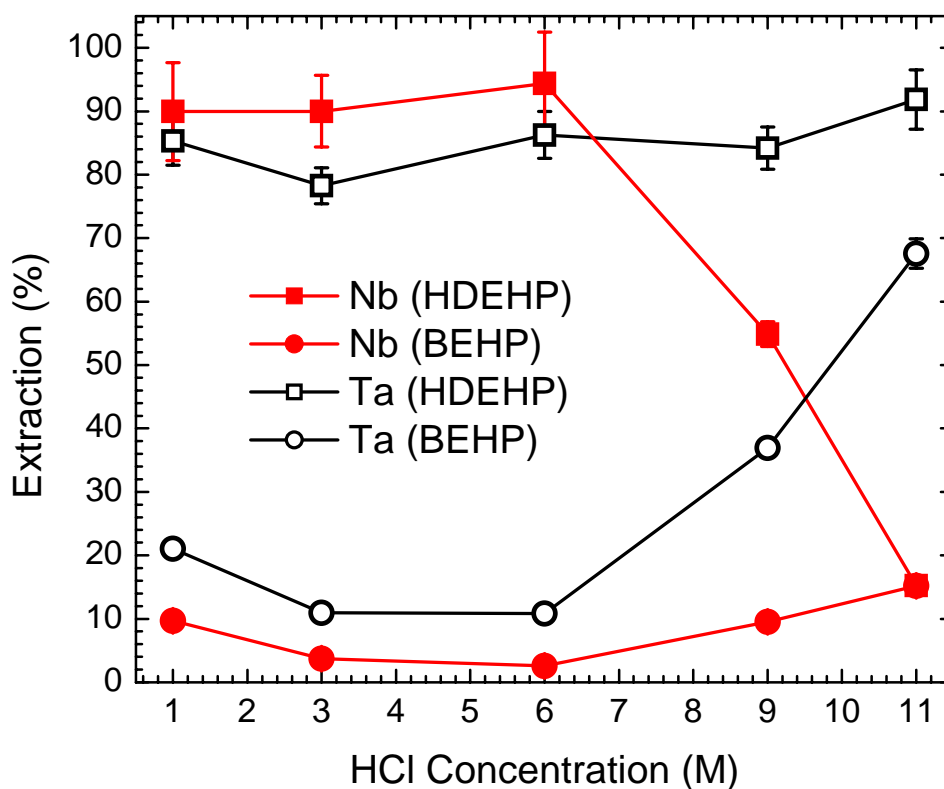
Fig. 5.5: Comparison of extraction yields for niobium (■,●, after 60 s mixing) and tantalum (□,○, after 90 s mixing). The organic phase was 0.01 M HDEHP (■,□) or 0.01 M BEHP (●,○) in CHCl$_3$. The aqueous phase consisted of 1 - 11 M HCl. Error bars are shown when larger than the symbols.

(1, 3, and 6 M HCl). When the acid concentration was increased above 6 M HCl, the yields decreased to $(55\pm2)\%$ at 9 M HCl and $(15\pm1)\%$ at 11 M HCl. The results from the HDEHP extractions are in agreement with those shown by Kimura when niobium was extracted from HCl solutions into 50% HDEHP in toluene [Kimura1960]. However, Das *et al.* observed that the niobium extraction yield increased from 18.6 to 32.2 % as the HCl concentration was increased from 0.8 to 5.6 N when using an organic phase of 0.01 M HDEHP in carbon tetrachloride [Das1981]. Both studies were performed using tracer levels of ^{95}Nb.

Experiments with semi-macroscopic amounts of niobium have determined that the niobium species change from polymeric cationic complexes based on $Nb(OH)_2Cl_2^+$ and $NbOCl_2^+$ at low HCl concentrations to neutral complexes like $Nb(OH)_2Cl_3$ around $3-6$ M HCl [Kim1973]. At $6-9$ M HCl, the predominant specie in solution is $Nb(OH)_2Cl_4^-$ [Kanzelmeyer1953; Kanzelmeyer1956] and is replaced by $NbOCl_4^-$, $NbOCl_5^{2-}$ and $NbCl_6^-$ above 11 M HCl [Sabatini1966]. Campderrós *et al.* suggest the formation of cationic $HNbOCl_3^+$ complexes if the H^+ concentration is raised above 8 M HCl [Campderrós2000]. From what is known about niobium complex formation, HDEHP and BEHP, the following general mechanisms for the extraction of niobium by HDEHP and BEHP can be postulated:

1. Ionic association of HDEHP dimers with cationic complexes at low HCl concentrations:
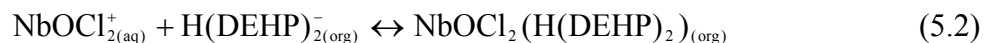
$$Nb(OH)_2Cl_{2(aq)}^+ + H(DEHP)_{2(org)}^- \leftrightarrow Nb(OH)_2Cl_2(H(DEHP)_2)_{(org)} \qquad (5.1)$$

$$NbOCl_{2(aq)}^+ + H(DEHP)_{2(org)}^- \leftrightarrow NbOCl_2(H(DEHP)_2)_{(org)} \qquad (5.2)$$

2. Adduct formation of neutral complexes and HDEHP dimers or BEHP at medium HCl concentrations:

$$Nb(OH)_2 Cl_{3(aq)} + HDEHP_{2(org)} \leftrightarrow Nb(OH)_2 Cl_3 (HDEHP)_{2(org)} \qquad (5.3)$$

$$Nb(OH)_2 Cl_{3(aq)} + BEHP_{(org)} \leftrightarrow Nb(OH)_2 Cl_3 (BEHP)_{(org)} \qquad (5.4)$$
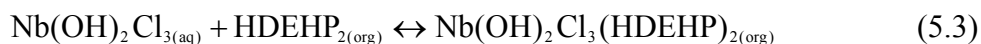
3. Ionic association of HDEHP dimers with cationic complexes at high HCl concentrations:

$$HNbOCl^+_{3(aq)} + H(DEHP)^-_{2(org)} \leftrightarrow HNbOCl_3 (H(DEHP)_2)_{(org)} \qquad (5.5)$$

Based upon our data, we can determine which mechanisms contribute to the total extraction. As BEHP only extracted small quantities of niobium, we conclude that $Nb(OH)_2 Cl_{3(aq)}$ is either not present in large amounts, or is not extractable through adduct formation with BEHP and HDEHP, thus eqns. (5.3) and (5.4) do not significantly contribute to the extraction. We also observed a decreasing extraction yield above 6 M HCl, suggesting that cationic niobium species are not present in solution, and by extension, that eqn. (5.5) does not contribute significantly to the extraction. Thus, eqns. (5.1) and (5.2) present the dominant extraction mechanisms.

5.1.3 Tantalum

Tantalum was extracted into solutions of 0.01 M HDEHP or 0.01 M BEHP in chloroform from 1-11 M HCl. The results are show in Fig. 5.5. For the extractions with BEHP, the yield decreased from 1 to 3 M HCl and began increasing after the HCl concentration was raised above 6 M. A maximum extraction of $(68\pm2)\%$ was observed for 11 M HCl and a minimum of $(11\pm1)\%$ at 3 and 6 M HCl. Over the whole acid concentration range studied, the extraction of tantalum by HDEHP remained above

>78%. A similar extraction pattern by HDEHP was seen from solutions of up to 1 M HCl in experiments by Kimura [Kimura1960]; however extraction yields were below those observed in this work. Das also investigated the extraction of tantalum by 0.01 M HDEHP in carbon tetrachloride and observed a decreasing extraction yield when the HCl concentration was raised above 1.6 N HCl [Das1981]. Both of these experiments were performed using ^{182}Ta, produced in the neutron irradiation of ^{181}Ta, and contain significant amounts of carrier. Differences between the experiments presented in [Das1981; Kimura1960] and those presented in this work are likely due to formation of different tantalum complexes. When tantalum is present in solution in semi-macroscopic amounts, the formation of polynuclear species in the form of $(TaO_{>1}Cl_{<3}nCl)_x$ hinders its extraction [Schäfer1959]. In this work, the tantalum concentration was ~10^{-16} M, preventing the formation of polynuclear species. In addition, the kinetics of forming complexes with O and OH$^-$ are slow. As such, on-line produced tantalum may have fewer of these complexes than off-line tracer solutions.

The data from the HDEHP and BEHP extractions in Fig. 5.5 show that niobium and tantalum have similar chemical behavior at $\leq$6 M HCl. This indicates that niobium and tantalum form similar complexes at $\leq$6 M HCl, leading to the conclusion that tantalum *may be* forming cationic complexes such as $Ta(OH)_2Cl_2^+$ and $TaOCl_2^+$. In addition, Campderrós *et al.* have suggested that $Ta(OH)Cl_4$ exists at low HCl concentrations and can be extracted by tributyl phosphate [Campderrós2000], a neutral complex exchanger similar to BEHP. Based on these assumptions, the following mechanisms can be *tentatively* postulated for extractions at $\leq$6 M HCl:

1. Ionic association of HDEHP with cationic complexes:

$$TaOCl_{2(aq)}^{+} + H(DEHP)_{2(org)}^{-} \leftrightarrow TaOCl_2(H(DEHP)_2)_{(org)} \qquad (5.6)$$

$$Ta(OH)_2Cl_{2(aq)}^{+} + H(DEHP)_{2(org)}^{-} \leftrightarrow Ta(OH)_2Cl_2(H(DEHP)_2)_{(org)} \qquad (5.7)$$
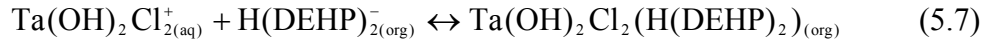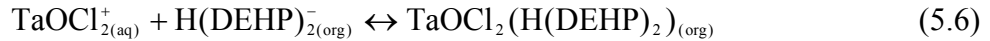
2. Adduct formation with BEHP at low HCl concentrations:

$$Ta(OH)_4Cl_{aq} + BEHP_{org} \leftrightarrow Ta(OH)_4Cl(BEHP)_{org} \qquad (5.8)$$
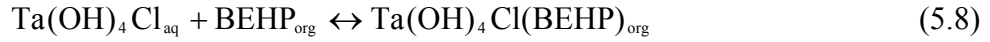
At high acid concentrations, anionic tantalum complexes should be the dominant species in solution. Electrodialysis experiments have shown that tantalum begins to form anionic species at acid concentrations approximately 1 M higher than those seen for niobium [Nabivanets1964; Nabivantes1962]. This would suggest the formation of $Ta(OH)_2Cl_4^{-}$ at >6 M HCl, $TaOCl_4^{-}$ at medium HCl concentrations and $TaCl_6^{-}$ above 12 M HCl [Pershina1998b]. We observed high extraction of tantalum by both HDEHP and BEHP at acid concentrations from 9 - 11 M, indicating that HDEHP and BEHP either form neutral complexes or that the formation of cationic species becomes favorable again with increasing hydrogen ion concentration. If tantalum has the tendency to form cationic complexes analogous to those observed by niobium at high hydrogen ion concentrations, such as $HTaOCl_3^{+}$, then the high extraction yields *may be* explained by ionic association of HDEHP and BEHP with cationic complexes:

$$HTaOCl_{3(aq)}^{+} + H(DEHP)_{2(org)}^{-} \leftrightarrow HTaOCl_3(H(DEHP)_2)_{(org)} \qquad (5.9)$$

$$HTaOCl_{3(aq)}^{+} + Cl_{(aq)}^{-} + BEHP_{(org)} \leftrightarrow HTaOCl_3Cl(BEHP)_{(org)} \qquad (5.10)$$

108

5.2 Extraction of Niobium and Tantalum from HCl/LiCl Solutions

5.2.1 Kinetics

For each aqueous phase, the samples were mixed for 10 - 60 s to obtain information regarding the amount of time the system needed to reach equilibrium. Results of these experiments are contained in Fig.s 5.6 - 5.9. Niobium extraction equilibrium was reached within 10 s at all H^+ concentrations studied for both of the extraction systems (See Fig. 5.6 and 5.8). Tantalum showed a different equilibrium behavior as equilibrium was reached within 10 s only when HDEHP was used as an extractant and the aqueous phase consisted of 1 or 3 M H^+. Equilibrium was not reached within 60 s at the other three H^+ concentrations when HDEHP was used as an extractant (See Fig. 5.7). In contrast, equilibrium was reached within 30 s when tantalum was extracted by BEHP from 11 M H^+ and not reached within 60 s when the H^+ concentration was decreased (See Fig. 5.9). Based on these results and the short half-lives of the isotopes studied, mixing times of 60 s were chosen for both the niobium and tantalum experiments.
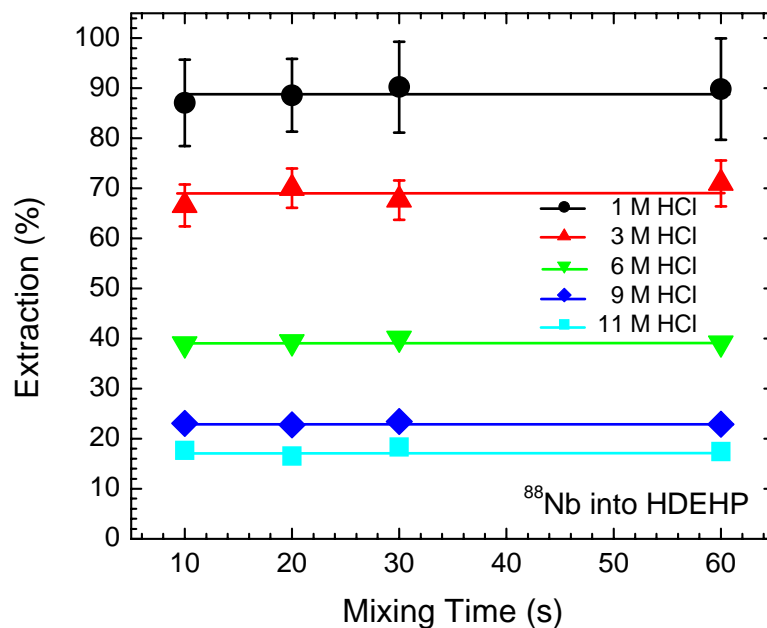
Fig. 5.6: Extraction of niobium from solutions of 12 M Cl⁻ and 1 (●), 3 (▲), 6 (▼), 9 (◆) or 11 (■) M H⁺ by 0.01 M HDEHP in CHCl₃ as a function of mixing time. Error bars are shown when larger than the symbol.
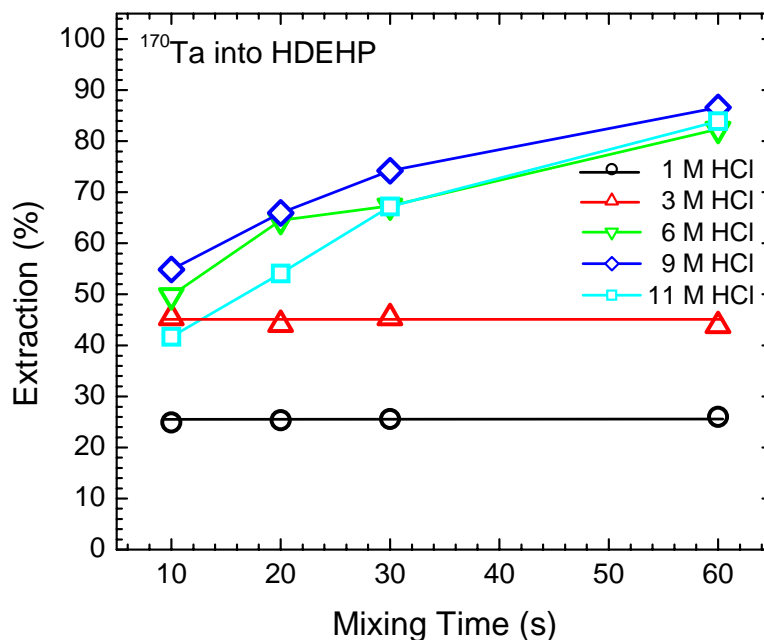
Fig. 5.7: Extraction of tantalum from solutions of 12 M Cl⁻ and 1 (○), 3 (△), 6 (▽), 9 (◇) or 11 (□) M H⁺ by 0.01 M HDEHP in CHCl₃ as a function of mixing time. Error bars are smaller than the symbols.
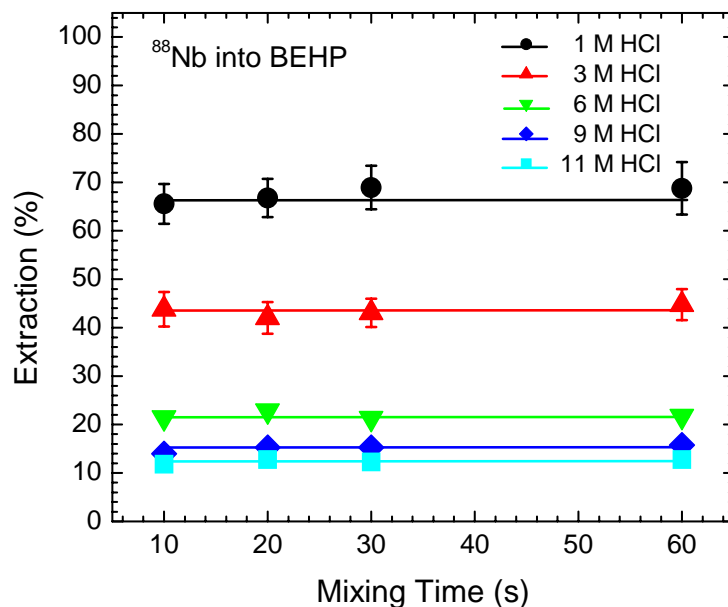
Fig. 5.8: Extraction of niobium from solutions of 12 M Cl⁻ and 1 (●), 3 (▲), 6 (▼), 9 (♦) or 11 (■) M H⁺ by 0.01 M BEHP in CHCl₃ as a function of mixing. Error bars are shown when larger than the symbol.
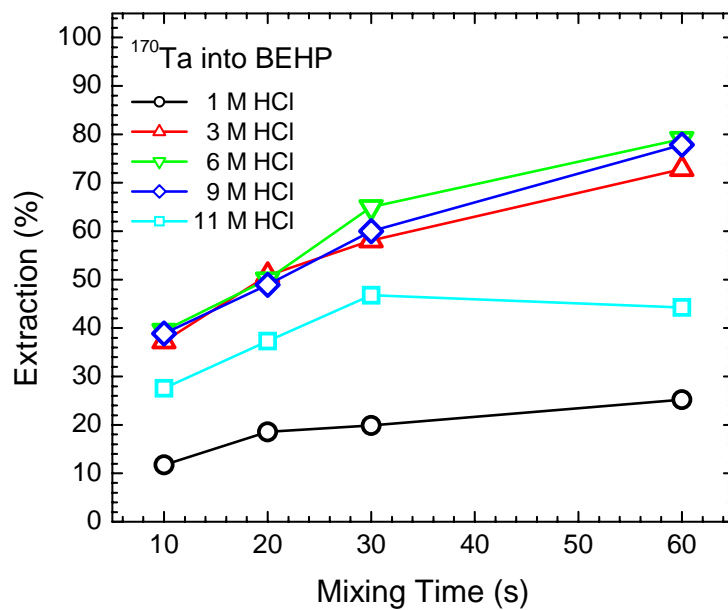
Fig. 5.9: Extraction of tantalum from solutions of 12 M Cl⁻ and 1 (○), 3 (Δ), 6 (▽), 9 (◊) or 11 (□) M H⁺ by 0.01 M BEHP in CHCl₃ as a function of mixing time. Error bars are smaller than the symbols.

5.2.2   Niobium

The extraction of niobium mixed HCl/LiCl solutions by 0.01 M HDEHP and 0.01 M BEHP in chloroform was studied at Cl^- concentrations of 12 M and over a H^+ concentration of 1 – 11 M, as shown in Fig. 5.10. When HDEHP is used, the extraction of niobium decreases from 90±10% to 17.4±1.4% as the H^+ is increased from 1 to 11 M. The extraction of niobium by BEHP followed a similar pattern. The maximum amount (69±5%) of niobium was extracted at 1 M H^+ and the extraction yield decreased with increasing H^+ concentration to a minimum of 12.7±0.4% at 11 M H^+. The low extraction yields at increased H^+ concentrations are consistent with observations made previously (see Chap. 5.1.1).
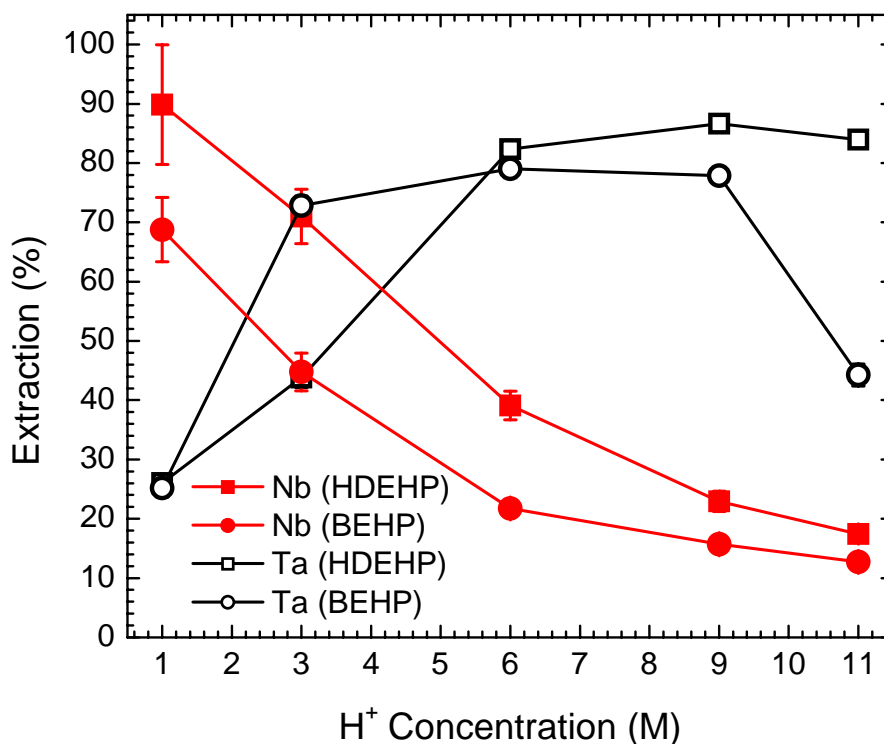
Fig. 5.10: Comparison of extraction yields for niobium (■,●) and tantalum (□,○) after 60 seconds of mixing. The organic phase was 0.01 M HDEHP (■,□) or 0.01 M BEHP (●,○) in CHCl₃. The aqueous phase consisted of 12 M Cl^- and 1 - 11 M H^+. Error bars are shown when larger than the symbols.

Experiments with semi-macroscopic amounts of niobium have also determined that cationic niobium species such as $Nb(OH)_2 Cl_2^+$ and $NbOCl_2^+$ exist at low HCl concentrations [Kim1973]. Kanzelmeyer *et al.* has also suggested that the predominant species in solution at high H^+ and Cl^- concentration is $Nb(OH)_2 Cl_4^-$ and that $Nb(OH)_3 Cl_2$ is formed at the H^+ concentration is lowered. [Kanzelmeyer1953; Kanzelmeyer1956] (see Chap 4.2.1 for a summary). Based upon this information we tentatively propose the following extraction mechanisms at low H^+ concentrations:

4. Adduct formation of the neutral complexes and HDEHP dimers or BEHP at low H^+ concentrations:

$$Nb(OH)_3 Cl_{2(aq)} + BEHP_{(org)} \leftrightarrow Nb(OH)_3 Cl_2 (BEHP)_{(org)} \qquad (5.12)$$

$$Nb(OH)_3 Cl_{2(aq)} + (HDEHP)_{2(org)} \leftrightarrow Nb(OH)_3 Cl_2 (HDEHP)_{2(org)} \qquad (5.13)$$
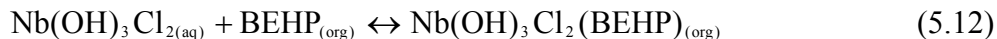
5. Ionic association of HDEHP dimers with cationic complexes at low H^+ concentrations:

$$Nb(OH)_2 Cl_{2(aq)}^+ + H(DEHP)_{2(org)}^- \leftrightarrow Nb(OH)_2 Cl_2 (H(DEHP)_2)_{(org)} \qquad (5.14)$$

$$NbOCl_{2(aq)}^+ + H(DEHP)_{2(org)}^- \leftrightarrow NbOCl_2 (H(DEHP)_2)_{(org)} \qquad (5.15)$$
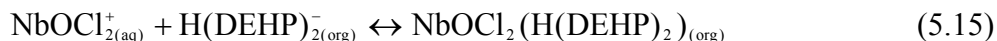
With increasing H^+ concentration, the formation of the anionic $Nb(OH)_2 Cl_4^-$ complex begins to dominant e, resulting in decreased extraction yields.

5.2.3   Tantalum

Fig. 5.10 contains the results of the extraction of tantalum by 0.01 M HDEHP or 0.01 M BEHP in chloroform from solutions of 12 M Cl^+ and 1 – 11 M H^+. Over the H^+ concentration range, the amount of tantalum extracted by HDEHP increased from 26±1%

113

to 87±1% as the H$^+$ concentration was raised from 1 to 9 M and then decreased slightly to 84±1% at 11 M H$^+$. The extraction with BEHP showed a similar pattern as the amount of tantalum that was extracted increased as the H$^+$ concentration was raised from 1 M (25±2%) to 6 M (79±1%). A decrease in extraction yield, to 44±2%, was then observed at 11 M H$^+$. The extraction yields observed at 11 M H$^+$ are consistent with observations made previously (see Chap. 5.1.1).

The difference between tantalum and niobium extractions as the H$^+$ concentration is increased indicates that niobium and tantalum are not forming similar complexes. The increase in the extraction yield of tantalum over the same concentration range for which the extraction of niobium decreases suggests that the formation of the anionic species, such as $Ta(OH)_2Cl_4^-$, is not favorable. It is also notable that the extraction of tantalum by HDEHP is below 50% at ≤3 M HCl. The extraction of tantalum by BEHP begins at lower H$^+$ concentrations than it does for HDEHP, while high extraction of tantalum by HDEHP occurs through 11 M H$^+$. These observations may suggest the formation of neutral complexes, e.g. $Ta(OH)_3Cl_2$, at medium H$^+$ concentrations and cationic species, e.g. $HTaOCl_3^+$, as the H$^+$ concentration is increased. From these assumptions, the following extraction mechanisms *may be* examples of the types of reactions between tantalum and HDEHP or BEHP:

1. Adduct formation of neutral complexes with HDEHP dimers or BEHP at medium H$^+$ concentrations:
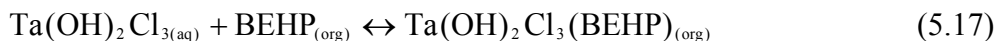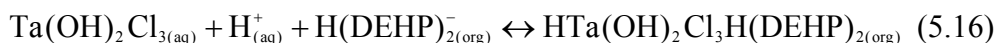
$$Ta(OH)_2Cl_{3(aq)} + H_{(aq)}^+ + H(DEHP)_{2(org)}^- \leftrightarrow HTa(OH)_2Cl_3H(DEHP)_{2(org)} \quad (5.16)$$

$$Ta(OH)_2Cl_{3(aq)} + BEHP_{(org)} \leftrightarrow Ta(OH)_2Cl_3(BEHP)_{(org)} \quad (5.17)$$

2. Ionic association of HDEHP dimers with cationic complexes at high H^+ concentrations:

$$HTaOCl_{3(aq)}^+ + H(DEHP)_{2(org)}^- \leftrightarrow HTaOCl_3(H(DEHP)_2)_{(org)} \qquad (5.18)$$

3. Adduct formation of HDEHP dimers with cationic complexes at high H^+ concentrations:

$$HTaOCl_{3(aq)}^+ + Cl_{(aq)}^- + HDEHP_{2(org)} \leftrightarrow HTaOCl_3Cl(HDEHP)_{2(org)} \qquad (5.19)$$
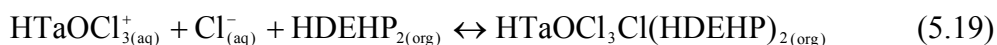
Eqn. (10) requires the existence of a deprotonated HDEHP complex in the same solutions that form a protonated $TaOCl_3$. As such, mechanisms similar to those proposed in eqn. (5.19) may more realistically represent extraction at high H^+ and Cl^- ion concentrations than eqn. (5.18).

5.3   Comparisons of Macro- and Microscopic Concentrations

5.3.1   Niobium

The extraction of niobium by HDEHP and BEHP was studied at three different metal concentrations: 10^{-6}, 10^{-10} and 10^{-16} M. These results are shown in Fig. 5.11. The behavior of extraction is very similar, regardless of niobium concentration. Differences between the different metal concentrations are only observed at low HCl concentrations when the extract is BEHP. In this case, the extraction of niobium is much higher for 10^{-6} M niobium. At low HCl and high niobium concentrations, the formation of neutral, polynuclear species is favored. The high extraction yields at 1 M HCl may be due to extraction of these polynuclear species.

115
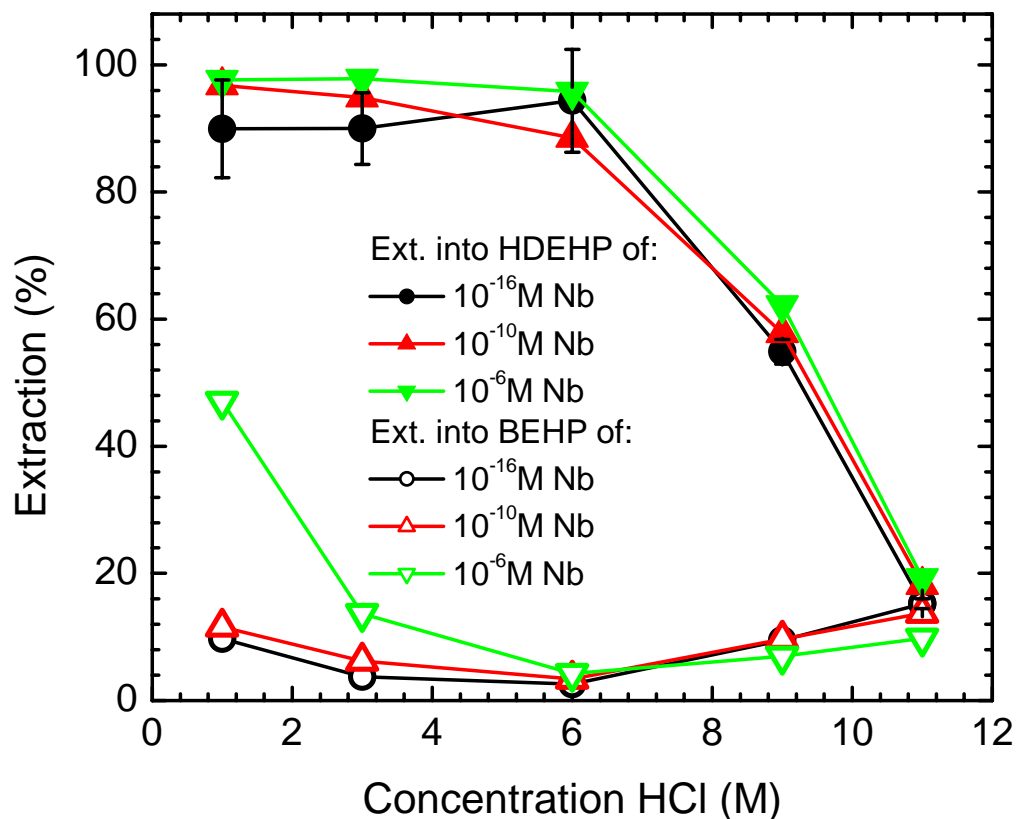
Fig. 5.11: Comparison of the extraction of 10^{-16} M ($\bullet$,$\circ$), 10^{-10} M ($\blacktriangle$,$\triangle$) and 10^{-6} M ($\blacktriangledown$,$\triangledown$) niobium into solutions of 0.01 M HDEHP ($\bullet$,$\blacktriangle$,$\blacktriangledown$) or BEHP ($\circ$,$\triangle$,$\triangledown$) in CHCl$_3$ as a function of HCl concentration. Error bars are shown when larger than the symbols.

5.3.2 *Tantalum*

The formation of polymeric or polynuclear species is well-known for tantalum. To determine whether the concentration of tantalum in the solution had an impact on the extraction yield, the extraction of 10^{-16} and 10^{-6} M tantalum by HDEHP and BEHP was studied as a function of HCl concentration. The results of these studies are shown in Fig. 5.12. The extraction behavior was observed to be very dependent on the concentration of metal in solution. At < 3 M HCl, higher extraction yields by both BEHP

and HDEHP were observed with the more concentrated metal solution (10^{-6} M). However, above 3 M HCl, the extraction yields were highest for the lower (10^{-16} M) metal concentration. Several factors may be influencing the observed difference:

i)   formation of polymeric species at low HCl concentrations. These species may be extracted more readily by HDEHP and BEHP.

ii) 'age' of the solutions: the extractions with 10^{-16} M tantalum were performed using short-lived, accelerator-produced tantalum while studies with 10^{-6} M tantalum were performed off-line, using long-lived isotopes. As the kinetics of forming complexes with O and OH⁻ are slow, on-line produced tantalum may have fewer of these complexes than off-line tracer solutions.

iii) Fluoride contamination: the tantalum used to produce the 10^{-6} M solution was first dissolved in fluoride. While a step was added to destroy the remaining fluoride, traces may have remained in solution
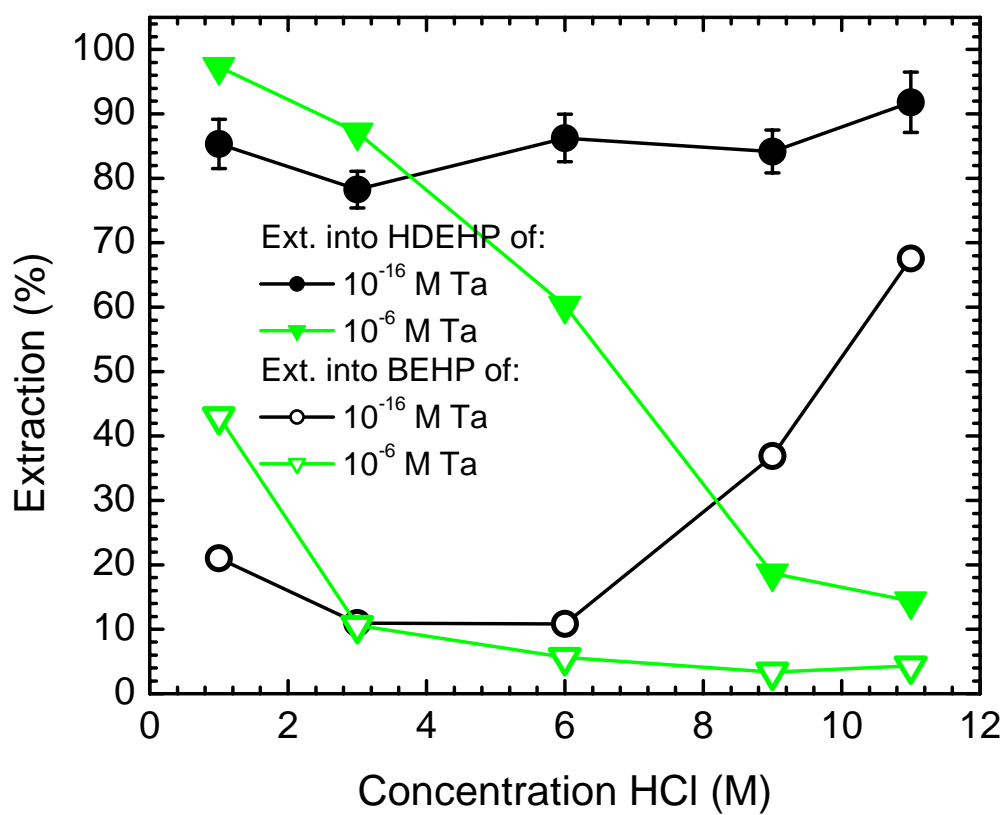
Fig. 5.12: Comparison of the extraction of 10^{-16} M ($\bullet$,$\circ$) and 10^{-6} M ($\blacktriangledown$,$\triangledown$) tantalum into solutions of 0.01 M HDEHP ($\bullet$,$\blacktriangledown$) or BEHP ($\circ$,$\triangledown$) in CHCl$_3$ as a function of HCl concentration. Error bars are shown when larger than the symbols.

6 Measurement of the ^{88g}Nb half-life and ^{74}Se(^{18}O,$p3n$) excitation function

6.1 The ^{88g}Nb Half-Life

The half-life of ^{88g}Nb has been measured several times previously, leading to values of 14.4±0.2 min [Oxorn1984] 14.3±0.3 min [Iafigliola1972] and 13.3±1.0 min [Doron1971]. During the experiments mentioned in this dissertation, the half-lives of reaction products collected at the back end of the BGS during the ^{74}Se(^{18}O,p3n) reaction were measured. The setup for these reactions was the same as described for the chemistry experiments (See Chap. 2.3.1). Reaction products recoiled out of the ^{74}Se target and were separated by the BGS. The evaporation residues (EVRs) were thermalized in the RTC, captured on KCl aerosols and transported to a collection apparatus. The aerosols were collected for 30 – 45 minutes and then dissolved in 3 mL dilute hydrochloric acid (HCl). The 3 mL aliquots were then counted using a HPGe γ–detector using counting intervals of 3 min. Four parallel experiments were performed and the spectra from each counting interval were summed.

Fig. 6.1 contains a sample spectrum obtained from the collected reaction products. Lines that are significantly above background are labeled. In addition to the ground state, ^{88}Nb is known to have a metastable state with a half-life of 7.7 min and several prominent γ-ray energies (271.80, 671.20, 1057.01 and 1082.53 keV) can be from the decay of either ^{88g}Nb and ^{88m}Nb [Oxorn1984]. However, ^{88m}Nb also contains lines at 262.04, 450.52 and 760.76 keV that are not present in the decay of ^{88g}Nb [Oxorn1984]. As these lines were not observed in any of the spectra from the reaction products, it was

determined that contamination in the 271.80, 671.20, 1057.01 and 1082.53 keV lines due to decay of ^{88m}Nb is negligible.

The ^{88g}Nb half-life was determined from the decay curves fitted to the 271.80, 671.20, 1057.01 and 1082.53 keV lines using first order exponentials, as shown in Fig. 6.2. These fits resulted in a weighted-average half-life of 14.56±0.11 min, consistent with and more precise than previous measurements [Iafigliola1972; Oxorn1984].
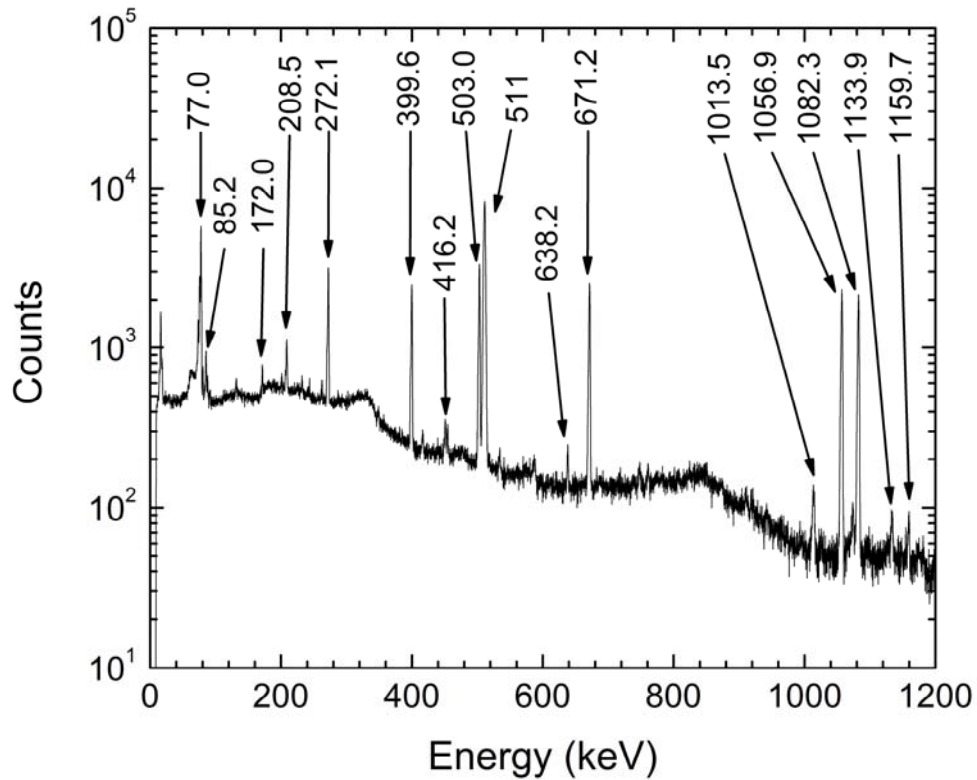
Fig. 6.1: Sample γ-ray spectrum of the recoil products obtained from a bombardment of ^{74}Se with ^{18}O, after separation by the BGS. Lines significantly above background are labeled with their energies in keV.
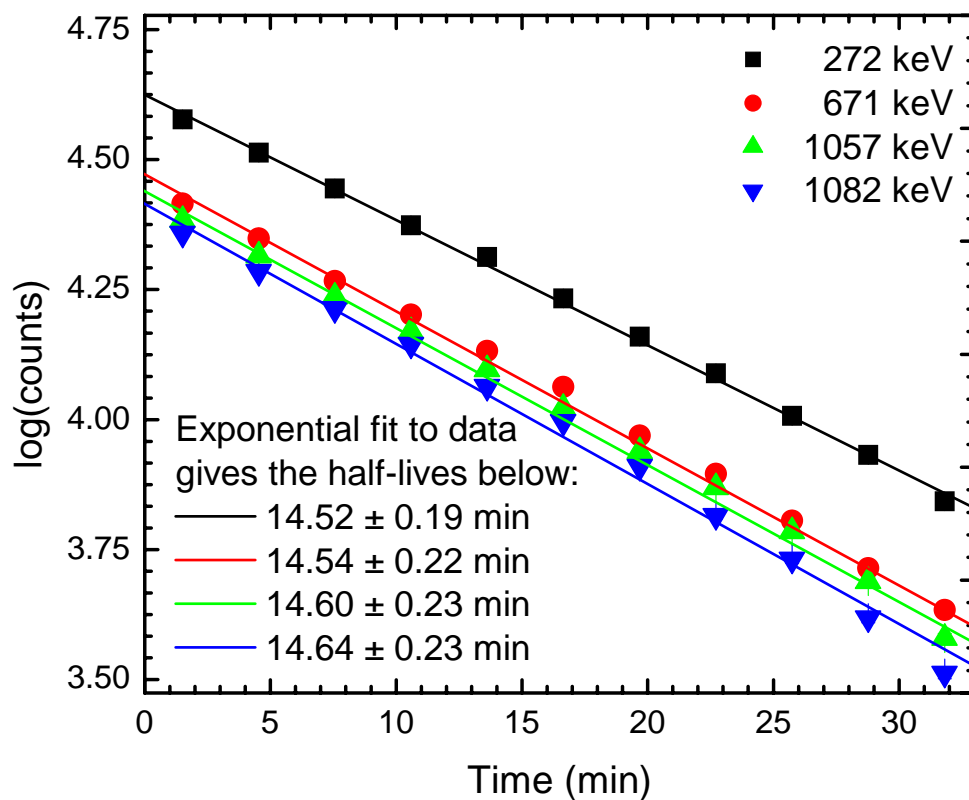
Fig. 6.2: Decay data and exponential fits to the data for the four prominent γ-ray lines. Error bars in the vertical direction are smaller than the symbols.

6.2 Measurement of the $^{74}Se(^{18}O,p3n)^{88}Nb$ Excitation Function

To best replicate the chemical conditions under which the transactinide elements are studied, it is necessary to study the lighter homologues at atom-at-a-time scales as well. As such, the $^{74}Se(^{18}O,p3n)$ excitation function was measured for the production of short-lived accelerator-produced ^{88g}Nb for use in the group five homologue chemistry experiments.

6.2.1　Experimental

The experimental setup is the same as the one described for the chemistry experiments in Chap. 2.3. Energy losses of the ^{18}O beam in C, Au, and Se were calculated with SRIM2006.02 [Ziegler2004]. On-line detection of Rutherford-scattered particles in two PIN diode detectors located at ±27° from the beam axis continuously monitored the product of target thickness and beam intensity. Relative energies were determined to within 0.1% by analysis of the pulse heights of the Rutherford-scattered projectiles from the various ^{18}O energies. The resulting center-of-target beam energies were 64.0, 68.6, 74.0, 78.9 and 83.9 MeV in the laboratory frame. Compound nucleus excitation energies were calculated using the relative beam energies with the experimental mass defects for ^{18}O, ^{74}Se and ^{88g}Nb [Audi2003]. The resulting ranges of compound nucleus excitation energies within the targets were 57.5±0.5, 61.1±0.5, 65.5±0.5, 69.4±0.5 and 73.4±0.5 MeV.

The efficiency for collecting ^{88}Nb EVRs at the BGS focal plane was modeled using a Monte Carlo simulation of the EVR trajectories in the BGS, as described in [Gregorich2003; Gregorich2005], and resulted in efficiencies (ε_{BGS}) of 36-44%, depending on the beam energy. The EVRs passed through a 3.3-μm mylar window at the back of the BGS, were thermalized in the ~1.3 bar of helium gas in the RTC, captured on KCl aerosols and transported to the collection site. After ten minutes of collection, the aerosols were dissolved in 3 mL dilute HCl and then assayed for four minutes on a HPGe γ-ray detector. Corrections were made for decay during collection, decay during counting, γ-ray intensities and efficiencies of the gas-jet, BGS and HPGe γ-ray detector.

Cross sections for the ^{74}Se(^{18}O, $p3n$)^{88}Nb reaction were then calculated using a weighted average of the 271.80, 671.20, 1057.01 and 1082.53 keV γ-ray lines.

6.2.2 ^{74}Se(^{18}O,p3n)^{88g}Nb Excitation Function

The excitation function for the ^{74}Se(^{18}O,$p3n$)^{88g}Nb reaction is shown in Figure 6.3 and the resulting cross sections and errors are listed in Table 6.4. Cross sections for the reaction were calculated using a weighted average of the 271.80, 671.20, 1057.01 and 1082.53 keV γ-ray lines. A maximum cross section of 495±(stat = 5, syst = 205) mb was observed at an ^{18}O energy of 74.0 MeV.
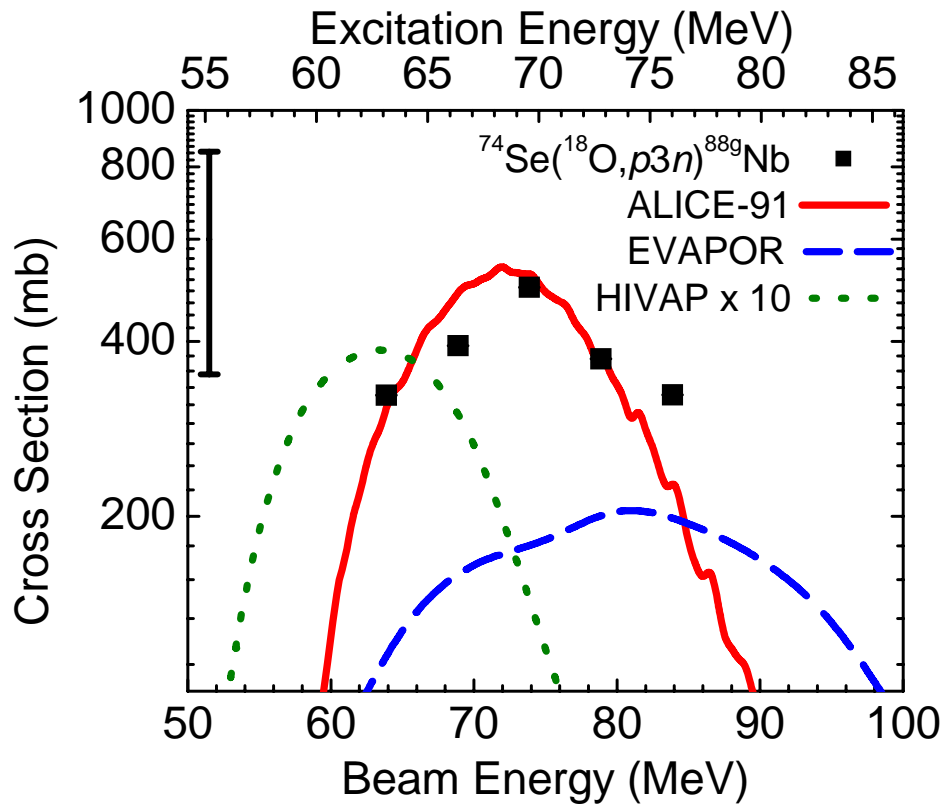
Fig. 6.3: Excitation function for the ^{74}Se(^{18}O, $p3n$)^{88}Nb reaction. The horizontal width of the symbols shows the energy spread of the beam within the target. In the vertical direction, statistical errors are smaller than the size of the symbols. The bar in the upper left-hand corner represents the size of the systematic errors at the 1σ level. Theoretical predictions from ALICE-91, EVAPOR and HIVAP are shown by the solid, dashed and dotted lines, respectively.

Table 1: Energies and cross sections for the ^{74}Se(^{18}O, $p3n$)^{88}Nb reaction.

Center-of-Target Beam Energy (MeV)	Excitation Energy (MeV)	Cross Section (mb)	Statistical Error (mb)	Systematic Error (mb)
64.0	57.5	325	5	135
68.6	61.1	395	5	160
74.0	65.5	495	5	205
78.9	69.4	375	5	155
83.9	73.4	325	5	135

6.2.3   Systematic Uncertainties

Systematic uncertainties in the measured cross sections are the result of seven main contributions:

i)   calculations of the cross sections were performed using the half-life measured in this work (14.56±0.11 min). This value has a 0.76% error, leading to a 1.2% error in the cross section measurement.

ii)   the uncertainty in the efficiency for transport of EVRs through the BGS and the mylar window and into the RTC. An uncertainty of 10% has been estimated for the transport of EVRs to the focal plane detector for the ^{48}Ca + $^{206-208}$Pb reactions by a comparison of the size and shape of the modeled and experimental focal plane position distributions [Gregorich2005]. However, since the (Z, A) of ^{88g}Nb is outside the range of the normal operation of the BGS, a more conservative uncertainty of 20% was used.

iii)   the angle of the Rutherford monitor detectors is known within 0.2° with respect to the beam direction. This results in a 3% uncertainty in the Rutherford cross section, corresponding to a 3% error in the EVR cross sections.

iv)   the uncertainty in the solid angle subtended by the collimators placed in front of the monitor detectors is dominant ed by uncertainty in the size of the opening and is estimated to contribute 4% to the systematic error in cross sections.

v)   between the target and the Rutherford monitor detectors are a series of screens that attenuate the scattered particles. In the ^{207}Pb(^{48}Ca,2n)^{253}No reaction, the ratio of ^{253}No EVRs in the focal plane detector to the Rutherford scattered ^{48}Ca ions was measured with and without the attenuation screens. The uncertainty in the attenuation factor was determined to be 5%.

vi)   the systematic uncertainty in the absolute energy from the 88-Inch Cyclotron is ~1%, resulting in energy uncertainties of 0.6 - 0.8 MeV and Rutherford scattering cross section uncertainties of 2%.

vii)   the gas-jet efficiencies have been measured to 30-70% in previous experiments [Düllmann2005; Kirbach1999], although the variation during an experiment has been measured at <5% [Gates2008b]. We conservatively estimate the gas-jet efficiency to be 50±20%.

Standard error propagation of the seven systematic contributions results in a systematic error of ~40%. Statistical uncertainties due to the number of counts observed are 1 - 2%.

6.2.4   Theoretical Predictions

We have compared the experimental cross sections to theoretical predictions from ALICE-91 [Blann1991], EVAPOR [Beene] and HIVAP [Reisdorf1992]. The ALICE-91 code calculates equilibrium (EQ) cross sections using the Weisskopf-Ewing model [Weisskopf1940]. ALICE-91 was previously found to accurately reproduce the results of reactions between ^{18}O and ^{65,63}Cu when COST = 1.5, a = A/9 and n_0 = 16

125

[Chowdhury2003].   Due to the similarity between the $^{16}O + ^{65,63}Cu$ and $^{18}O + ^{74}Se$ reactions, we have chosen to use COST = 1.5 and a = A/9. In this work, n_0 was 18. A comparison of the experimental and theoretical values is shown in Fig. 4. Theoretical values from HIVAP underestimate the experimental cross sections by a factor of 10. HIVAP also predicts that the centroid of the excitation function occurs 10 MeV below the energy obtained experimentally.   EVAPOR underestimates the experimental cross sections by a factor of 3 and predicts that the centroid of the excitation function occurs at excitation energies that are 10 MeV higher than those observed experimentally. EVAPOR also predicts a broader excitation function than that observed experimentally. ALICE-91 accurately reproduces the height and width of the experimental excitation function. Similar agreement between experimental data and theoretical predictions from ALICE-91 were observed in [Chowdhury2003] for the *pxn* reactions with ^{18}O and $^{65,63}Cu$.

7   Conclusion and Future Work

7.1   *Conclusions*

7.1.1   Reactions

In this dissertation, the $1n$ and $2n$ excitation functions for the $^{208}\text{Pb}(^{51}\text{V},\text{x}n)^{259\text{-x}}\text{Db}$ reaction were measured and we re-measured the $1n$ excitation function for the $^{209}\text{Bi}(^{50}\text{Ti},n)^{258}\text{Db}$ reaction. The maximum cross section, $\sigma_{\text{max}} = 5910 \pm 810$ pb, of the $^{209}\text{Bi}(^{50}\text{Ti},n)$ reaction is larger than the maximum, $\sigma_{\text{max}} = 2160 \pm 530$ pb, of the $^{208}\text{Pb}(^{51}\text{V},n)$ reaction. The FBD model suggests that these differences are due to the effect of the height of the Coulomb + nuclear barrier on σ_{cap}. The maximum cross sections of the $2n$ excitation functions for these two target and beam combinations were identical within the error bars. The FBD model predicts that the $^{209}\text{Bi}(^{50}\text{Ti},2n)^{258}\text{Db}$ should have a larger cross section due to higher values of σ_{cap}.

7.1.2   Off-Line Extraction Systems

The extraction of niobium and tantalum was investigated using a variety of organophosphorus compounds in chloroform. Aqueous phases were HCl or mixtures of

HCl and LiCl. When LiCl was added to the aqueous phase, the extractions reached equilibrium in a shorter amount of time. Large differences in extraction were observed between the two elements. From the off-line studies, extractions with HDEHP and BEHP were chosen for further investigation using short-lived, accelerator-produced isotopes of niobium and tantalum.

7.1.3   On-Line Extraction Systems

The extraction of the group V elements, niobium and tantalum, from HCl and mixed HCl/LiCl media by 0.01 M HDEHP and 0.01 M BEHP was investigated as a function of HCl or H$^+$ concentration and phase mixing time in this work. For the HCl systems, different behaviors for niobium and tantalum were observed when comparing extraction yield as a function of mixing time, as well as a function of HCl concentration. By increasing the HCl concentration, it was possible to observe the decrease in the formation of cationic species for niobium. For tantalum the existence of highly extractable species was observed up to 11 M HCl, where the formation of anionic tantalum species should dominant e. The higher acid concentrations provide suitable separation of niobium and tantalum for both of the systems investigated. It is also possible to use the higher acid concentrations to investigate the kinetics of dubnium and determine its similarity to niobium or tantalum.

When niobium and tantalum were extracted from solutions of mixed HCl/LiCl media, different extraction behavior was observed at both low (1 M) and high (6 - 9 M) H$^+$ concentrations. The amount of time needed for each system to reach equilibrium is also significantly different between the two elements. However, both niobium and tantalum reach equilibrium within 10 s when the extractant was HDEHP and the aqueous

phase consisted of 1 or 3 M H^+. Under these conditions, niobium and tantalum also show large differences in extraction behavior: as the H^+ concentration was increased, a decrease was observed in the amount of niobium that was extracted, while the amount of tantalum extracted increased over the same acid range. The fast kinetics and drastically different chemical behavior make this region of the system suitable for the study of the chemical properties of dubnium.

7.2   Future Work

7.2.1   Reactions

The peak of both the 1*n* and 2*n* excitation functions occurs below the fusion plus nuclear barrier. However, the expected peak of the 3*n* exit channel will be above the barrier and σ_{cap} for the two reactions will be the same over the excitation function. Investigation of the 3*n* excitation function would allow for determination of the effect of P_{CN} on EVR formation. In addition, more studies need to be undertaken with coupled reaction pairs, investigating 1*n*, 2*n* and possibly 3*n* excitation functions to better understand the effect of the entrance channel on the production of transactinide elements.

Presently at LBNL, only ^{208,207}Pb, ^{209}Bi and ^{233,238}U targets are available for transactinide production. In this dissertation, the production of dubnium using ^{208}Pb and ^{209}Bi targets was discussed. ^{238}U targets have also been used to produce isotopes of dubnium [Gregorich2007].   Using reactions with these three targets and the most neutron-rich projectiles, isotopes of $^{257-261}$Db have been produced. The longest-lived of these isotopes is ^{258}Db with a half-life of $4.4^{+0.9}_{-0.6}$ s. However, for chemistry experiments, it is preferable to have much longer lived isotopes. ^{262}Db is the longest-lived isotope with

a half-life of 34 ± 4 s and can be produced through the $^{244}\mathrm{Pu}(^{23}\mathrm{Na},5n)$ reaction. Development and implementation of $^{244}\mathrm{Pu}$ targets for the BGS are in progress at LBNL to study the chemistry of the transactinide elements.

7.2.2   Extraction Systems

The chemistry of niobium and tantalum is complex and little understood due to the formation of polymeric, colloidal and polynuclear species. This specifically hinderers the understanding of these elements on the microscopic scale, as the formation of these species is prohibited by the low metal concentrations. Spectroscopic studies to determine what monomeric species exist at low metal concentrations would be of the most use. In addition, a more in-depth examination of the region between 10^{-10} and 10^{-6} M metal would be valuable to obtain a better understanding of where the cross-over from polymeric to monomeric species occurs.

The LiCl/HCl systems show fast kinetics and good separation between niobium and tantalum. These systems are appropriate for the on-line chemistry of dubnium. However, very little information regarding speciation of dubnium can be determined from these studies, mainly due to the lack of understanding about the speciation of niobium and tantalum. Focus should be placed on understanding the chemistry of the homologues in complex solutions.

8   References

[Alberi1976]   Alberi, J. L. and V. Radeka (1976). "Position Sensing by
                    Charge Division." IEEE Transactions on Nuclear Science
                    23(1): 251-258.

[Audi2003]   Audi, G., O. Bersillon, J. Blachot and A. H. Wapstra
                    (2003). "The NUBASE evaluation of nuclear and decay
                    properties." Nuclear Physics **A729**(1): 3-128.

[Beene]   Beene, J. R. and N. G. Nicolis "The computer code
                    EVAPOR." (unpublished).

[Bemis1981]   Bemis, C. E., P. F. Dittner, R. L. Ferguson, D. C. Hensley,
                    F. Plasil and F. Pleasonton (1981). "Spontaneous-fission
                    branching in the decay of ^{259}104." Physical Review C
                    23(1): 555-558.

[Bemis1977a]   Bemis, C. E., P. F. Dittner, R. J. Silva, R. L. Hahn, J. R.
                    Tarrant, L. D. Hunt and D. C. Hensley (1977a).
                    "Production, L x-ray identification, and decay of the
                    nuclide ^{260}105." Physical Review C **16**(3): 1146.

[Bemis1977b]   Bemis, C. E., R. L. Ferguson, F. Plasil, R. J. Silva, G. D.
                    O'Kelley, M. L. Kiefer, R. L. Hahn, D. C. Hensley, E. K.
                    Hulet and R. W. Lougheed (1977b). "Mass Asymmetry and
                    Total-Kinetic-Energy Release in the Spontaneous Fission
                    of ^{262}[105]." Physical Review Letters **39**(20): 1246.

[Blann1991]   Blann, M. (1991). ALICE-91. Gif-sur-Yvette, France, NEA
                    Data Bank.

131

[Campderrós2000]   Campderrós, M. E. and J. Marchese (2000). "Facilitated transport of niobium(V) and tantalum (V) with supported liquid membrane using TBP as carrier." <u>Journal of Membrane Science</u> **164**(1-2): 205-210.

[Chowdhury2003]   Chowdhury, D. P., R. Guin, S. K. Saha and M. Sudersanan (2003). "Excitation functions of heavy ion induced nuclear reactions between ^{16}O ion beam and natural copper: Measurements, analysis and its applicability in TLA study." <u>Nuclear Instruments and Methods in Physics Research Section B: Beam Interactions with Materials and Atoms</u> **211**(3): 288-296.

[Das1981]   Das, N. R., B. Nandi and S. N. Bhattacharyya (1981). "Tracer Scale Solvent-Extraction Separation of Tantalum from Niobium Using Di-(2-Ethylhexyl)-Phosphoric Acid as Extractant." <u>Journal of Radioanalytical Chemistry</u> **62**(1-2): 53-60.

[Davies1968]   Davies, J. E. D. and D. A. Long (1968). "The Vibrational Spectra of Titatnium Tetrachloride-Hydrochloric Acid and Titanium Tetrachloride-Tri-n-butyl Phosphate Systems and the Hexachloro-anions of Zirconium(IV), Hafnium(IV), Niobium(V), and Tantalum(V)." <u>J. Chem. Soc.</u>: 2560.

[Doron1971]   Doron, T. A. and M. Blann (1971). "Decay scheme studies of short-lived isotopes of 69 [less-than over equal to] A [less-than over equal to] 88 produced by heavy-ion bombardment." <u>Nuclear Physics A</u> **161**(1): 12-48.

[Dragojević2008]   Dragojević, I., K. E. Gregorich, Ch. E. Düllmann, M. A. Garcia, J. M. Gates, S. L. Nelson, L. Stavsetra, R. Sudowe and H. Nitsche (2008). "The influence of projectile neutron number in the ^{208}Pb(^{48}Ti,n)^{255}Rf and ^{208}Pb(^{50}Ti,n)^{257}Rf reactions." <u>In preparation</u>.

[Druin1971]   Druin, V. A., A. G. Demin, Y. P. Kharitonov, G. N. Akapiev, V. I. Rudd, G. Y. Sung-Ching-Yang, L. P. Chelnokov and K. A. Gavrilov (1971). <u>Soviet Journal of Nuclear Physics</u> **13**: 139.

[Düllmann2006]   Düllmann, Ch. E. (2006). <u>Physical Preseparation: a Powerful New Method for Transactinide Chemists</u>. International Symposium on Exotic Nuclei, Khanty-Mansiysk (Russia), AIP.

[Düllmann2005]   Düllmann, Ch. E., C. M. Folden III, K. E. Gregorich, D. C. Hoffman, D. Leitner, G. K. Pang, R. Sudowe, P. M. Zielinski and H. Nitsche (2005). "Heavy-ion-induced production and physical preseparation of short-lived isotopes for chemistry experiments." Nuclear Instruments and Methods in Physics Research Section A: Accelerators, Spectrometers, Detectors and Associated Equipment **551**(2-3): 528-539.

[Eskola1971]   Eskola, K., P. Eskola, M. Nurmia and A. Ghiorso (1971). "Studies of Lawrencium isotopes with Mass Numbers 255 Through 260." Physical Review C **4**(2): 632-642.

[Essel2000]   Essel, H. G. and N. Kurz (2000). "The General Purpose Data Acquisition System MBS." IEEE Transactions on Nuclear Science **47**(2): 337.

[Firestone1996]   Firestone, R. B. and V. S. Shirley, Eds. (1996). Table of Isotopes. New York, Wiley.

[Flerov1970]   Flerov, G. N. (1970). "Soviet Synthesis of Element 105." Science **170**(3953): 15.

[Flerov1968]   Flerov, G. N., V. A. Druin, A. G. Demin, Y. V. Lobanov, N. K. Skobelev, G. N. Akapiev, B. V. Fefilov, I. V. Kolesov, K. A. Gavrilov, Y. P. Kharitonov and L. P. Chelnokov (1968).Joint Institute for Nuclear Research Report.

[Flerov1971]   Flerov, G. N., Yu. Ts. Oganessian, Y. V. Lobanov, Y. A. Lasarev, S. P. Tretiakova, I. V. Kolesov and V. M. Plotko (1971). "On the synthesis of element 105." Nuclear Physics A **160**(1): 181-192.

[Folden2004a]   Folden III, C. M. (2004a). Development of Odd-Z-Projectile Reactions for Transactinide Element Synthesis. Department of Chemistry. Berkeley, University of California, Berkeley. **Ph. D.**

[Folden2004b]   Folden III, C. M., K. E. Gregorich, Ch. E. Düllmann, H. Mahmud, G. K. Pang, J. M. Schwantes, R. Sudowe, P. M. Zielinski, H. Nitsche and D. C. Hoffman (2004b). "Development of an Odd-Z-Projectile Reaction for Heavy Element Synthesis: $^{208}Pb(^{64}Ni,n)^{271}Ds$ and $^{208}Pb(^{65}Cu,n)^{272}111$." Physical Review Letters **93**(21): 212702.

[Folden2006]   Folden III, C. M., S. L. Nelson, Ch. E. Düllmann, J. M. Schwantes, R. Sudowe, P. M. Zielinski, K. E. Gregorich, H. Nitsche and D. C. Hoffman (2006). "Excitation function for the production of ^{262}Bh (Z = 107) in the odd-Z-projectile reaction ^{208}Pb(^{55}Mn, n)." Physical Review C (Nuclear Physics) **73**(1): 014611-11.

[Gan2001]   Gan, Z. G., Z. Qin, H. M. Fan, X. G. Lei, Y. B. Xu, J. J. He, H. Y. Liu, X. L. Wu, J. S. Guo, X. H. Zhou, S. G. Yuan and G. M. Jin (2001). "A new alpha-particle-emitting isotope ^{259}Db." Eur. Phys. J. A **10**: 21-25.

[Gates2008a]   Gates, J. M., M. A. Garcia, K. E. Gregorich, Ch. E. Düllmann, I. Dragojević, J. Dvorak, R. Eichler, C. M. Folden III, W. Loveland, S. L. Nelson, G. K. Pang, L. Stavsetra, R. Sudowe, A. Türler and H. Nitsche (2008a). "Synthesis of rutherfordium isotopes in the ^{238}U(^{26}Mg, xn)$^{264-x}$Rf reaction and study of their decay properties." Physical Review C (Nuclear Physics) **77**: 034603.

[Gates2008b]   Gates, J. M., R. Sudowe, M. N. Ali, M. G. Calvert, I. Dragojević, P. A. Ellison, M. A. Garcia, N. Gharibyan, K. E. Gregorich, S. L. Nelson, S. H. Neumann, T. Parsons-Moss, L. Stavsetra and H. Nitsche (2008b). "Extraction of niobium and tantalum isotopes using organophosphorus compounds – Part I – Extraction of 'carrier-free' metal concentrations from HCl solutions." Radiochimica Acta (submitted).

[Ghiorso1970]   Ghiorso, A. (1970). "New Element Hahnium, Atomic Number 105." Physical Review Letters **24**(26): 1498.

[Ghiorso1971a]   Ghiorso, A. (1971a). "Disputed Discovery of Element 105." Science **171**(3967): 127.

[Ghiorso1971b]   Ghiorso, A., M. Nurmia, K. Eskola and P. Eskola (1971b). "Two New Alpha-Particle Emitting Isotope of Element 105, ^{261}Ha and ^{262}Ha." Phys. Rev. C **4**(5): 1850-1853.

[Ghiorso1988]   Ghiorso, A., S. Yashita, M. E. Leino, L. Frank, J. Kalnins, P. Armbruster, J. P. Dufour and P. K. Lemmertz (1988). "Sassy, a gas-filled magnetic separator for the study of fusion reaction products." Nuclear Instruments and Methods in Physics Research Section A: Accelerators, Spectrometers, Detectors and Associated Equipment **269**(1): 192-201.

[Gober1992]   Gober, M. K., J. V. Kratz, H. P. Zimmerman, M. Schädel, W. Brüchle, E. Schimpf, K. E. Gregorich, A. Türler, N. J. Hannink, K. R. Czerwinski, B. Kadkhodayan, D. M. Lee, M. J. Nurmia, D. C. Hoffman, H. W. Gäggeler, D. T. Jost, J. Kovacs, U. W. Scherer and A. Weber (1992). "Chemical Properties of Element 105 in Aqueous Solution: Extraction into Diisobutylcarbinol." Radiochimica Acta **57**: 77-84.

[Greenwood2003]   Greenwood, N. N. (2003). "Vanadium to dubnium: from confusion through clarity to complexity." Catalysis Today **78**: 5-11.

[Gregorich1991]   Gregorich, K. E. (1991). "Maximum likelihood decay curve fits by the simplex method." Nuclear Instruments and Methods in Physics Research Section A: Accelerators, Spectrometers, Detectors and Associated Equipment **302**(1): 135-142.

[Gregorich2007]   Gregorich, K. E., Ch. E. Düllmann, W. Loveland, C. M. Folden III, J. M. Gates, M. A. Garcia, R. Sudowe, L. Stavsetra, I. Dragojević, S. L. Nelson, G. K. Pang, P. M. Zielinski, Y. H. Chung, B. Eichler, M. Schädel, A. Türler, A. Yakushev, J. Dvorak, D. C. Hoffman and H. Nitsche (2007). Heavy element formation in compound nucleus reactions with ^{238}U targets.Lawrence Berkeley National Laboratory Report: LBNL-63617.

[Gregorich2003]   Gregorich, K. E., T. N. Ginter, W. Loveland, D. Peterson, J. B. Patin, C. M. Folden III, D. C. Hoffman, D. M. Lee, H. Nitsche, J. P. Omtvedt, L. A. Omtvedt, L. Stavsetra, R. Sudowe, P. A. Wilk, P. M. Zielinski and K. Aleklett (2003). "Cross-section limits for the ^{208}Pb(^{86}Kr, n)^{293}118 reaction." European Physical Journal A **18**: 633-638.

[Gregorich1988]   Gregorich, K. E., R. A. Henderson, D. M. Lee, M. J. Nurmia, R. M. Chasteler, H. L. Hall, D. A. Bennett, G. C.M., R. B. Chadwich, J. D. Leyba and D. C. Hoffman (1988). "Aqueous Chemistry of Element 105." Radiochim. Acta **43**: 223-231.

[Gregorich2005]   Gregorich, K. E., W. Loveland, D. Peterson, P. M. Zielinski, S. L. Nelson, Y. H. Chung, Ch. E. Düllmann, C. M. Folden III, K. Aleklett, R. Eichler, D. C. Hoffman, J. P. Omtvedt, G. K. Pang, J. M. Schwantes, S. Soverna, P. Sprunger, R. Sudowe, R. E. Wilson and H. Nitsche (2005). "Attempt to confirm superheavy element production in the ^{48}Ca + ^{238}U reaction." Physical Review C **72**(1): 014605.

[Gregorich2000]   Gregorich, K. E. and V. Ninov (2000). "Superheavy Elements with the Berkeley Gas-Filled Separator." Journal of Nuclear and Radiochemical Sciences **1**(1): 1-4.

[Heßberger2007]   Heßberger, F. P. private communication (2007).

[Heßberger2001]   Heßberger, F. P., S. Hofmann, D. Ackermann, V. Ninov, M. Leino, G. Münzenberg, S. Saro, A. Y. Lavrentev, A. G. Popeko, A. V. Yeremin and C. Stodel (2001). "Decay properties of neutron-deficient isotopes ^{256,257}Db, ^{255}Rb, and ^{252,253}Lr." European Physical Journal A **12**: 57-67.

[Heßberger1985]   Heßberger, F. P., G. Münzenberg, S. Hofmann, Y. K. Agarwal, K. Poppensieker, W. Reisdorf, K. H. Schmidt, J. R. H. Schneider, W. F. W. Schneider, H. J. Schött and P. Armbruster (1985). "The New Isotopes ^{258}105, ^{257}105, ^{254}Lr and ^{253}Lr." Z. Phys. A **322**: 557-566.

[Hoffman1971]   Hoffman, D. C., F. O. Lawrence, J. L. Mewherter and F. M. Rourke (1971). "Detection of Plutonium-244 in Nature." Nature **234**: 132.

[Hoffman2006]   Hoffman, D. C., D. M. Lee and V. Pershina (2006). Transactinide Elements and Future Elements. The Chemistry of the Actinide and Transactinide Elements. L. R. Morss, Springer.

[Hyde1987]   Hyde, E. K. and D. C. Hoffman (1987). "A History and Analysis of the Discovery of Elements 104 and 105." Radiochimica Acta **42**: 57-102.

[Iafigliola1972]   Iafigliola, R., R. Turcotte, R. B. Moore and J. K. P. Lee (1972). "The levels of 88Zr observed in the decay of 88gNb and 88mNb." Nuclear Physics A **182**(2): 400-410.

[Kanzelmeyer1953]   Kanzelmeyer, J. H. and H. Freund (1953). "Ultraviolet Spectrophotometric Determination of Niobium in Hydrochloric Acid." Analytical Chemistry **25**(12): 1807.

[Kanzelmeyer1956]   Kanzelmeyer, J. H., J. Ryan and H. Freund (1956). "The Nature of Niobium(V) in Hydrochloric Acid Solution." Journal of the American Chemical Society **78**: 3020.

[Kim1973]   Kim, J. I., H. Lagally and H.-J. Born (1973). "Ion exchange in aqueous and in aqueous-organic solvents : Part I. Anion-exchange behaviour of Zr, Nb, Ta and Pa in aqueous HCl-HF and in HCl-HF-organic solvent." Analytica Chimica Acta **64**(1): 29.

[Kimura1960]   Kimura, K. (1960). "Inorganic Extraction Studies on the System between Bis(2-ethyl hexyl)-orthophosphoric Acid and Hydrochloric Acid (I)." Bulletin of the Chemical Society of Japan **33**(8): 1038.

[Kimura1961]   Kimura, K. (1961). "Inorganic Extraction Studies on the System between Bis(2-ethylhexyl)-orthophosphoric Acid and Hydrochlorid Acid. II." Bulletin of the Chemical Society of Japan **34**(1): 63.

[Kirbach2002]   Kirbach, U. W., C. M. Folden III, T. N. Ginter, K. E. Gregorich, D. M. Lee, V. Ninov, J. P. Omtvedt, J. B. Patin, N. K. Seward and D. A. Strellis (2002). "The Cryo-Thermochromatographic Separator (CTS): : A new rapid separation and [alpha]-detection system for on-line chemical studies of highly volatile osmium and hassium (Z=108) tetroxides." Nuclear Instruments and Methods in Physics Research Section A: Accelerators, Spectrometers, Detectors and Associated Equipment **484**(1-3): 587-594.

[Kirbach1999]   Kirbach, U. W., K. Gregorich, V. Ninov, D. M. Lee, J. B. Patin, D. A. Shaughnessy, D. A. Strellis, P. A. Wilk, D. C. Hoffman and H. Nitsche (1999). The Recoil product Transfer Chamber (RTC): A new interface for heavy element chemistry studies at the Berkeley Gas-filled Separator.Lawrence Berkeley National Laboratory Report.

[Krane1988]   Krane, K. S. (1988). Introductory Nuclear Physics. New York, John Wiley & Sons, Inc.

[Kratz2003]   Kratz, J. V. (2003). "Critical Evaluation of the Chemical Properties of the Transactinide Elements." Pure and Applied Chemistry **75**(1): 103-138.

[Kratz1992] Kratz, J. V., M. K. Gober, H. P. Zimmermann, M. Schädel, W. Brüchle, E. Schimpf, K. E. Gregorich, A. Türler, N. J. Hannink, K. R. Czerwinski, B. Kadkhodayan, D. M. Lee, M. J. Nurmia, D. C. Hoffman, H. Gäggeler, D. Jost, J. Kovacs, U. W. Scherer and A. Weber (1992). "New nuclide ^{263}Ha." Physical Review C **45**(3): 1064.

[Kratz1989] Kratz, J. V., H. P. Zimmerman, U. W. Schere, M. Schädel, W. Brüchle, K. E. Gregorich, C. M. Gannett, H. L. Hall, C. M. Henderson, D. M. Lee, J. D. Leyba, M. Nurmia, D. C. Hoffman, H. Gäggeler, D. Jost, U. Baltensperger, Y. Nai-Qi, A. Türler and C. Lienert (1989). "Chemical Properties of Element 105 in Aqueous Solution: Halide Complex Formation and Anion Exchange into Triisoctyl Amine." Radiochim. Acta **48**: 121-133.

[Loveland2005] Loveland, W. private communication (2005).

[Loveland2002] Loveland, W., K. E. Gregorich, J. B. Patin, D. Peterson, C. Rouki, P. M. Zielinski and K. Aleklett (2002). "Search for the production of element 112 in the ^{48}Ca+ ^{238}U reaction." Physical Review C **66**(4): 044617.

[Möller1995] Möller, P., J. R. Nix, W. D. Myers and W. J. Swiatecki (1995). "Nuclear Ground-State Masses and Deformations." Atomic Data and Nuclear Data Tables **59**(2): 185-381.

[Myers1994] Myers, W. D. and W. J. Świątecki (1994). Table of Nuclear Masses according to the 1994 Thomas-Fermi Model.Lawrence Berkeley National Laboratory Report: LBNL-36803.

[Nabivanets1962] Nabivanets, B. I. (1962). "The state of tantalum(V) in nitric, hydrochloric, and sulphuric acid solutions." Russian Journal of Inorganic Chemistry **7**(12): 1428-1432.

[Nabivanets1964] Nabivanets, B. I. (1964). "State of niobium(V) in solutions of nitric, hydrochloric, and sulphuric acids." Russian Journal of Inorganic Chemistry **9**(5): 590-593.

[Nabivantes1962] Nabivantes, B. I. (1962). Russian Journal of Inorganic Chemistry **7**: 1428.

[Nelson2008]	Nelson, S. L., C. M. Folden III, K. E. Gregorich, I. Dragojević, Ch. E. Düllmann, R. Eichler, M. A. Garcia, J. M. Gates, R. Sudowe and H. Nitsche (2008). "Comparison of Complementary Reactions for the Production of ^{262,261}Bh." <u>unpublished</u>.
[Ninov1998]	Ninov, V., K. Gregorich and C. A. McGrath (1998). <u>The Berkeley Gas-Filled Separator</u>. ENAM 98: Exotic Nuclei and Atomic Masses, Woodbury, New York, American Institute of Physics.
[Oganessian2007]	Oganessian, Yu. Ts. (2007). "Study of Heavy Nuclei at FLNR (Dubna)." <u>Journal of Nuclear and Radiochemical Sciences</u> **8**(2): 39-45.
[Oganessian2004]	Oganessian, Yu. Ts., V. K. Utyonkoy, Y. V. Lobanov, F. S. Abdullin, A. N. Polyakov, I. V. Shirokovsky, Y. S. Tsyganov, G. G. Gulbekian, S. L. Bogomolov, A. N. Mezentsev, S. Iliev, V. G. Subbotin, A. M. Sukhov, A. A. Voinov, G. V. Buklanov, K. Subotic, V. I. Zagrebaev, M. G. Itkis, J. B. Patin, K. J. Moody, J. F. Wild, M. A. Stoyer, N. J. Stoyer, D. A. Shaughnessy, J. M. Kenneally and R. W. Lougheed (2004). "Experiments on the synthesis of element 115 in the reaction ^{243}Am(^{48}Ca,xn)$^{291 - x}$115." <u>Physical Review C (Nuclear Physics)</u> **69**(2): 021601-5.
[Oxorn1984]	Oxorn, K. and S. K. Mark (1984). "The beta decay of ^{88g}Nb and ^{88m}Nb." <u>Zeitschrift Fur Physik a-Hadrons and Nuclei</u> **316**: 97-104.
[Patin2002]	Patin, J. B. (2002). Experimental Cross Sections for Reactions of Heavy Ions and ^{208}Pb, ^{209}Bi, ^{238}U, and ^{248}Cm Targets.Lawrence Berkeley National Laboratory Report: LBNL-49593.
[Paulus1998]	Paulus, W., J. V. Kratz, E. Strub, S. Zauner, W. Brüchle, V. Pershina, M. Schädel, B. Schausten, J. L. Adams, K. E. Gregorich, D. C. Hoffman, M. R. Lane, C. Laue, D. M. Lee, C. A. McGrath, D. K. Shaughnessy, D. A. Strellis and E. R. Sylwester (1998). "Extraction of the fluoride-, chloride-, and bromide complexes of the elements Nb, Ta, Pa, and 105 into aliphatic amines." <u>J. Alloy. Comp.</u>: 292-295.

139

[Paulus1999]	Paulus, W., J. V. Kratz, E. Strub, S. Zauner, W. Brüchle, V. Pershina, M. Schädel, B. Schausten, J. L. Adams, K. E. Gregorich, D. C. Hoffman, M. R. Lane, C. Laue, D. M. Lee, C. A. McGrath, D. K. Shaughnessy, D. A. Strellis and E. R. Sylwester (1999). "Chemical Properties of Element 105 in Aqueous Solution: Extraction of Fluoride-, Chloride-, and Bromide Complexes of the Group-5 Elements into an Aliphatic Amine." Radiochim. Acta **84**: 69-77.
[Pershina1996]	Pershina, V. (1996). "Electronic Structure and Properties of the Transactinides and Their Compounds." Chemical Review **96**: 1977-2010.
[Pershina1998a]	Pershina, V. (1998a). "Solution Chemistry of Element 105. Part I: Hydrolysis of Group 5 Cations: Nb, Ta, Ha and Pa." Radiochim. Acta **80**: 65-73.
[Pershina1998b]	Pershina, V. (1998b). "Solution Chemistry of Element 105. Part II: Hydrolysis and Complex Formation of Nb, Ta, Ha and Pa in HCl Solutions." Radiochim. Acta **80**: 75-84.
[Pershina1993]	Pershina, V. and B. Fricke (1993). "Relativistic effects in physics and chemistry of element 105. IV. Their influence on the electronic structure and related properties." Journal of Chemical Physics **99**(12): 9720-9729.
[Pyykkö1988]	Pyykkö, P. (1988). "Relativistic Effects in Structural Chemistry." Chemical Reviews **88**(3): 563-594.
[Recommendations1994]	Recommendations, I. (1994). "Names and symbols of transfermium elements." Pure and Applied Chemistry **66**(12): 2419-2421.
[Recommendations1997]	Recommendations, I. (1997). "Names and symbols of transfermium elements." Pure and Applied Chemistry **69**(12): 2471-2473.
[Reisdorf1992]	Reisdorf, W. and M. Schädel (1992). "How well do we understand the synthesis of heavy elements by heavy-ion induced fusion?" Zeitschrift Fur Physik a-Hadrons and Nuclei **343**: 47-57.
[Rydberg2004]	Rydberg, J., M. Cox, C. Musikas and G. R. Choppin (2004). Solvent Extraction Principles and Practice. New York, USA, Marcel Dekker.

[Sabatini1966]   Sabatini, A. and I. Bertini (1966). "Far-Infrared Spectra of Oxochloro and Oxobromo Complexes of Nb(V), Mo(V), and W(V)." Inorganic Chemistry **5**(2): 204.

[Schädel2003]   Schädel, M. (2003). The chemistry of the superheavy elements. Dordrecht, The Netherlands, Kluwer Academic Publishers.

[Schädel1989]   Schädel, M., W. Brüchle, E. Jäger, E. Schimpf, J. V. Kratz, U. W. Scherer and H. P. Zimmermann (1989). "ARCA II - A New Apparatus for Fast, Repetitive HPLC Separations." Radiochimica Acta **48**: 179-176.

[Schädel1992]   Schädel, M., W. Brüchle, E. Schimpf, H. P. Zimmerman, M. K. Gober, J. V. Kratz, N. Trautmann, H. W. Gäggeler, D. T. Jost, J. Kovacs, U. W. Scherer, A. Weber, K. E. Gregorich, A. Türler, K. R. Czerwinski, N. J. Hannink, B. Kadkhodayan, D. M. Lee, M. J. Nurmia and D. C. Hoffman (1992). "Chemical Properties of Element 105 in Aqueous Solution: Cation Exchange Separations with alpha-Hydroxyisobutyric Acid." Radiochim. Acta **57**: 85-92.

[Schäfer1959]   Schäfer, H. (1959). "Die Methoden zur Trennung der Elemente Niob und Tantal und ihre Grundlagen Beiträge zur Chemie der Elemente Niob und Tantal XIX)." Angewandte Chemie **71**: 152-160.

[Schmidt2000]   Schmidt, K. H. (2000). "A new test for random events of an exponential distribution." European Physical Journal A **8**: 141-145.

[Sears1992]   Sears, V. F. (1992). "Neutron Scattering Lengths and Cross Sections." Neutron News **3**(3): 26-37.

[Segrè1977]   Segrè, E. (1977). Nuclei and Particles: An Introduction to Nuclear and Subnuclear Physics. Reading, Massachusetts, Bengamin/Cummings.

[Świątecki2003]   Świątecki, W. J., K. Siwek-Wilczyńska and J. Wilczyński (2003). "Fusion by Diffusion." Acta Physica Polonica B **34**(4): 2049-2071.

[Świątecki2005]   Świątecki, W. J., K. Siwek-Wilczyńska and J. Wilczyński (2005). "Fusion by diffusion. II. Synthesis of transfermium elements in cold fusion reactions." Physical Review C (Nuclear Physics) **71**(1): 014602-16.

[Trubert1998]   Trubert, D., M. Hussonnois, C. Le Naour, L. Brillard, F. Monroy Guzman, J. F. Le Du, V. Servajean, V. Barci, B. Weiss, G. Ardisson, O. Constantinescu and Yu. Ts. Oganessian (1998). "Comportement chimique de quelques atomes de rutherfordium (Rf, Z=104) et dubnium (Db, Z=105) produits a Orsay." Chim. Phys et Theor.: 643-649.

[Trubert2002]   Trubert, D., C. Le Naour, F. Monroy Guzman, M. Hussonnois, L. Brillard, J. F. Le Du., O. Constantinescu, J. Gasparro, V. Barci, B. Weiss and G. Ardisson (2002). "Chemical isolation of dubnium (element 105) in fluroide media." Radiochim. Acta **90**: 127-132.

[Weisskopf1940]   Weisskopf, V. F. and D. H. Ewing (1940). "On the Yield of Nuclear Reactions with Heavy Elements." Physical Review **57**(6): 472.

[Ziegler2004]   Ziegler, J. F. (2004). "SRIM-2003." Nuclear Instruments and Methods in Physics Research Section B: Beam Interactions with Materials and Atoms **219-220**: 1027-1036.

[Zimmermann1993]   Zimmermann, H. P., M. K. Gober, J. V. Kratz, M. Schädel, W. Brüchle, E. Schimph, K. E. Gregorich, A. Türler, K. R. Czerwinski, N. J. Hannink, B. Kadkhodayan, D. M. Lee, M. J. Nurmia, D. C. Hoffman, H. W. Gäggeler, D. T. Jost, J. Kovacs, U. W. Scherer and A. Weber (1993). "Chemical Properties of Element 105 in Aqueous Solution: Back Extraction from Triisooctyl Amine in to 0.5 M HCl." Radiochim. Acta **60**: 11-16.

[Zvára1974]   Zvára, I., V. Aikhler, V. Z. Belov, T. S. Zvarova, Y. S. Korotkin, M. R. Shalaevskii, V. A. Shchegolev and M. Yussonnua (1974). "Gas Chromatography and Thermochromatography in the Study of Transuranium Elements." Soviet Radiochemistry **16**: 709-715.

[Zvára1976]   Zvára, I., V. Z. Belov, V. P. Domanov and M. R. Shalaevskii (1976). "Chemical Isolation of Neilsbohrium and Ekatantalum in the Form of the Anhydrous Bromide II. Experiments with a spontaneously Fissioning Isotope of Neilsbohrium." <u>Soviet Radiochemistry</u> **18**: 328-334.

9 Appendix:

9.1 Actual Acid Concentrations:

Table 9.1: Actual HCl and H^+ concentrations for the off- and on-line extractions experiments.

HCl Concentration (M)	Actual Concentration (M)		H^+ Concentration (M)	Actual Concentration (M)
1	1.00		1	0.98
3	2.94		3	3.05
6	5.82		6	6.02
9	8.81		9	8.98
11	11.06		11	10.97

9.2 Kinetics Data for Off-Line Experiments

9.2.1 Extractions from HCl Solutions

Table 9.2: Data for the extraction of ^{95}Nb (10^{-10} M) from HCl solutions by 0.01 M HDEHP in $CHCl_3$ (Fig. 4.2).

Mixing Time (s)	1 M HCl Ext (%)	3 M HCl Ext (%)	6 M HCl Ext (%)	9 M HCl Ext (%)	11 M HCl Ext (%)
10	65.85 ± 0.37	65.76 ± 0.36	74.59 ± 0.43	49.51 ± 0.30	19.15 ± 0.12
20	85.92 ± 0.55	88.20 ± 0.55	82.99 ± 0.52	57.68 ± 0.36	18.63 ± 0.11
30	91.28 ± 0.60	91.52 ± 0.61	90.08 ± 0.78	58.61 ± 0.39	18.27 ± 0.11
40	94.38 ± 0.78	93.85 ± 0.69	88.39 ± 0.61	59.31 ± 0.42	18.25 ± 0.14
60	96.80 ± 0.84	94.87 ± 0.75	88.51 ± 0.51	57.81 ± 0.44	18.17 ± 0.13

Table 9.3: Data for the extraction of ^{95}Nb (10^{-10} M) from HCl solutions by 0.01 M BEHP in $CHCl_3$ (Fig. 4.3).

Mixing Time (s)	1 M HCl Ext (%)	3 M HCl Ext (%)	6 M HCl Ext (%)	9 M HCl Ext (%)	11 M HCl Ext (%)
10	10.94 ± 0.15	4.00 ± 0.04	2.93 ± 0.03	8.57 ± 0.06	19.48 ± 0.31
20	15.75 ± 0.16	4.97 ± 0.03	3.15 ± 0.04	8.96 ± 0.06	17.04 ± 0.16
30	12.02 ± 0.11	4.15 ± 0.04	3.11 ± 0.03	8.65 ± 0.05	15.30 ± 0.15
40	6.50 ± 0.06	4.51 ± 0.04	3.20 ± 0.04	9.70 ± 0.08	15.14 ± 0.15
60	11.57 ± 0.12	6.21 ± 0.05	3.41 ± 0.04	9.69 ± 0.06	13.73 ± 0.10

Table 9.4: Data for the extraction of ^{95}Nb (10^{-10} M) from HCl solutions by 0.01 M DEHPA in CHCl$_3$ (Fig. 4.4).

Mixing Time (s)	1 M HCl Ext (%)	3 M HCl Ext (%)	6 M HCl Ext (%)	9 M HCl Ext (%)	11 M HCl Ext (%)
10	71.83 ± 0.58	73.61 ± 0.48	87.88 ± 1.08	86.73 ± 0.91	42.22 ± 0.47
20	84.15 ± 0.97	81.97 ± 1.13	93.47 ± 1.52	90.81 ± 1.14	41.73 ± 0.37
30	89.73 ± 1.05	88.73 ± 1.40	92.88 ± 1.37	90.90 ± 0.94	42.75 ± 0.32
40	85.98 ± 0.89	88.01 ± 1.23	93.68 ± 1.41	90.97 ± 0.97	40.87 ± 0.41
60	90.90 ± 1.31	84.38 ± 1.29	93.68 ± 1.47	90.79 ± 1.02	38.18 ± 0.35

Table 9.5: Data for the extraction of ^{95}Nb (10^{-10} M) from HCl solutions by 0.01 M DiOPA in CHCl$_3$ (Fig. 4.5).

Mixing Time (s)	1 M HCl Ext (%)	3 M HCl Ext (%)	6 M HCl Ext (%)	9 M HCl Ext (%)	11 M HCl Ext (%)
10	56.51 ± 0.43	63.56 ± 0.75	65.72 ± 0.65	26.13 ± 0.23	4.46 ± 0.07
20	72.91 ± 0.79	74.99 ± 0.99	88.31 ± 1.29	31.78 ± 0.28	2.67 ± 0.06
30	81.23 ± 0.79	87.80 ± 1.16	89.39 ± 1.19	39.62 ± 0.33	2.27 ± 0.04
40	83.47 ± 0.73	89.23 ± 1.00	90.84 ± 0.94	36.52 ± 0.24	3.69 ± 0.07
60	88.23 ± 1.14	91.11 ± 1.19	91.15 ± 0.95	35.59 ± 0.25	1.56 ± 0.04

Table 9.6: Data for the extraction of ^{182}Ta (10^{-6} M) from HCl solutions by 0.01 M HDEHP in CHCl$_3$ (Fig. 4.6).

Mixing Time (s)	1 M HCl Ext (%)	3 M HCl Ext (%)	6 M HCl Ext (%)	9 M HCl Ext (%)	11 M HCl Ext (%)
10	65.37 ± 0.89	38.34 ± 0.73	12.77 ± 0.09	2.35 ± 0.03	0.66 ± 0.02
20	76.73 ± 1.03	55.92 ± 1.14	25.35 ± 0.28	3.92 ± 0.04	2.27 ± 0.05
30	84.88 ± 0.27	64.73 ± 0.78	30.86 ± 0.26	9.58 ± 0.12	4.01 ± 0.07
40	86.16 ± 1.07	66.98 ± 1.06	39.65 ± 0.43	11.23 ± 0.12	6.31 ± 0.16
60	95.09 ± 1.74	76.65 ± 0.76	44.54 ± 0.45	12.68 ± 0.11	7.77 ± 0.12
90	97.31 ± 1.56	87.13 ± 1.22	60.24 ± 0.82	18.66 ± 0.14	14.38 ± 0.17

Table 9.7: Data for the extraction of ^{182}Ta (10^{-6} M) from HCl solutions by 0.01 M BEHP in CHCl$_3$ (Fig. 4.7).

Mixing Time (s)	1 M HCl Ext (%)	3 M HCl Ext (%)	6 M HCl Ext (%)	9 M HCl Ext (%)	11 M HCl Ext (%)
10	1.84 ± 0.26	2.43 ± 0.08	0.60 ± 0.03	0.48 ± 0.01	0.30 ± 0.01
20	7.78 ± 0.17	1.58 ± 0.06	1.21 ± 0.06	0.59 ± 0.02	0.86 ± 0.02
30	13.16 ± 0.22	1.70 ± 0.08	1.15 ± 0.05	1.58 ± 0.03	0.86 ± 0.03
40	15.00 ± 0.26	1.60 ± 0.08	2.52 ± 0.10	1.45 ± 0.03	1.46 ± 0.04
60	27.32 ± 0.39	4.61 ± 0.14	2.99 ± 0.07	1.90 ± 0.04	1.15 ± 0.04
90	42.98 ± 0.66	10.58 ± 0.27	5.61 ± 0.15	3.34 ± 0.04	4.30 ± 0.08

9.2.2 Extractions from HCl/LiCl Solutions

Table 9.8: Data for the extraction of ^{95}Nb (10^{-10} M) from HCl/LiCl solutions by 0.01 M HDEHP in CHCl$_3$ (Fig. 4.10).

Mixing Time (s)	1 M H$^+$/ 12 M Cl$^-$ Ext (%)	3 M H$^+$/ 12 M Cl$^-$ Ext (%)	6 M H$^+$/ 12 M Cl$^-$ Ext (%)	9 M H$^+$/ 12 M Cl$^-$ Ext (%)	11 M H$^+$/ 12 M Cl$^-$ Ext (%)
10	93.26 ± 1.00	67.87 ± 0.74	43.07 ± 0.38	20.93 ± 0.18	16.53 ± 0.25
20	94.53 ± 1.24	68.36 ± 0.92	43.10 ± 0.48	20.45 ± 0.24	15.58 ± 0.14
30	94.52 ± 1.28	67.81 ± 0.92	41.70 ± 0.47	19.09 ± 0.26	15.61 ± 0.19
60	94.53 ± 1.31	67.37 ± 0.90	40.73 ± 0.44	20.28 ± 0.16	15.51 ± 0.18

Table 9.9: Data for the extraction of ^{95}Nb (10^{-10} M) from HCl/LiCl solutions by 0.01 M BEHP in CHCl$_3$ (Fig. 4.11).

Mixing Time (s)	1 M H$^+$/ 12 M Cl$^-$ Ext (%)	3 M H$^+$/ 12 M Cl$^-$ Ext (%)	6 M H$^+$/ 12 M Cl$^-$ Ext (%)	9 M H$^+$/ 12 M Cl$^-$ Ext (%)	11 M H$^+$/ 12 M Cl$^-$ Ext (%)
10	60.78 ± 0.56	40.48 ± 0.40	22.42 ± 0.32	18.30 ± 0.23	15.51 ± 0.29
20	64.65 ± 0.63	43.27 ± 0.58	23.45 ± 0.34	18.65 ± 0.23	13.94 ± 0.27
30	66.02 ± 0.67	43.16 ± 0.43	22.92 ± 0.33	17.63 ± 0.20	14.47 ± 0.23
60	68.89 ± 0.68	44.64 ± 0.62	21.67 ± 0.31	16.86 ± 0.18	14.71 ± 0.15

Table 9.10: Data for the extraction of ^{95}Nb (10^{-10} M) from HCl/LiCl solutions by 0.01 M HDEHP in CHCl$_3$ (Fig. 4.12).

Mixing Time (s)	0.5 M H$^+$/ 1 M Cl$^-$ Ext (%)	0.5 M H$^+$/ 3 M Cl$^-$ Ext (%)	0.5 M H$^+$/ 6 M Cl$^-$ Ext (%)	0.5 M H$^+$/ 9 M Cl$^-$ Ext (%)	0.5 M H$^+$/ 11 M Cl$^-$ Ext (%)
10	89.10 ± 0.81	91.62 ± 1.51	81.17 ± 0.85	97.30 ± 1.52	98.35 ± 2.53
20	95.02 ± 1.17	90.19 ± 1.50	76.35 ± 0.74	94.97 ± 1.26	98.72 ± 2.19
30	95.27 ± 1.51	89.36 ± 1.50	76.45 ± 0.76	94.97 ± 1.98	98.57 ± 2.62
40	96.60 ± 1.30	92.32 ± 1.45	75.62 ± 0.69	97.32 ± 1.45	98.92 ± 3.18
60	95.42 ± 1.41	90.97 ± 1.67	76.18 ± 0.75	96.08 ± 1.40	98.86 ± 2.59

Table 9.11: Data for the extraction of ^{182}Ta (10^{-6} M) from HCl/LiCl solutions by 0.01 M HDEHP in CHCl$_3$ (Fig. 4.13).

Mixing Time (s)	0.5 M H$^+$/ 1 M Cl$^-$ Ext (%)	0.5 M H$^+$/ 3 M Cl$^-$ Ext (%)	0.5 M H$^+$/ 6 M Cl$^-$ Ext (%)	0.5 M H$^+$/ 9 M Cl$^-$ Ext (%)	0.5 M H$^+$/ 11 M Cl$^-$ Ext (%)
10	35.37 ± 0.73	27.64 ± 1.11	37.57 ± 0.28	27.54 ± 0.32	27.16 ± 0.17
20	89.65 ± 1.02	82.24 ± 1.03	46.25 ± 0.36	35.23 ± 0.25	37.53 ± 0.54
30	93.25 ± 1.53	85.78 ± 2.51	53.05 ± 0.42	41.50 ± 0.44	38.17 ± 0.28
40	95.29 ± 1.35	88.74 ± 1.32	55.18 ± 0.46	43.32 ± 0.47	36.01 ± 0.37
60	96.98 ± 2.16	90.97 ± 1.68	54.00 ± 0.51	43.10 ± 0.82	40.68 ± 0.62

9.3 *Kinetics Data for On-Line Experiments*

9.3.1 Extractions from HCl Solutions

Table 9.12: Data for the extraction of ^{88g}Nb from HCl solutions by 0.01 M HDEHP in CHCl$_3$ (Fig. 5.1).

Mixing Time (s)	1 M HCl Ext (%)	3 M HCl Ext (%)	6 M HCl Ext (%)	9 M HCl Ext (%)	11 M HCl Ext (%)
10	44.37 ± 1.55	63.37 ± 2.01	60.22 ± 2.44	47.95 ± 1.63	14.42 ± 0.87
20	68.30 ± 2.76	81.96 ± 3.58	84.63 ± 4.29	53.21 ± 1.86	14.90 ± 0.87
30	84.16 ± 4.10	88.28 ± 4.51	92.65 ± 7.55	54.29 ± 1.96	14.77 ± 0.82
40	85.75 ± 4.17	90.02 ± 5.31	94.29 ± 7.70	54.67 ± 1.92	13.87 ± 0.76
60	89.96 ± 7.70	90.00 ±5.64	94.37 ± 8.09	54.88 ± 1.94	15.25 ± 0.75

Table 9.13: Data for the extraction of ^{170}Ta from HCl solutions by 0.01 M HDEHP in CHCl$_3$ (Fig. 5.2).

Mixing Time (s)	1 M HCl Ext (%)	3 M HCl Ext (%)	6 M HCl Ext (%)	9 M HCl Ext (%)	11 M HCl Ext (%)
10	54.78 ± 3.55	23.74 ± 0.80	31.43 ± 0.91	28.42 ± 0.84	56.99 ± 1.40
20	63.67 ± 2.96	34.58 ± 1.16	40.92 ± 1.20	44.46 ± 1.20	68.85 ± 1.83
30	68.76 ± 2.78	39.39 ± 1.35	53.79 ± 1.50	54.30 ± 1.40	75.11 ± 2.20
40	71.34 ± 3.23	55.41 ± 1.82	63.69 ± 1.88	61.42 ± 1.70	78.96 ± 2.29
60	76.08 ± 3.50	64.25 ± 2.04	77.19 ± 2.58	73.31 ± 2.12	86.85 ± 3.22
90	85.66 ± 4.27	78.26 ± 2.85	86.26 ± 3.69	84.18 ± 3.33	91.84 ± 4.68

Table 9.14: Data for the extraction of ^{88g}Nb from HCl solutions by 0.01 M BEHP in CHCl$_3$ (Fig. 5.3).

Mixing Time (s)	1 M HCl Ext (%)	3 M HCl Ext (%)	6 M HCl Ext (%)	9 M HCl Ext (%)	11 M HCl Ext (%)
10	9.88 ± 0.59	5.37 ± 0.36	2.94 ± 0.22	8.95 ± 0.52	14.65 ± 0.70
20	10.83 ± 0.67	4.64 ± 0.34	2.67 ± 0.23	8.57 ± 0.55	14.28 ± 0.71
30	10.29 ± 0.65	4.19 ± 0.30	2.70 ± 0.28	9.08 ± 0.54	15.12 ± 0.74
40	10.22 ± 0.67	3.64 ± 0.31	2.49 ± 0.25	8.54 ± 0.56	15.76 ± 0.74
60	9.72 ± 0.61	3.75 ± 0.30	2.59 ± 0.25	9.51 ± 0.56	15.22 ± 0.76

Table 9.15: Data for the extraction of ^{170}Ta from HCl solutions by 0.01 M BEHP in CHCl$_3$ (Fig. 5.4).

Mixing Time (s)	1 M HCl Ext (%)	3 M HCl Ext (%)	6 M HCl Ext (%)	9 M HCl Ext (%)	11 M HCl Ext (%)
10	37.55 ± 1.41	17.21 ± 0.86	13.92 ± 0.61	19.06 ± 0.70	29.79 ± 1.00
20	27.28 ± 1.07	14.63 ± 0.74	12.26 ± 0.59	20.83 ± 0.74	39.15 ± 1.20
30	24.29 ± 0.96	13.66 ± 0.71	11.94 ± 0.57	24.14 ± 0.78	44.08 ± 1.38
40	22.75 ± 1.05	12.51 ± 0.57	12.86 ± 0.65	27.78 ± 0.89	49.50 ± 1.61
60	22.83 ± 1.12	11.28 ± 0.63	11.56 ± 0.55	31.16 ±1.00	58.40 ± 2.03
90	21.03 ± 1.09	10.98 ± 0.70	10.85 ± 0.57	36.92 ± 1.28	67.58 ± 2.33

9.3.2   Extractions from HCl/LiCl Solutions

Table 9.16: Data for the extraction of ^{88g}Nb from HCl/LiCl solutions by 0.01 M HDEHP in CHCl$_3$ (Fig. 5.6).

Mixing Time (s)	1 M H$^+$/ 12 M Cl$^-$ Ext (%)	3 M H$^+$/ 12 M Cl$^-$ Ext (%)	6 M H$^+$/ 12 M Cl$^-$ Ext (%)	9 M H$^+$/ 12 M Cl$^-$ Ext (%)	11 M H$^+$/ 12 M Cl$^-$ Ext (%)
10	87.10 ± 8.64	66.62 ± 4.18	38.95 ± 2.22	23.09 ± 1.58	17.66 ± 1.33
20	88.61 ± 7.28	70.04 ± 3.92	39.33 ± 2.22	22.75 ± 1.71	16.54 ± 1.56
30	90.24 ± 9.09	67.66 ± 3.94	40.07 ± 2.39	23.43 ± 1.77	18.30 ± 1.52
60	89.85 ± 10.11	71.01 ± 4.60	39.13 ± 2.41	22.91 ± 1.72	17.44 ± 1.39

Table 9.17: Data for the extraction of ^{170}Ta from HCl/LiCl solutions by 0.01 M HDEHP in CHCl$_3$ (Fig. 5.7).

Mixing Time (s)	1 M H$^+$/ 12 M Cl$^-$ Ext (%)	3 M H$^+$/ 12 M Cl$^-$ Ext (%)	6 M H$^+$/ 12 M Cl$^-$ Ext (%)	9 M H$^+$/ 12 M Cl$^-$ Ext (%)	11 M H$^+$/ 12 M Cl$^-$ Ext (%)
10	24.93 ± 0.69	45.43 ± 2.16	49.78 ±1.90	54.86 ± 1.53	41.68 ± 1.27
20	25.36 ± 0.80	44.09 ± 1.48	64.50 ±1.26	65.93 ± 1.17	54.09 ± 1.68
30	25.56 ± 1.53	45.40 ± 1.66	67.35 ± 1.25	74.19 ± 1.04	67.23 ± 1.15
60	26.01 ± 1.08	43.84 ± 1.70	82.34 ± 0.85	86.63 ± 0.69	83.93 ± 0.68

Table 9.18: Data for the extraction of ^{88g}Nb from HCl/LiCl solutions by 0.01 M BEHP in CHCl$_3$ (Fig. 5.8).

Mixing Time (s)	1 M H$^+$/ 12 M Cl$^-$ Ext (%)	3 M H$^+$/ 12 M Cl$^-$ Ext (%)	6 M H$^+$/ 12 M Cl$^-$ Ext (%)	9 M H$^+$/ 12 M Cl$^-$ Ext (%)	11 M H$^+$/ 12 M Cl$^-$ Ext (%)
10	65.56 ± 4.08	43.81 ± 3.54	21.46 ± 1.95	13.95 ± 0.57	11.82 ± 0.52
20	66.77 ± 3.94	42.03 ± 3.28	22.88 ± 1.82	15.28 ± 0.90	12.73 ± 0.53
30	68.92 ± 4.50	43.06 ± 2.93	21.35 ± 0.81	15.29 ± 0.70	12.29 ± 0.58
60	68.78 ± 5.42	44.77 ± 3.19	21.75 ± 0.78	15.73 ± 0.66	12.73 ± 0.44

Table 9.19: Data for the extraction of ^{170}Ta from HCl/LiCl solutions by 0.01 M BEHP in CHCl$_3$ (Fig. 5.9).

Mixing Time (s)	1 M H$^+$/ 12 M Cl$^-$ Ext (%)	3 M H$^+$/ 12 M Cl$^-$ Ext (%)	6 M H$^+$/ 12 M Cl$^-$ Ext (%)	9 M H$^+$/ 12 M Cl$^-$ Ext (%)	11 M H$^+$/ 12 M Cl$^-$ Ext (%)
10	11.75 ± 0.86	37.27 ± 1.98	39.49 ± 2.14	38.86 ± 1.46	27.56 ± 1.03
20	18.59 ± 1.26	50.84 ± 2.53	50.05 ± 2.48	48.95 ± 1.76	37.31 ± 1.38
30	19.86 ± 1.27	58.13 ± 2.36	65.01 ± 1.68	60.04 ± 2.89	46.80 ± 1.88
60	25.20 ± 1.54	72.84 ± 1.57	79.04 ± 1.32	77.88 ± 1.28	44.26 ± 1.86

9.4 Kinetics Data for Comparison of Macro- and Microscopic Concentrations

Table 9.20: Data for the extraction of ^{95}Nb (10^{-6} M) from HCl solutions by 0.01 M HDEHP in CHCl$_3$ (Fig. 5.11).

Mixing Time (s)	1 M HCl Ext (%)	3 M HCl Ext (%)	6 M HCl Ext (%)	9 M HCl Ext (%)	11 M HCl Ext (%)
10	92.25 ± 0.85	83.65 ± 1.00	80.55 ± 0.74	54.93 ± 0.36	22.65 ± 0.27
20	96.17 ± 1.22	91.16 ± 1.32	91.02 ± 0.98	64.13 ± 0.58	21.01 ± 0.13
30	97.75 ± 1.39	94.79 ± 1.48	94.94 ± 1.15	64.19 ± 0.59	22.09 ± 0.18
40	96.50 ± 1.78	96.27 ± 1.79	95.03 ± 1.28	63.23 ± 0.34	20.94 ± 0.18
60	97.68 ± 1.94	97.86 ± 2.52	95.83 ± 1.52	62.24 ± 0.44	19.31 ± 0.11

Table 9.21: Data for the extraction of ^{95}Nb (10^{-6} M) from HCl solutions by 0.01 M BEHP in CHCl$_3$ (Fig. 5.12).

Mixing Time (s)	1 M HCl Ext (%)	3 M HCl Ext (%)	6 M HCl Ext (%)	9 M HCl Ext (%)	11 M HCl Ext (%)
10	29.16 ± 0.18	5.31 ± 0.09	2.81 ± 0.05	6.06 ± 0.07	10.70 ± 0.18
20	39.03 ± 0.23	8.84 ± 0.13	3.53 ± 0.05	7.18 ± 0.11	10.33 ± 0.10
30	35.49 ± 0.24	7.94 ± 0.13	4.50 ± 0.07	6.63 ± 0.12	10.43 ± 0.12
40	48.73 ± 0.37	10.59 ± 0.19	4.86 ± 0.09	7.01 ± 0.07	10.42 ± 0.16
60	47.09 ± 0.39	13.67 ± 0.23	4.28 ± 0.08	6.94 ± 0.10	9.80 ± 0.10